

DUD
NAVAL F
MONTE
LIBRARY
ATE SCHOOL
CALIFORNIA 93943

NAVAL POSTGRADUATE SCHOOL

Monterey, California



THESIS

NUMERICAL SIMULATIONS OF THE RESPONSE OF
INTENSE OCEAN CURRENTS TO ATMOSPHERIC FORCING

by

David Adamec

March 1985

Thesis Advisor:

R.L. Elsberry

Approved for public release; distribution is unlimited.

T221684

REPORT DOCUMENTATION PAGE		READ INSTRUCTIONS BEFORE COMPLETING FORM
1. REPORT NUMBER	2. GOVT ACCESSION NO.	3. RECIPIENT'S CATALOG NUMBER
4. TITLE (and Subtitle) Numerical Simulations of the Response of Intense Ocean Currents to Atmospheric Forcing.		5. TYPE OF REPORT & PERIOD COVERED Ph.D. Thesis; March 1985
		6. PERFORMING ORG. REPORT NUMBER
7. AUTHOR(s) David Adamec		8. CONTRACT OR GRANT NUMBER(s)
9. PERFORMING ORGANIZATION NAME AND ADDRESS Naval Postgraduate School Monterey, California 93943		10. PROGRAM ELEMENT, PROJECT, TASK AREA & WORK UNIT NUMBERS
11. CONTROLLING OFFICE NAME AND ADDRESS Naval Postgraduate School Monterey, California 93943		12. REPORT DATE March 1985
		13. NUMBER OF PAGES 99
14. MONITORING AGENCY NAME & ADDRESS (if different from Controlling Office)		15. SECURITY CLASS. (of this report) Unclassified
		15a. DECLASSIFICATION DOWNGRADING SCHEDULE
16. DISTRIBUTION STATEMENT (of this Report) Approved for public release; distribution is unlimited.		
17. DISTRIBUTION STATEMENT (of the abstract entered in Block 20, if different from Report)		
18. SUPPLEMENTARY NOTES		
19. KEY WORDS (Continue on reverse side if necessary and identify by block number) Ocean simulations; Atmospheric forcing; Gulf Stream; Bottom topography; Momentum mixing; Surface cooling; Wind forcing		
20. ABSTRACT (Continue on reverse side if necessary and identify by block number) The two and three-dimensional response of strong ocean currents to atmospheric forcing is studied using numerical simulations. In particular, surface cooling is explored as a possible mechanism for explaining an observed 100 km southward shift in the mean position of the Gulf Stream during winter. The magnitude and direction of the cross-stream circulation is highly dependent on whether or not a vertical mixing of momentum occurs when the water column convectively adjusts in response to the surface cooling. A weak		

cross-stream flow toward the higher sea-surface temperatures occurs in the surface layer if momentum mixing does not occur, whereas a stronger flow toward the lower sea-surface temperatures results if momentum mixing does take place. The response in the three-dimensional simulations is very similar to the two-dimensional simulations in the immediate vicinity of the front. The response due to horizontal cooling gradients is not large enough to displace the Gulf Stream appreciably southward in any of the numerical simulations. By contrast, a moderate increase in the zonal wind stress is more effective in displacing the core of the current system than are strong gradients in the surface cooling. The position of the Gulf Stream has also been observed to change as it encounters changes in the bottom topography. The simulated adjustment of the flow to a 200 m seamount is consistent with the conservation of potential vorticity. The inclusion of surface forcing does not affect the adjustment to the topography in any of the simulations, and does not steer the flow toward (away from) the topography so that the characteristics of the downstream flow are changed.

Approved for public release; distribution is unlimited.

Numerical Simulations of the Response of
Intense Ocean Currents to Atmospheric Forcing

by

David Adamec

B.S., Florida State University, 1976

M.S., Florida State University, 1978

Submitted in partial fulfillment of the
requirements for the degree of

DOCTOR OF PHILOSOPHY

from the

NAVAL POSTGRADUATE SCHOOL
March 1985

14035
A 225
2.1

DUDLEY KNOX LIBRARY
NAVAL POSTGRADUATE SCHOOL
MONTEREY, CALIFORNIA 93943

ABSTRACT

The two and three-dimensional response of strong ocean currents to atmospheric forcing is studied using numerical simulations. In particular, surface cooling is explored as a possible mechanism for explaining an observed 100 km southward shift in the mean position of the Gulf Stream during winter. The magnitude and direction of the cross-stream circulation is highly dependent on whether or not a vertical mixing of momentum occurs when the water column convectively adjusts in response to the surface cooling. A weak cross-stream flow toward the higher sea-surface temperatures occurs in the surface layer if momentum mixing does not occur, whereas a stronger flow toward lower sea-surface temperatures results if momentum mixing does take place. The response of three-dimensional simulations is very similar to the two-dimensional simulations in the immediate vicinity of the front. The response due to horizontal cooling gradients is not large enough to displace the Gulf Stream appreciably southward in any of the numerical simulations. By contrast, a moderate increase in the zonal wind stress is more effective in displacing the core of the current system than are strong gradients in the surface cooling. The position of the Gulf Stream has also been observed to change as it encounters changes in the bottom topography. The simulated adjustment of flow to a 200 m seamount is consistent with the conservation of potential vorticity. The inclusion of surface forcing does not affect the adjustment to the topography in any of the simulations, and does not steer the flow toward (away from) the topography so that the characteristics of the downstream flow are changed.

TABLE OF CONTENTS

I.	INTRODUCTION -----	12
II.	THE MODEL -----	16
III.	TWO-DIMENSIONAL SIMULATIONS -----	28
	A. EFFECT OF VERTICAL MIXING OF HEAT ONLY (EXPERIMENT 3-1) -----	32
	B. EFFECT OF MOMENTUM MIXING (EXPERIMENT 3-2) -----	37
	C. EFFECT OF WIND FORCING (EXPERIMENTS 3-3 AND 3-4) -----	45
IV.	THREE-DIMENSIONAL SIMULATIONS -----	55
	A. EFFECT OF VERTICAL MIXING OF HEAT ONLY (EXPERIMENT 4-1) -----	56
	B. EFFECT OF MOMENTUM MIXING (EXPERIMENT 4-2) -----	62
	C. EFFECT OF WIND FORCING (EXPERIMENT 4-3) -----	69
V.	EFFECTS DUE TO TOPOGRAPHY -----	73
	A. SURFACE CURRENT FORCED AWAY FROM SEAMOUNT (EXPERIMENT 5-1) -----	78
	B. SURFACE CURRENT FORCED TOWARD SEAMOUNT (EXPERIMENT 5-2) -----	84
VI.	SUMMARY AND CONCLUSIONS -----	88
	APPENDIX A - STABILITY ANALYSIS -----	93
	LIST OF REFERENCES -----	95
	INITIAL DISTRIBUTION LIST -----	98

LIST OF FIGURES

Figure	PAGE
2-1. Initial temperature field of the upper 250 m in the vicinity of the simulated Gulf Stream front. The contour interval is 1.0°C . -----	19
2-2. Cross-section of the initial geostrophic velocities of the upper 250 m in the vicinity of the front (side face), and the east-west distribution of the surface cooling (top face). The contour interval for the velocities is 40 cm s^{-1} , and the contour interval for the cooling is 190 W m^{-2} (increasing toward the southeast). -----	21
2-3. Surface pressure field and the daily mean distribution of the surface wind stress (N-m), sensible heat flux (W m^{-2}) and latent heat flux (W m^{-2}) during AMTEX 1974 from Kondo (1976). The top row is February 22, the middle row is February 24 and the bottom row is February 26. -----	22
2-4. Daily mean distribution of the latent heat flux (W m^{-2}) and surface wind stress (N-m) on 26 February during AMTEX 1974 (from Kondo, 1976). The contour interval for the heat flux is 100 W m^{-2} , and the contour interval for the wind stress is 0.1 N-m . -----	24
2-5. Distribution of the average latent heat flux over the North Atlantic during February (from Gorshkov, 1978). The contour interval is 20 W m^{-2} . -----	25
2-6. Time series of latent heat flux at Station Ryofu during AMTEX 1974 (from Agee and Howley, 1977). -----	26

3-1.	Average of the v component of velocity for hours 51-72 for Experiment 3-1. The contour interval is 0.1 cm s^{-1} and negative contours are dashed. The flow is positive northward (to the left). The arrow indicates the position of the warm edge of the surface front. -----	33
3-2.	Average of the change in the u component of velocity for hours 51-72 for Experiment 3-1. The contour interval is 1 cm s^{-1} and negative contours are dashed. -----	35
3-3.	Combined effect of horizontal and vertical advection on the temperature tendency at hour 72 for Experiment 3-1. The values are multiplied by 10^5 . The contour interval is $0.5 \times 10^{-5} \text{ }^{\circ}\text{C s}^{-1}$ and negative contours are dashed. -----	36
3-4.	Change in temperature at hour 72 for Experiment 3-1. The contour interval is 0.25°C and negative contours are dashed. -----	38
3-5.	As in Fig. 3-1 except for Experiment 3-2 and the contour interval is 1 cm s^{-1} . -----	40
3-6.	As in Fig. 3-2 except for Experiment 3-2 and the contour interval is 2 cm s^{-1} . -----	41
3-7.	Average of the vertical velocity for hours 51-72 for Experiment 3-2. The contour interval is 0.002 cm s^{-1} and negative (downward) contours are dashed. The values have been multiplied by 100. -----	43
3-8.	As in Fig. 3-2 except for Experiment 3-3 and the contour interval is 2 cm s^{-1} . -----	46
3-9.	As in Fig. 3-1 except for Experiment 3-3 and the contour interval is 1 cm s^{-1} . -----	48
3-10.	As in Fig. 3-7 except for Experiment 3-3. ---	49
3-11.	As in Fig. 3-1 except for Experiment 3-4, the contour interval is 1 cm s^{-1} , and for values of y between -200 and 0 km. -----	50

3-12.	As in Fig. 3-2 except for Experiment 3-4 and for values of y between -200 and 0 km. -----	52
3-13.	As in Fig. 3-4 except for Experiment 3-4 and for values of y between -200 and 0 km. -----	53
4-1.	Surface v component at hour 72 for Experiment 4-1. Negative values indicate southward flow.	57
4-2.	Changes in surface temperature (solid lines) and the velocities (arrows) at hour 72 for Experiment 4-1. The length of the arrows is proportional to the departure from a control run without forcing. The maximum departure is about 8 cm s^{-1} . The contour interval is 0.5°C . -----	59
4-3.	Surface v component at day 18 for a simulation using a cooling rate six times smaller than the first simulation of Experiment 4-1. The contour interval is 0.1 cm s^{-1} . -----	61
4-4.	As in Fig. 4-1 except for Experiment 4-2 and the contour interval is 0.5 cm s^{-1} where the flow is positive (northward), and 0.1 cm s^{-1} where the flow is negative (southward). -----	63
4-5.	Time series of the instantaneous v component at the surface (dashed line) and filtered v component (solid line) at $x = 1100 \text{ km}$ and $y = 188 \text{ km}$ for Experiment 4-2. -----	65
4-6.	Change in surface u component of velocity at hour 72 for Experiment 4-2. Negative values indicate a reduction in the eastward current maximum. The contour interval is 2 cm s^{-1} . --	67
4-7.	As in Fig. 4-2 except for Experiment 4-2, and the maximum departure is about 16 cm s^{-1} . ---	68
4-8.	As in Fig. 4-2 except for Experiment 4-3, and the maximum departure is about 35 cm s^{-1} . ---	71

5-1.	South-to-north cross-section of the initial zonal velocities used in the simulations which include effects due to topography. The contour interval is 20 cm s^{-1} , and positive flow is toward the east. -----	75
5-2.	Dependence of the amplitude of the response of the flow on non-dimensional height for the initial conditions and topography used throughout Section V. -----	76
5-3.	Surface temperature at day 6 of for the first simulation of Experiment 5-1. The contour interval is 1.0°C . -----	79
5-4.	West-to-east cross-section of temperature along $y = 128 \text{ km}$ at day 6 for Experiment 5-1. The contour interval is 1.0°C . -----	80
5-5.	As in Fig. 5-3 except that the seamount is centered at $x = 640 \text{ km}$ and $y = 144 \text{ km}$. -----	82
5-6.	Difference in surface temperature fields at day 6 of Experiment 5-1 between the simulation which is forced by an eastward wind stress and a simulation which is not forced. The contour interval is 0.5°C . -----	83
5-7.	As in Fig. 5-3 except for Experiment 5-2. ---	85
5-8.	As in Fig. 5-6 except for Experiment 5-2. ---	87

LIST OF SYMBOLS

A_M	Horizontal eddy viscosity; $1.6 \times 10^7 \text{ m}^4 \text{ s}^{-1}$
A_T	Horizontal eddy conductivity; $1.6 \times 10^7 \text{ m}^4 \text{ s}^{-1}$
C_p	Specific heat of water
D	Total depth of water column
f	Coriolis parameter
g	Gravity
H	Thickness of upper layer
K_M	Vertical eddy viscosity; $5 \times 10^{-5} \text{ m}^2 \text{ s}^{-1}$
K_T	Vertical eddy conductivity; $5 \times 10^{-5} \text{ m}^2 \text{ s}^{-1}$
P	Pressure
T, T_0	Temperature and reference temperature
u	East-west component of velocity
v	North-south component of velocity
w	Vertical component of velocity
Q	Surface heat flux per unit area
α	Coefficient of thermal expansion
ρ, ρ_0	Density and reference density

ACKNOWLEDGMENTS

I am very thankful to Dr. Russell Elsberry for his time and the guidance he provided throughout the course of this research. His true dedication to quality research will always be very much appreciated.

I would also like to thank Dr. Robert Haney for his comments and suggestions regarding this research and to Drs. Terry Williams, Mary Alice Rennick, Gordon Latta and Bill Garwood for their time and service on my committee.

The help provided by Mr. Steve Lamont in the printing phases of this dissertation is also very much appreciated.

Finally, I would like to thank my wife Michele who was a constant source of encouragement over the past three years.

This research was funded by the Office of Naval Research under contract number NR 083-275, program element 61153N. Computer time was supplied by the W.R. Church Computer Center at the Naval Postgraduate School.

I. INTRODUCTION

Over the past decade there has been conflicting observational and theoretical evidence over the role of air-sea fluxes of sensible and latent heat during cyclogenesis. Using data from the Air Mass Transfer Experiment, Wei (1979) concluded that air-sea fluxes of sensible and latent heat did not contribute significantly to the available potential energy during cyclogenesis. However, there is evidence which suggests that ocean heat fluxes may be important for cyclogenesis at specific geographic locations. Baker (1979) finds that most cyclogenetic events in the southern hemisphere occur along the sub-polar ocean front. Sanders and Gyakum (1980) find that a positive correlation exists between areas of explosive cyclogenesis and locations of sea-surface temperature gradients. Sandgathe (1981) investigated changes in the evolution of model cyclones when the air-sea fluxes were removed. He selectively removed surface fluxes and found both changes in the intensification of an initial cyclone and in the development of secondary lows. The studies by Baker (1979), Sanders and Gyakum (1980) and Sandgathe (1981) suggest that knowledge of the locations of sea-surface temperature gradients may be needed for accurate prediction of cyclogenesis over the ocean.

According to Sanders and Gyakum (1980), most explosive cyclogenetic events over the Atlantic Ocean occur in the vicinity of the Gulf Stream. There is a baroclinic zone associated with the Gulf Stream current which can be traced from Cape Hatteras eastward for hundreds of kilometers. The horizontal ocean temperature differences are not compensated by salinity effects, and there is an associated baroclinic jet with a front that behaves similarly to an atmospheric front. The local momentum balances in the Gulf Stream are similar to the momentum balances of an atmospheric front (Roden, 1976). The Gulf Stream temperature front tends to be vertical in the upper 50-100 m and then slopes steeply (about 100 m/10 km) toward the south with increasing depth.

Much study has been devoted to the understanding of the large-scale balances of the Gulf Stream. The review article by Veronis (1981) provides an excellent background on these studies. The investigation presented here deals with local balances and the effects of surface forcing on the Gulf Stream. The processes which form and maintain the Gulf Stream current system are not addressed.

Most ocean front response studies have focused on wind forcing only (DeSzoeko, 1980; Cushman-Roisin, 1981; and Camerlengo, 1982). Recent studies have also considered the effects of a surface buoyancy flux in the forcing of oceanic fronts. Cushman-Roisin (1984) investigated the role of the large-scale buoyancy flux in maintaining the subtropical front in the North Pacific Ocean. Adamec and Garwood (1985) included a surface buoyancy flux in addition to wind forcing and demonstrated that the near-surface advective response of the ocean is enhanced when the surface buoyancy flux is downward (heating).

Of particular interest is an investigation by Nof (1983) who studied the response of the Gulf Stream as it flowed into a region of cooling. The response of the Gulf Stream was examined because of the large cooling rates observed east of Cape Hatteras (Budyko, 1963; Worthington, 1976). Nof assumed the density structure could be represented by two layers and that the lower layer was motionless. A density increase of $1 \times 10^{-3} \text{ gm cm}^{-3}$ over 1200 km in the downstream (eastward) direction was specified to simulate surface cooling of the ocean. Also, surface cooling was allowed to occur south of a 0.5 m s^{-1} eastward jet only. A southward cross-stream component developed in response to a zonal pressure gradient which resulted from the along-stream gradient in surface cooling (density increase). A power series solution for a steady state, inviscid, Boussinesq flow yielded cross-stream velocities of 3 cm s^{-1} , which could lead to displacements as large as 90 km in a season.

The displacements predicted by Nof appear to be consistent with Fuglister's (1972) isotherm analysis of the Gulf Stream during the 1965-1966 winter, which showed a 100 km north-to-south

displacement of the 5°C and 10°C isotherms. Halliwell and Mooers (1983) provide additional evidence for a southward shift in the Gulf Stream front during winter based on an empirical orthogonal function analysis of satellite infrared imagery. In that study, the average monthly position of long-period meanders is displaced 45 km southward between October and February, 1975-1978. Nof's result that a steepening of the frontal interface will occur during winter is consistent with Worthington's (1976) isotherm analyses of the Gulf Stream east of the Grand Banks.

The Gulf Stream is a highly variable meandering current system that parallels the temperature front. Because the front and the current penetrate very deep into the water column, the effect of gradients in the underlying topography may be important in determining the path of the Gulf Stream. The Gulf Stream frequently passes over areas where there are large changes in the bottom topography. The New England Seamount Chain in the western Atlantic has features which rise 3 km above the surrounding ocean floor. There are observations which indicate that the seamount chain significantly affects the path of the Gulf Stream extension. Vastano and Warren (1976) observed drastic path changes as the Gulf Stream flowed over the New England Seamount Chain. Richardson (1981) observed that the New England Seamount Chain is a favored area for large-scale meanders and warm core ring generation. In addition, the topography appears to be responsible for a 100 km southeastward deflection of the current system.

The overall objective of this research is to aid in understanding the effects of local atmospheric forcing on strong ocean currents such as the Gulf Stream. Particular attention is paid to those processes that displace the current system equatorward in the winter season. Because of a lack of detailed observations of the response of the Gulf Stream to surface forcing, and because the response of the ocean to surface forcing is expected to be nonlinear, numerical simulations are used to model the complex processes and response of the ocean.

The research is described in five major sections. Section II briefly describes the ocean models and initial conditions used in this investigation. The objective of Section III is to use numerical simulations to understand the effects of local atmospheric forcing on strong ocean currents. Processes that modify the oceanic thermal and momentum structure when a cross-stream cooling gradient is imposed are highlighted. A cross-stream cooling gradient is specified by extracting more heat on the warm side of the Gulf Stream front than on the cold side. The response due to an increase in the southward and eastward wind stress is also investigated to determine the relative importance of the additional effect of wind stress and those effects due to cooling only. Because downstream variations are not treated in these two-dimensional simulations, the Nof (1983) process is excluded.

Section IV extends the results of Section III and includes the effects of along-stream variations in the forcing. The purpose of this section is to simulate numerically the three-dimensional response of an intense ocean current system such as the Gulf Stream as it flows into a region of surface cooling. The relative importance of the cross-stream and along-stream cooling gradients near the initial position of the associated baroclinic zone is discussed in detail.

Section V uses a multi-level primitive equation model with σ -coordinates to investigate the effect of wind forcing on a stratified flow similar to the Gulf Stream as it flows over bottom topography. One of the major goals of Section V is to determine if surface forcing affects the adjustment of the flow to the topography so that the mean position of the current system is significantly altered. Section VI summarizes the results of this research and suggests areas for future study.

II. THE MODEL

A multi-level, nonlinear primitive equation model is used in these experiments to simulate the Gulf Stream response to atmospheric forcing. The governing equations in flux form for an ocean circulation model which predicts the shear currents in an ocean of uniform depth D are written in Cartesian coordinates as

$$u_t = - (uu)_x - (vu)_y - (wu)_z + fv + A_M \nabla^4 u + K_M u_{zz} + \overline{(uu)}_x + \overline{(vu)}_y - \frac{\hat{P}_x}{\rho_o} \quad (2.1)$$

$$v_t = - (uv)_x - (vv)_y - (wv)_z - fu + A_M \nabla^4 v + K_M v_{zz} + \overline{(uv)}_x + \overline{(vv)}_y - \frac{\hat{P}_y}{\rho_o} \quad (2.2)$$

$$T_t = - (uT)_x - (vT)_y - (wT)_z + A_T \nabla^4 T + K_T T_{zz} \quad (2.3)$$

$$u_x + v_y + w_z = 0 \quad (2.4)$$

$$P_z = - \rho g \quad (2.5)$$

$$\rho = \rho_o (1 - \alpha(T - T_o)) \quad (2.6)$$

where \sim represents a vertical average over the entire depth and \hat{P} is $P - \overline{P}$, which can be calculated using (2.5). The symbols are defined in the List of Symbols.

The ocean is assumed to be hydrostatic and incompressible, and density is prescribed to be a linear function of temperature alone. A rigid lid is specified by setting the vertical velocity to zero at the top and bottom of the domain, so that the integrated divergence over the entire depth of the water column is zero. Furthermore, the vertical average of the horizontal velocity components is zero, so that the model predicts only the vertical shear in the horizontal velocities. The barotropic components which are a result of a dynamic adjustment in the ocean are assumed to be smaller than the currents induced by the surface forcing. All calculations in the simulations presented throughout this study are performed on an f plane at 36°N .

The effects of diffusion are calculated using a biharmonic (∇^4) operator in the horizontal and a Laplacian ($\partial^2/\partial z^2$) operator in the vertical. The values for the horizontal eddy coefficients are chosen such that for the largest currents the Reynolds number based on the grid size is of order 1. That is, the advective and diffusive terms in the strong current regions will have a comparable magnitude for scales the order of Δx . The model also includes a generalized convective adjustment scheme based on a local gradient Richardson number: if the Richardson number falls below a critical value (0 for these simulations), then similar adjustments of heat and momentum occur so that the new adjusted profile will have a local gradient Richardson number slightly larger than the critical value. The details of the adjustment scheme are given in Adamec *et al.* (1981). Zero is used as the critical Richardson number in these simulations to isolate those effects due to convective overturning only in response to the surface cooling. The consequences of using a larger critical Richardson number are discussed in Section III.

The response is due to surface forcing only, as there is no flux of heat or momentum across the north and south boundaries or the bottom. The surface boundary forcing due to wind stress and heat flux enters through boundary conditions on $K_M (u_z, v_z)$ and $K_T (T_z)$, respectively. Variations in the x-direction (downstream) are ignored for all two-dimensional simulations. The total horizontal extent (resolution) of the two-dimensional region is 400 km (2 km). The vertical resolution varies logarithmically from 6 m near the surface to 100 m at 1000 m in 20 levels.

The horizontal dimensions (resolution) of the three-dimensional domain is 1280 km (20 km) in the east-west direction and 256 km (4 km) in the north-south direction. The vertical extent is 1000 m, and the vertical resolution varies logarithmically from 10 m near the surface to 200 m at 1000 m in 10 levels. The east and west lateral boundaries are open in the three-dimensional simulations and are prescribed using a variation of Orlanski's (1976) boundary condition as discussed by Camerlengo and O'Brien (1980).

The effect of topography is often included in baroclinic ocean models by specifying the vertical velocity as a bottom boundary condition, $w = -\mathbf{V} \cdot \nabla D$, as in Huppert and Bryan (1975) and Semtner and Mintz (1977). The numerical model in these simulations uses the so-called σ -coordinate transformation, which was introduced by Phillips (1957). The σ -coordinate is a redefinition of the vertical coordinate that allows for variations in the depth of the fluid.

The new vertical coordinate is defined by $\sigma = z/D$, where D is the local depth of the fluid. The horizontal coordinate and velocity components are defined on constant σ -surfaces. The governing equations for the flow are similar to the equations in Cartesian coordinates except for the pressure gradients. The horizontal gradient of pressure in σ -coordinates is

$$\nabla P = \frac{\sigma}{D} P_{\sigma} \nabla D, \quad (2.7)$$

and the hydrostatic equation is

$$P_{\sigma} = -\rho g D. \quad (2.8)$$

The equations in σ -coordinates are solved in a similar manner to that used for primitive equation models that use z as the vertical coordinate. The vertical resolution of sigma in these simulations varies logarithmically from 0.01 near the surface to 0.20 at $\sigma = -1$ in 10 levels. The topography used is a Gaussian-shaped seamount which extends 200 m above a 1000 m ocean floor. The seamount extends approximately 120 km in the x and y directions.

The initial conditions for temperature are derived from a smoothed version of a hydrographic section across the Gulf Stream at 38°N during mid-November 1970 (United States Naval Oceanographic Office, 1970) and are shown in Fig. 2-1. The horizontal sea-surface temperature gradient is 6°C in 20 km. On the northern side of the front, the temperature is uniform to a depth of 60 m, while the water is well-mixed to a depth of 100 m on the southern side. Notice also that the vertical stability below the mixed layer on the northern side is greater than the vertical stability on the southern side. As a result, the maximum horizontal temperature gradient

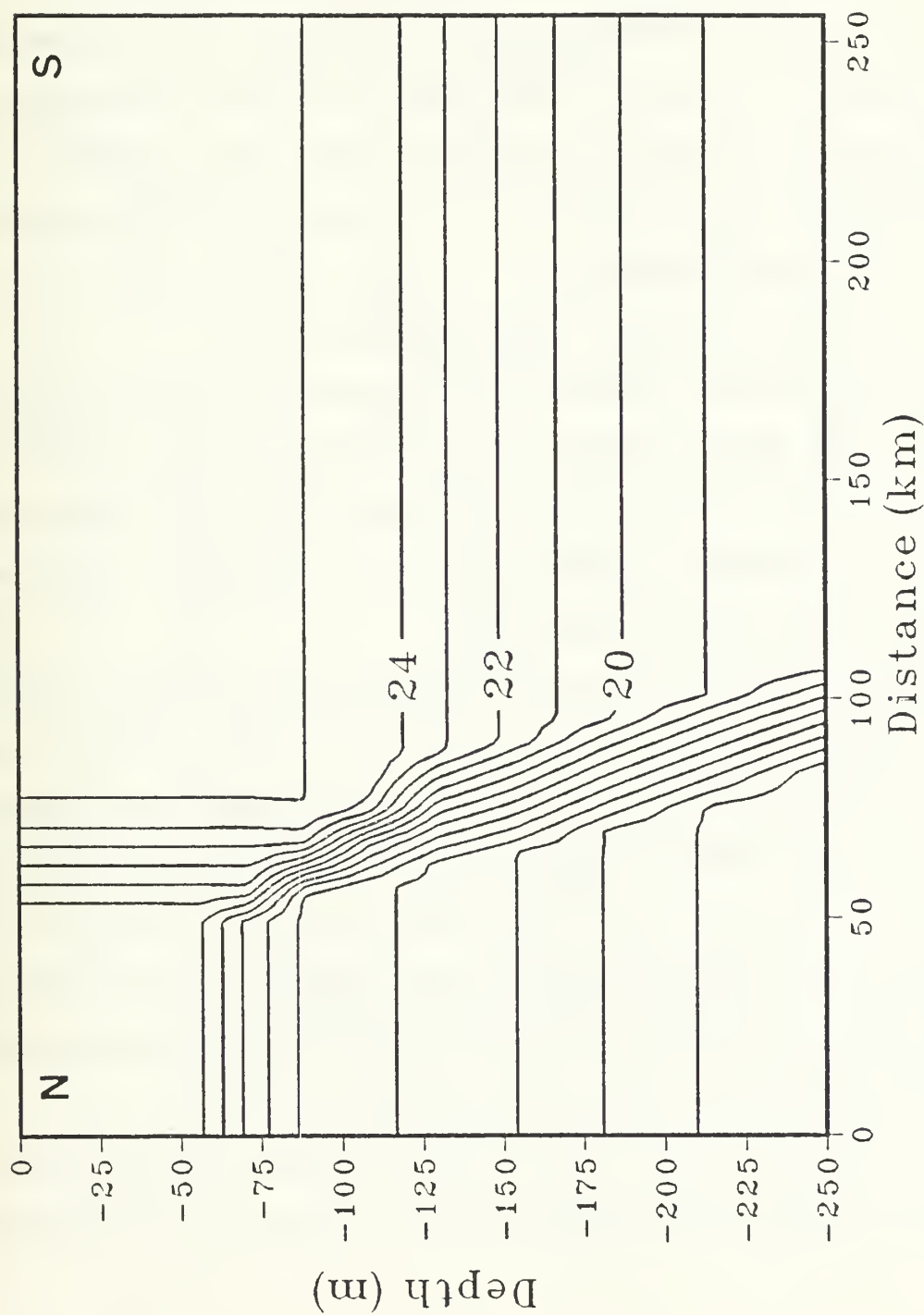


Figure 2-1. Initial temperature field of the upper 250 m in the vicinity of the simulated Gulf Stream front. The contour interval is 1.0 °C.

occurs at a depth of 100 m. Assuming geostrophic balance, the initial zonal velocities (Fig. 2-2) are eastward with a maximum value at the surface near 2.0 m s^{-1} .

Rather than inferring a cooling rate from the observed along-stream density increase as in Nof (1983), a surface cooling is specified. The x-y dependence of the surface cooling (Fig. 2-2) is similar to the x-y dependence of the density increases used by Nof. The upward heat flux increases from zero at $x = 320 \text{ km}$ to a maximum value at $x = 1000 \text{ km}$. Cooling is assumed to be directly proportional to the sea-surface temperature, so maximum cooling occurs on the warm side of the surface front. The initial cooling in the two-dimensional simulations is identical to the cooling in the three-dimensional simulations for $x > 1000 \text{ km}$. As in Nof (1983), there is no cooling north of the front. The maximum value for the cooling is 970 W m^{-2} .

The evaporative and sensible heat fluxes are directly proportional to the air-sea temperature difference in the bulk aerodynamic formulation. If the temperature of the air is assumed to be uniform over areas of non-uniform sea-surface temperatures, then the cooling will be largest where the sea-surface temperatures are highest. The choice of a cooling function which increases toward higher sea-surface temperatures seems justified.

The choice of a cooling function which increases in the along-stream direction is more difficult to justify. The Air Mass Transformation Experiment (AMTEX) was conducted south of Japan during February 1974 and 1975. One of the scientific objectives of AMTEX was to investigate the physical processes by which cold continental air is modified through interactions with the sea. The experiment was conducted in a location where cold continental air originating from the Asian land mass was modified through interaction with the warm waters of the Kuroshio. An array of observing stations enabled a comprehensive study of the heat and momentum transfer between the atmosphere and the ocean.

Kondo (1976) described the time evolution of the observed synoptic weather pattern, surface wind stress and sensible and latent heat fluxes during a cold outbreak (Fig. 2-3). As the cold air

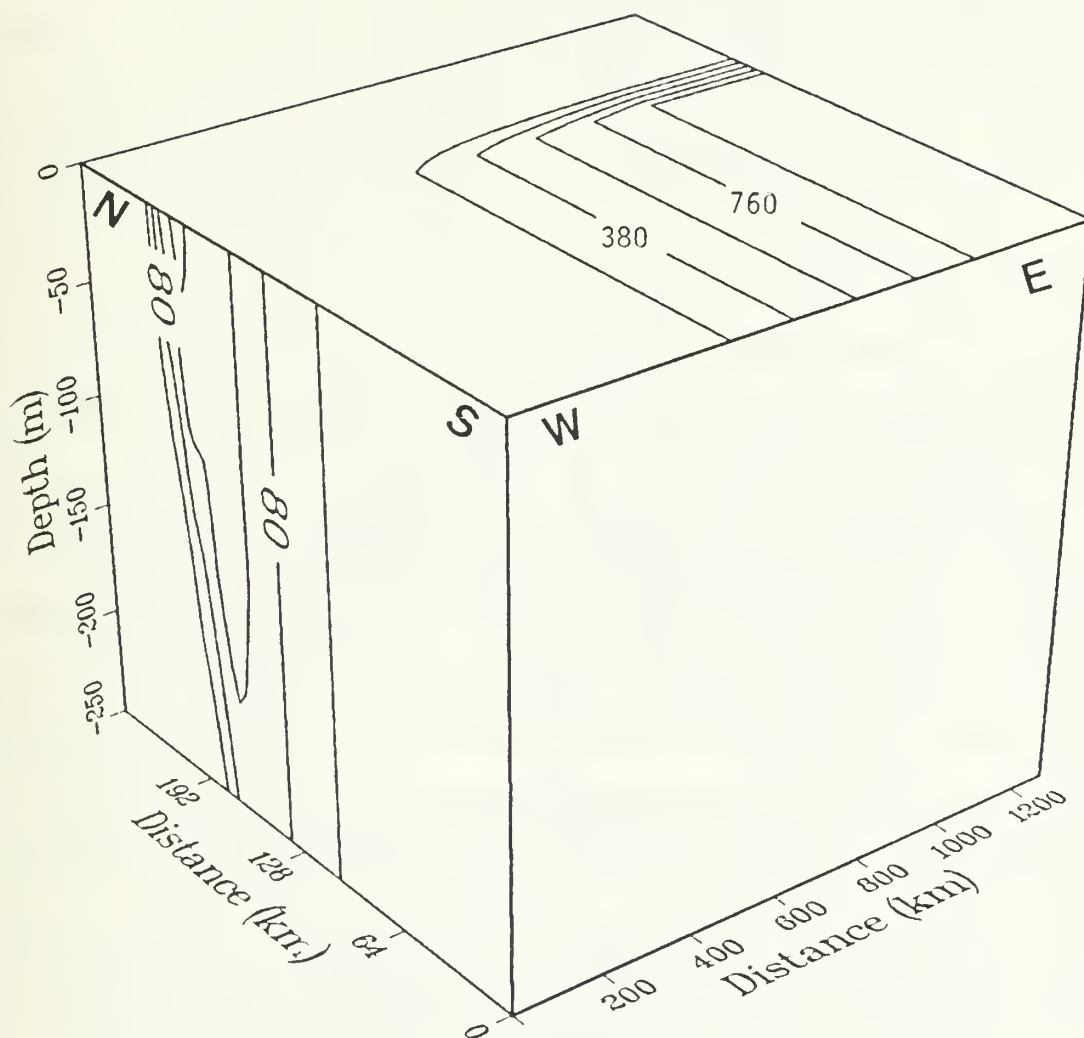


Figure 2-2. Cross-section of the initial geostrophic velocities of the upper 250 m in the vicinity of the front (side face), and the east-west distribution of the surface cooling (top face). The contour interval for the velocities is 40 cm s^{-1} , and the contour interval for the cooling is 190 W m^{-2} (increasing toward the southeast).

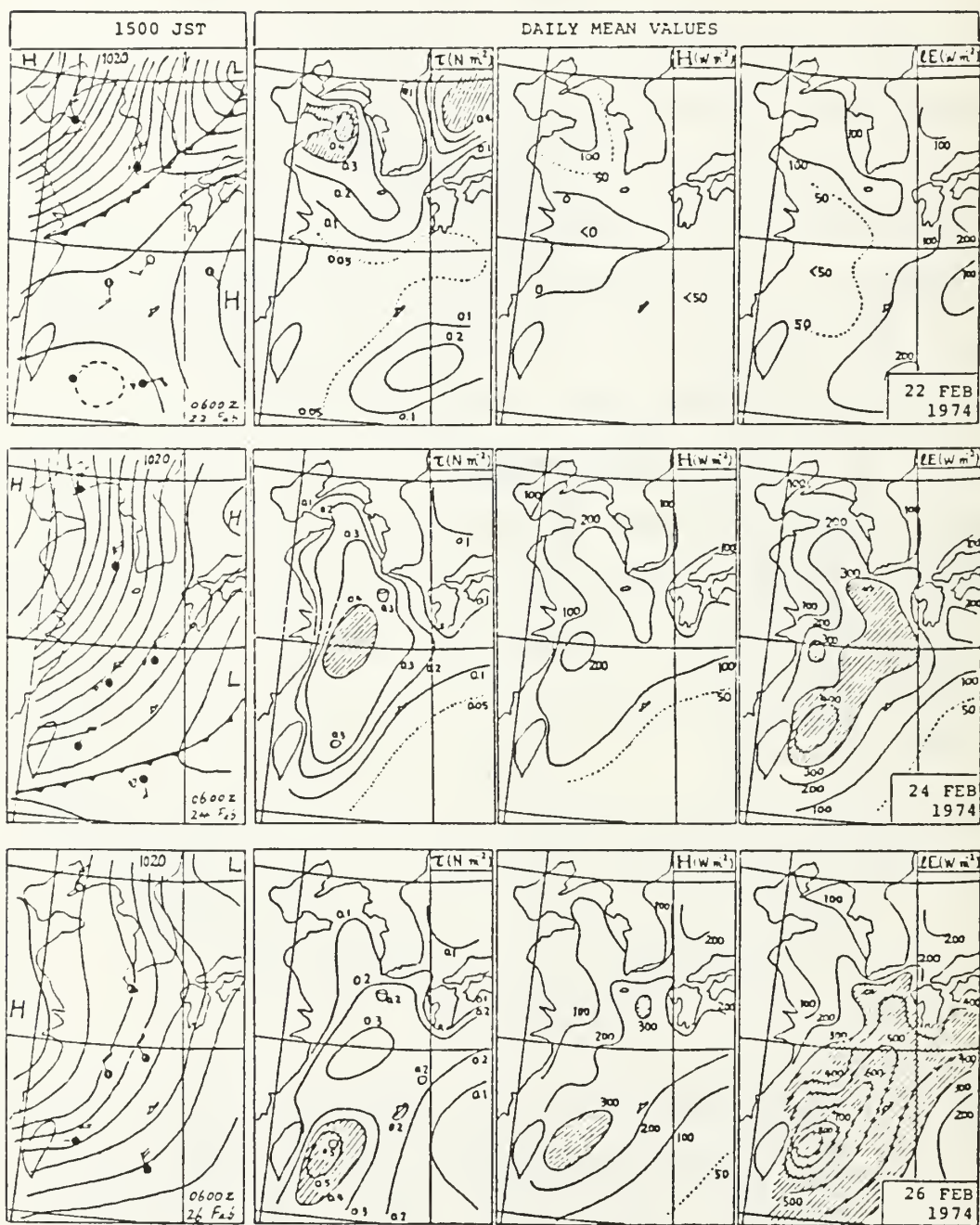


Figure 2-3. Surface pressure field and the daily mean distribution of the surface wind stress ($N m^{-2}$), sensible heat flux ($W m^{-2}$) and latent heat flux ($W m^{-2}$) during AMTEX 1974 (from Kondo, 1976). The top row is February 22, the middle row is February 24 and the bottom row is February 26.

penetrates southward, the values of the surface heat and momentum fluxes become larger so that by 26 February the maximum wind stress is about 0.5 N-m (directed southward as seen in left frames) and the sensible and latent heat fluxes are in excess of 300 W m^{-2} and 800 W m^{-2} , respectively. The maximum values of the heat and momentum fluxes occur initially near the coast, but progress further southward with the leading edge of the cold air. The maximum heat fluxes are located over the Kuroshio as the cold air is modified by interaction with the ocean (Kondo, 1976). An enlargement of the latent heat flux and surface wind stress patterns relative to the position of the Kuroshio on 26 February is shown in Fig. 2-4. The maximum values of the heat and momentum fluxes occur to the south of the mean path of the Kuroshio, and there is a cross-stream gradient in the heat flux. Notice that the Kuroshio is approaching these maxima from the south, so that the cooling and wind stress is increasing in the downstream direction. The specification of cooling increases in the downstream direction in the numerical simulations is consistent with these measurements.

Observations in the Atlantic support the choice of a cooling function which increases in the downstream direction for seasonal time scales. Gorshkov (1978) presents a monthly average of latent heat flux over the North Atlantic during February (Fig. 2-5) based on 70 years of ship observations. The maximum values occur off the east coast of the United States and are concurrent with the mean position of the Gulf Stream. The Gulf Stream flows from the south toward these maximum values and thus experiences a downstream increase in surface cooling. The maximum value of the average latent heat flux is 180 W m^{-2} .

In all of the simulations presented in this investigation, the surface forcing is applied impulsively. A time series of the computed latent heat flux from a study by Agee and Howley (1977) at Station Ryofu, which was located within the path of the Kuroshio during AMTEX 1974, is shown in Fig. 2-6. A rapid increase in surface cooling is evident at the initial stages of the cold outbreak on 22 February. The values of the latent heat flux rise from 50 W m^{-2} to over 800

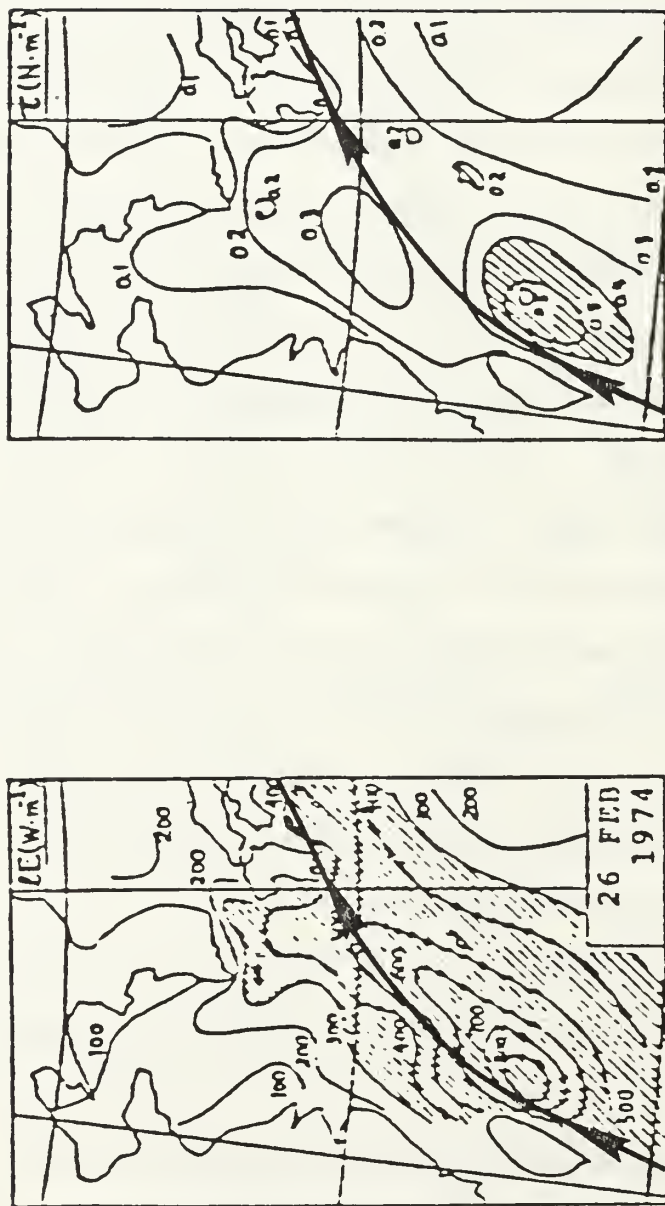


Figure 2-4. Daily mean distribution of the latent heat flux ($W m^{-2}$) and surface wind stress ($N m^{-2}$) on 26 February during AMTEX 1974₂ (from Kondo, 1976). The contour interval for the heat flux is $100 W m^{-2}$ and the contour interval for the wind stress is $0.1 N m^{-2}$.

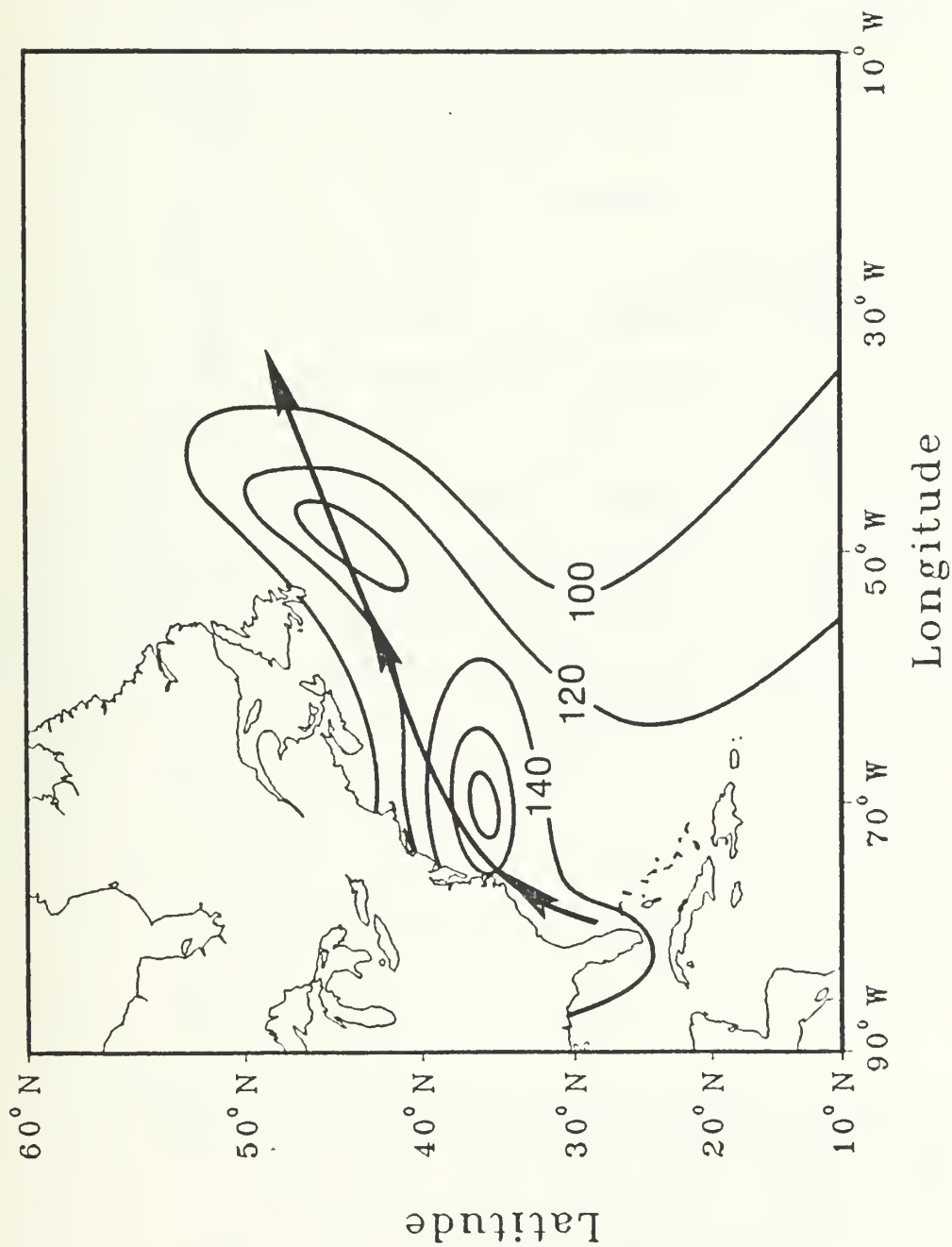


Figure 2-5. Distribution of the average latent heat flux over the North Atlantic during February (from Gorshkov, 1978). The contour interval is 20 W m^{-2} .

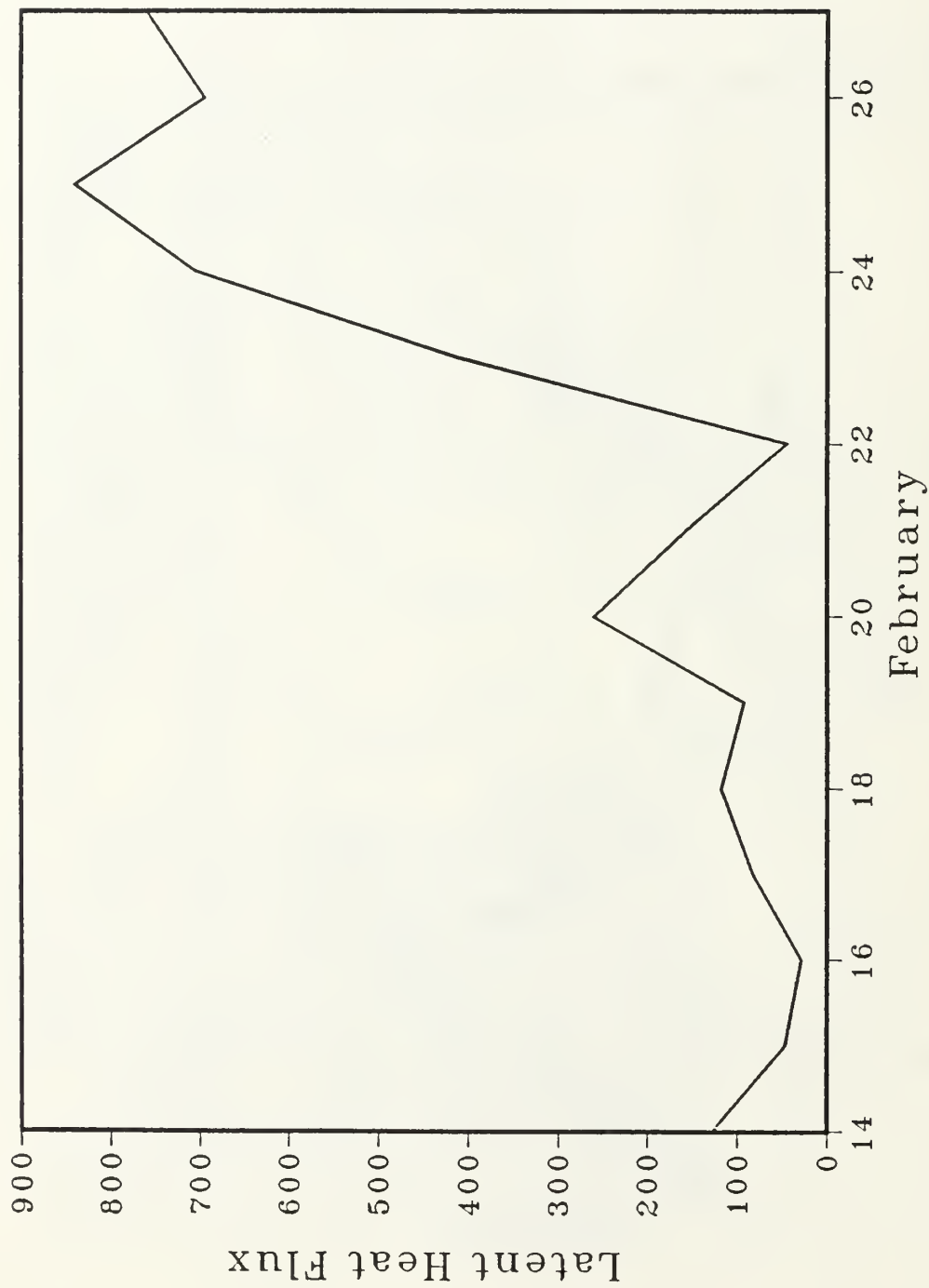


Figure 2-6. Time series of latent heat flux (W m^{-2}) at Station Ryofu during AMTEX 1974 (from Agee and Howley, 1977).

W m^{-2} . The computed value of the latent heat flux combined with an estimated maximum sensible heat flux of 300 W m^{-2} is about 15% greater than the maximum heat flux used in the simulations (970 W m^{-2}). Similar cooling rates during cold outbreaks have also been observed in the Gulf of Mexico by Huh *et al.* (1984).

These simulations also investigate the role of wind forcing as a possible mechanism for shifting the Gulf Stream. The maximum wind stress used in these simulations is 0.2 N-m , which is near the low end of values for the observed wind stress during the cold outbreak during AMTEX 1974 (Fig. 2-4). Two directions of the wind stress are considered. The first is from the north, which is the dominant direction of the wind during the outbreak of 22 February 1974 (Fig. 2-3), and the other is from the west. An increase in the eastward wind stress is considered because Gorshkov (1978) found that the average wind over the Gulf Stream increases to $5\text{-}7 \text{ m s}^{-1}$ in the eastward direction during winter. A value of 0.2 N-m is consistent with the observed values of the wind stress. The simulations presented here are designed to study the response of the Gulf Stream once it has left the coast near Cape Hatteras (Fig. 2-5). The observations during AMTEX 1974 were taken over the northward flowing Kuroshio before it leaves the coast of Asia. It is felt that the relative direction of the applied wind stress to the Gulf Stream realistically depicts outbreaks which originate from the cold continent to the north and west.

III. TWO-DIMENSIONAL SIMULATIONS

The experiments in this section examine the two-dimensional effect of a horizontal gradient in the cooling across a strong ocean frontal feature such as the Gulf Stream. Such a gradient in cooling may occur when a nearly uniform mass of cold air flows over the sea-surface temperature gradient. An analytic model with very simple mixed-layer dynamics is used first to aid in understanding the response of an ocean front to cross-stream cooling. A more sophisticated numerical solution of the problem follows in later sections.

Consider a hydrostatic fluid whose temperature is a constant T_1 down to depth $z = -H$, and then a constant T_2 for the remainder of the water column to depth $z = -D$. The governing equations for linear inviscid shear flow on an f plane are given by

$$u_t - fv = 0 \quad (3.1)$$

$$v_t + fu = - \frac{\hat{P}_y}{\rho_o} \quad (3.2)$$

where u and v are the Eulerian horizontal components of velocity, and ρ_o is the density of the fluid at a reference temperature T_o . In this study, x is positive to the east and is the downstream direction, y is positive to the north and is the cross-stream direction and z is positive up. For simplicity, variations in the x -direction have been ignored and the wind stress is assumed to be zero. A single equation for v can be found by taking a local time derivative of (3.2) and substituting from (3.1) to obtain

$$v_{tt} + f^2v = - \frac{\hat{P}_{yt}}{\rho_o} \quad (3.3)$$

If density is prescribed to be a linear function of temperature alone, then it is possible to write an expression for P in terms of temperature as

$$\hat{P} = \int_z^0 \rho g (1 - \alpha(T - T_o)) \, d\lambda - \frac{1}{D} \int_{-D}^0 \int_z^0 \rho g (1 - \alpha(T - T_o)) \, d\lambda \, dz \quad (3.4)$$

where α is the coefficient of thermal expansion and g is the acceleration due to gravity. The first term on the right side of (3.4) is the pressure, and the second term is the vertical average of the pressure. Taking a local time derivative of (3.4) removes all terms in the integrand which are not multiplied by T_t . If changes in temperature are due solely to surface heat flux, which is assumed to penetrate to depth $z = -H$, then the local rate of change of temperature can be written

$$\begin{aligned} T_t &= - \frac{Q}{\rho_o C_p H} & 0 \geq z \geq -H \\ T_t &= 0 & -H > z \geq -D \end{aligned} \quad (3.5)$$

where Q is the upward surface heat flux. There is no change in temperature below $z = -H$. Substituting (3.5) into the time derivative of the first term on the right side of (3.4) yields

$$\begin{aligned} P_t &= - \frac{\alpha g}{C_p} Q \frac{z}{H} & 0 \geq z \geq -H \\ P_t &= \frac{\alpha g}{C_p} Q & -H > z \geq -D \end{aligned} \quad (3.6)$$

or by performing the integrations and removing the vertical average,

$$\begin{aligned} \hat{P}_t &= - \frac{\alpha g}{C_p} Q \left(\frac{z}{H} + 1 - \frac{H}{2D} \right) & 0 \geq z \geq -H \\ \hat{P}_t &= \frac{\alpha g}{C_p} Q \frac{H}{2D} & -H > z \geq -D \end{aligned} \quad (3.7)$$

Differentiating (3.7) with respect to y and substituting the expression for \hat{P}_{yt} into (3.3) yields an equation for v forced by a gradient in the surface cooling

$$\begin{aligned} v_{tt} + f^2 v &= \frac{\alpha g}{\rho_o C_p} Q_y \left(\frac{z}{H} + 1 - \frac{H}{2D} \right) & 0 \geq z \geq -H \\ v_{tt} + f^2 v &= - \frac{\alpha g}{\rho_o C_p} Q_y \frac{H}{2D} & -H > z \geq -D \end{aligned} \quad (3.8)$$

It was assumed in (3.8) that H is not a function of y , which is not the case for the initial temperature structure in the numerical simulations (Fig. 2-1). A horizontal temperature gradient can also be induced by variations in H with uniform surface cooling. The contribution of the

variation in the upper layer thickness (δH) to a variation in the surface cooling (δQ) for forming horizontal temperature gradients is measured by the ratio ($\delta H/H$): ($\delta Q/Q$). For the initial conditions and cooling used in the numerical simulations, ($\delta H/H$) \sim 0.1, while ($\delta Q/Q$) \sim 1.0. Thus, the ratio is about 0.1, which indicates that the gradient in the surface cooling is more important in forming horizontal temperature differences than is the gradient in the thickness of the upper layer. This justifies the derivation of (3.8) which will be used to interpret the numerical solutions shown in this section.

The free response of (3.8) is inertial motion. Obtaining a particular solution to the forced problem requires assumptions about the heating rate Q . If the right side of (3.8) is assumed to be constant in time, then a particular steady state solution of (3.8) is

$$\begin{aligned} v &= \frac{\alpha g}{\rho_o C_p f^2} Q_y \left(\frac{z}{H} + 1 - \frac{H}{2D} \right) & 0 \leq z \leq -H \\ v &= - \frac{\alpha g}{\rho_o C_p f^2} Q_y \frac{H}{2D} & -H > z \geq -D \end{aligned} \quad (3.9)$$

The forced solution in the upper layer is a cross-stream velocity that is directly proportional to and in the direction of the horizontal gradient of upward heat flux.

An interesting application of this simple model can be made in the case of an existing surface temperature front. If a bulk aerodynamic formulation is assumed, then Q (latent and sensible heat fluxes) is directly proportional to the air-sea temperature difference. If the air temperature is constant, then Q has the same form as the sea-surface temperature. Consider now the special case of sea-surface temperature decreasing linearly with y , i.e. colder to the north, then $Q_y < 0$ is a constant. The forced solution near the surface is a southward cross-stream velocity. The physical interpretation is that a gradient in the surface cooling reduces the horizontal temperature gradient in the upper layer and consequently reduces the horizontal pressure gradient. If the front is initially in geostrophic balance, the cooling creates a supergeostrophic flow, i.e. the magnitude of the Coriolis term exceeds the pressure gradient term. The result is a cross-stream current directed

to the right of the geostrophic flow, or in the direction of the larger upward surface heat flux. It is interesting to notice that the cross-stream velocity predicted by (3.9) is independent of time if the heat flux remains constant. Using values of 9.81 m s^{-2} for g , 1000 kg m^{-3} for ρ_o , $4186 \text{ J kg}^{-1} \text{ }^\circ\text{C}^{-1}$ for C_p , $2 \times 10^{-4} \text{ }^\circ\text{C}^{-1}$ for α , 100 m for H , 1000 m for D , and 970 W m^{-2} in 20 km for Q at 36 N yields a value of 0.31 cm s^{-1} for the surface cross-stream velocity. The average of the cross-stream velocity for the upper layer is 0.16 cm s^{-1} .

It is possible to show that the linear forced response in the along-stream flow is given by

$$\begin{aligned} u(t) &= u(0) + \frac{\alpha g}{\rho_o C_p f} Q_y \left(\frac{z}{H} + 1 - \frac{H}{2D} \right) t & 0 \geq z \geq -H \\ u(t) &= u(0) - \frac{\alpha g}{\rho_o C_p f} Q_y \frac{H}{2D} t & -H > z \geq -D \end{aligned} \quad (3.10)$$

which is linearly dependent on time. As long as a north-south gradient in the upward heat flux persists, the upper layer horizontal temperature and pressure gradients and associated zonal geostrophic velocities are diminished.

The implication is that cross-stream cooling due to an atmospheric heat flux will both reduce and displace southward the north-south temperature gradient at the sea surface. While the induced cross-stream velocity is not very large (about 1/10 the value in the process treated by Nof, 1983), additional effects not considered by the linear theory above, such as the vertical exchange of momentum due to convection, may have a significant effect on the internal response of the ocean.

The numerical experiments designed to extend the above linear analysis are divided into three classes. The first class includes cases in which vertical redistribution of heat only is permitted as the upper layer cools and sinks due to interaction with the cold atmosphere. The second class includes both the exchange of heat and of momentum in the convective adjustment problem. That is, the convective overturning in the column is assumed to mix momentum as well as heat uniformly in the vertical. The third class includes cases which consider the additional effect of an

increase in the southward and eastward wind stress. Both heat and momentum are allowed to be mixed by the convective overturning when wind stress forcing is included.

In each of the simulations in this section, the response fields will be shown as a deviation from a control simulation which uses zero forcing. Because of the large gradients in temperature and zonal velocity, part of the response in any simulation will be due to diffusive effects only. Since those effects are not the primary interest, the diffusive response in a zero-forcing simulation is removed to isolate the response due to surface forcing. In addition, the flow fields are averaged over 21 hours to filter the inertial response. Hence a flow field at hour 72 is actually the average of the flow for hours 51-72.

A. EFFECT OF VERTICAL MIXING OF HEAT ONLY (EXPERIMENT 3-1)

A southward (negative) surface v component is evident after 72 hours of integration as shown in Fig. 3-1. The response in the v field is mainly confined to the upper 100 m in the region of the surface front. The maximum magnitude is slightly greater than 0.3 cm s^{-1} , which is in good agreement with the above linear theory. The instantaneous values of the v components at hour 72 (not shown) are remarkably similar to the averaged v components shown in Fig. 3-1, which indicates almost no time dependence in the forced flow.

To illustrate the physical processes that determine the response of the front to the imposed cooling, the contribution of the individual terms to the time tendencies in (2.1), (2.2) and (2.3) were calculated. An inspection of the terms comprising the average v tendency for hours 51-72 reveals that the difference between the pressure gradient and Coriolis terms is an order of magnitude larger than any of the other terms in (2.2). Thus, the tendency for the cross-stream flow is being accurately described by (3.2). As in the analytic work above, the surface cooling is reducing the north-south pressure gradient so that the Coriolis term is slightly larger than the pressure gradient term. The imbalance produces a southward flow opposite to the mean pressure gradient near the surface front. The along-front flow is constantly adjusted so that by hour 72,

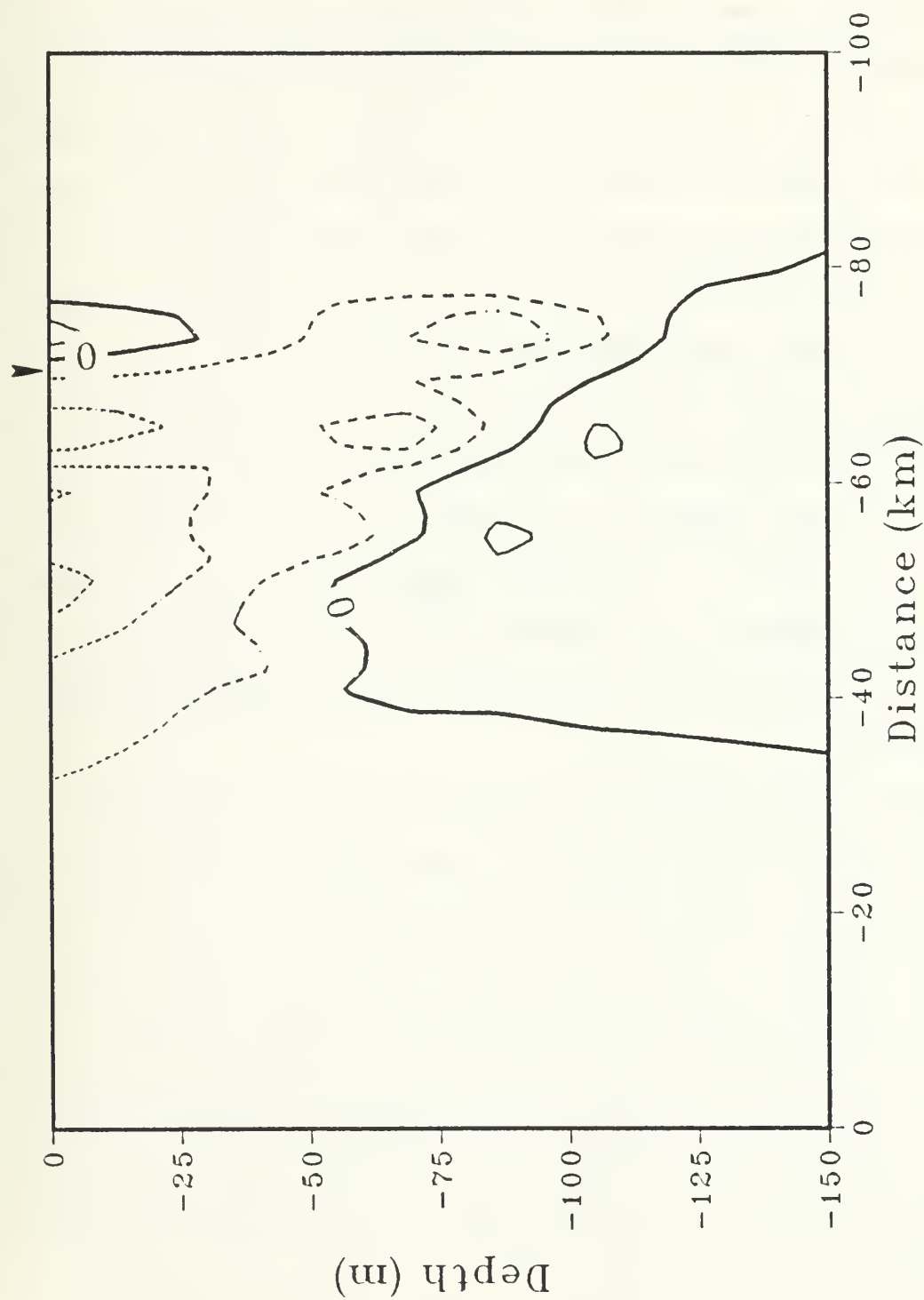


Figure 3-1. Average of the v component of velocity for hours 51-72 for Experiment 3-1. The contour interval is 0.1 cm s^{-1} and negative contours are dashed. The flow is positive northward (to the left). The arrow indicates the position of the warm edge of the surface front.

the magnitude of the u component of velocity has been reduced by over 0.08 m s^{-1} , as shown in Fig. 3-2. The change in u is also confined to the upper 100 m in the region near the surface front.

Although the sense of the horizontal cooling gradient is to destroy the ocean front, the dynamic response of the near-surface flow is thermally indirect (warm water sinking and cold water rising) and this tends to steepen the front and maintain it at its initial position. Notice that the largest southward flow occurs on the warm edge of the front where the cooling is greatest. Hence, the flow is divergent on the cool side of the front and upwelling occurs. There is also a small region of positive v near the surface at $y = -80 \text{ km}$, which indicates convergence and downwelling on the warm side of the front. An indication of the effect of the indirect circulation is shown in Fig. 3-3 which illustrates the temperature tendency due to the combined effect of horizontal and vertical advection. Advective processes increase the temperature on the warm side of the front and lower the temperature on the cold side of the front. The zero tendency line is located at the warm edge of the front, and the strongest tendencies occur at the surface on either side of the warm edge of the front. The horizontal advective term is the contribution from the effect of confluence (diffluence) in the strengthening (weakening) of the horizontal temperature gradient. The vertical advective term represents the effect of a differential tilting of the isotherms from the horizontal.

By taking a horizontal derivative of the temperature tendency field, one obtains the frontogenetic tendency. The contribution from the advective terms is closely related to the geostrophic frontogenetic tendencies discussed by both Sawyer (1956) and Eliassen (1962). If frontogenesis is defined as areas where $d/dt (-\partial T / \partial y) > 0$, then the advective tendency for frontogenesis is positive at the warm edge of the surface front and negative on either side of the warm edge. The nonlinear terms are acting to strengthen the surface front at the warm edge of the front. Sawyer and Eliassen also considered the effect of a cross-front shear on the horizontal temperature gradient. Since no variation in the x -direction is included here, the effect of cross-front shear is zero.

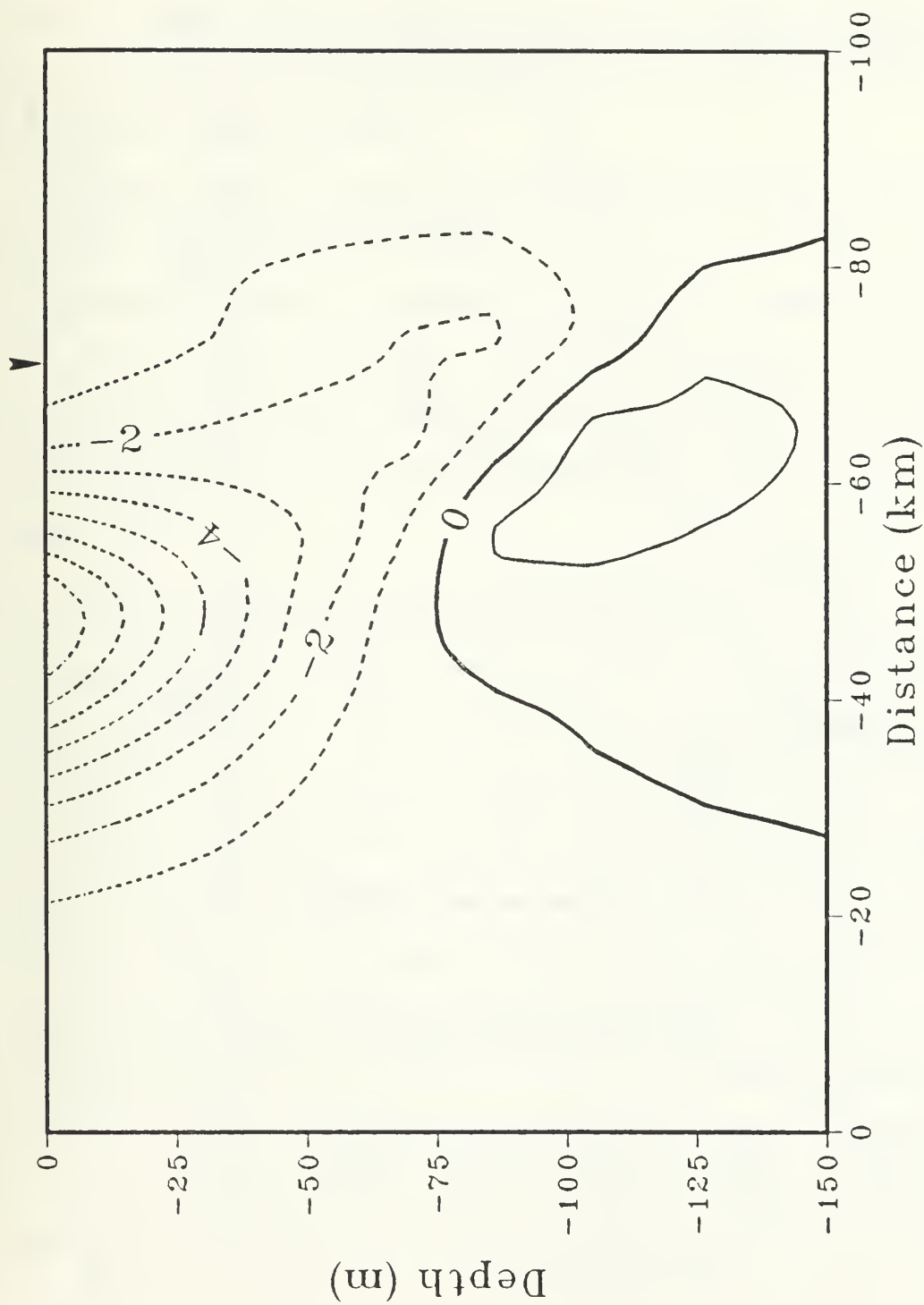


Figure 3-2. Average of the change in the u component of velocity for hours 51-72 for Experiment 3-1. The contour interval is 1 cm s⁻¹ and negative contours are dashed.

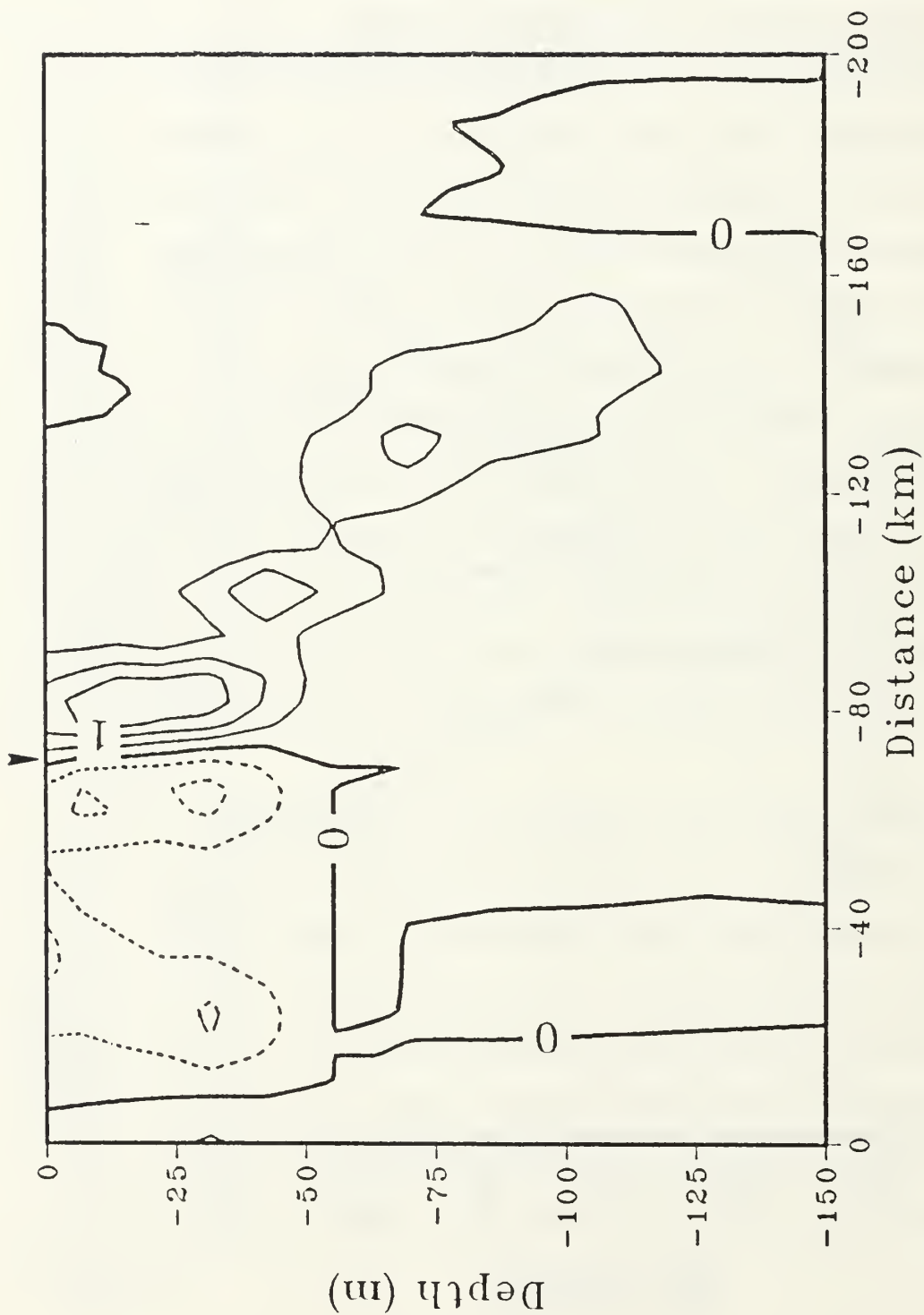


Figure 3-3. Combined effect of horizontal and vertical advection on the temperature tendency at hour 72 for Experiment 3-1. The values are multiplied by 10^5 . The contour interval is $0.5 \times 10^{-5} \text{ } ^\circ\text{C}^{-1}$ and negative contours are dashed.

The temperature change after 72 hours (Fig. 3-4) reflects an advective effect. A maximum temperature change of -0.82°C occurs south of the warm edge of the surface front. The temperature response closer to the warm edge of the surface front, but where the cooling is just as strong, is not as great (-0.69°C) due to the tendency of the horizontal convergence of heat to oppose the effect of surface cooling. For this simulation, the vertical extent of the cooling is constrained by the initial well-mixed layer.

In summary, a horizontal cooling gradient produces a very small cross-stream velocity which is not likely to affect the position of a baroclinic zone as strong as the Gulf Stream. Although the cooling produces a southward component in the flow, any tendency to displace the surface front is offset by the vertical velocity tending to steepen the front and maintain the front at its initial position. The temperature response includes changes that are not uniform over areas where the surface heat flux is uniform. The largest temperature response occurs at the warm edge of the surface front.

B. EFFECT OF MOMENTUM MIXING (EXPERIMENT 3-2)

The convective adjustment used above exchanges heat between adjacent levels to produce a temperature profile that is at least neutrally buoyant. Unlike temperature, exchanges of momentum usually occur on the same time scales of the mean flow or in this case, $1/f$. However, if surface cooling is forcing convective overturning, very little can be said about the time scale of the turbulent exchange of momentum. If the convection is sufficiently strong, then all properties of the water are likely to be mixed between adjacent layers. In laboratory experiments of flows with large Reynolds number, Thorpe (1973) found that both the heat and momentum profiles attained similar shapes when the Richardson number dropped below a critical value for short (order of seconds) time scales, which indicates that heat and momentum were being exchanged similarly. Although the exchange of momentum between layers has not been investigated in great detail, there have been numerical simulations which have shown the exchange of momentum in

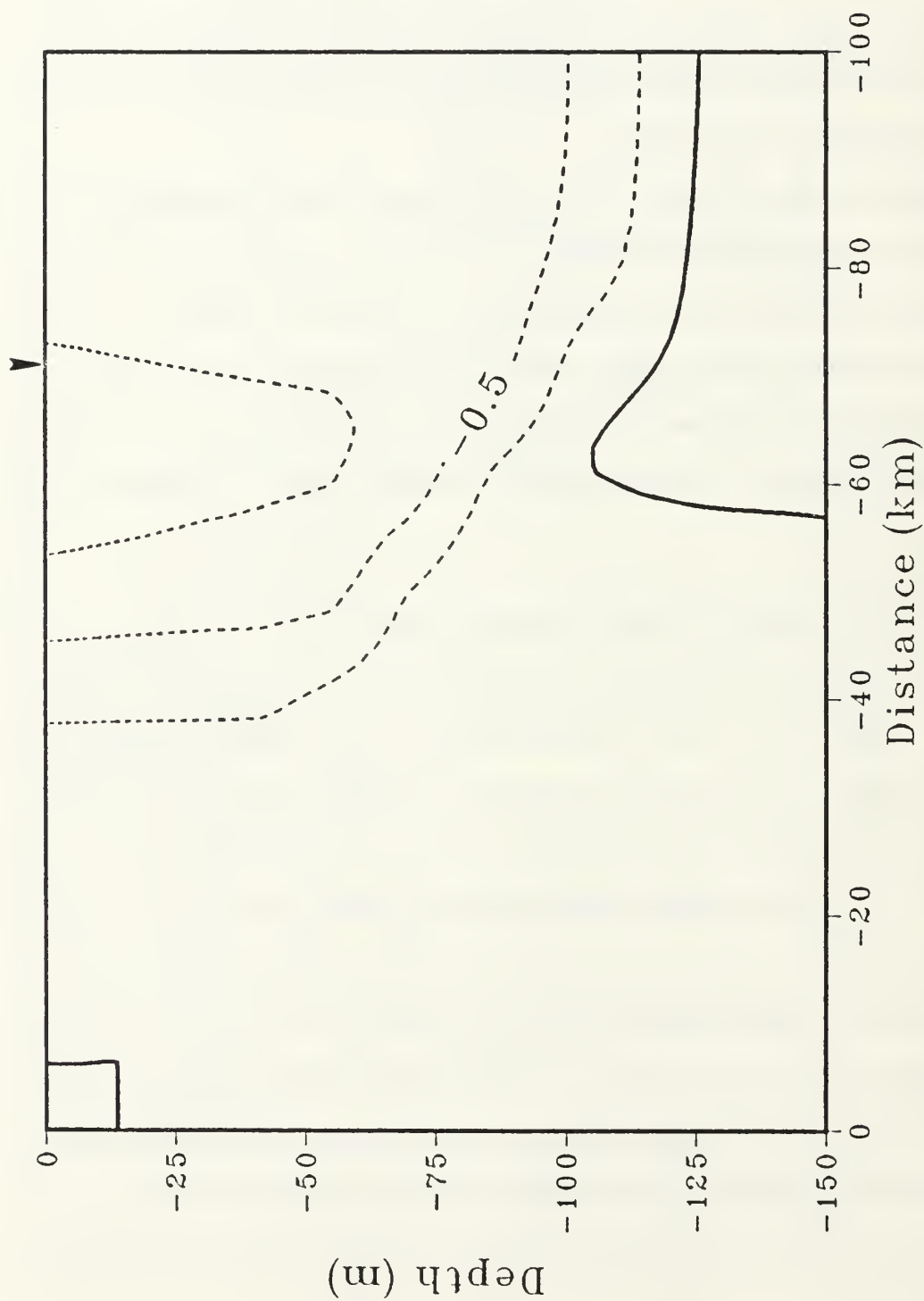


Figure 3-4. Change in temperature at hour 72 for Experiment 3-1. The contour interval is 0.25 °C and negative contours are dashed.

an adjustment problem to be an important influence (Adamec *et al.*, 1981; Schopf and Cane, 1983).

The response in the frontal simulation with identical forcing to Experiment 3-1, but with momentum mixing included, is very different from the previous simulation. The v components after 72 hours for this simulation are shown in Fig. 3-5. The most important differences from Experiment 3-1 are the reversal of sign near the surface and that the values are an order of magnitude larger. Below the surface, the flow is to the south. Here, as in Experiment 3-1, the horizontal pressure gradient and Coriolis acceleration are the largest terms in the v momentum equation by at least one order of magnitude. However, the absolute value of the pressure gradient force is larger than the absolute value of the Coriolis acceleration near the surface front.

The difference in the response of the v components can simply be explained in terms of the momentum mixing. When surface cooling occurs, the gradient Richardson number is less than the critical value. The relatively high momentum near the surface is mixed with relatively low momentum immediately below, so that the surface currents decrease relative to their initial values. Immediately below the surface layer, the currents increase. As the Coriolis term decreases at the surface, and the pressure gradient term is not decreased by a similar amount, the flow becomes sub-geostrophic and a flow down the mean pressure gradient occurs (positive v components, Fig. 3-5). Below the surface layer where u has increased due to the turbulent exchange with relatively higher momentum from above, the Coriolis term is larger than the pressure gradient, and the response in v is up the mean pressure gradient (negative).

The changes in the u component after 72 hours (Fig. 3-6) are consistent with these arguments. Notice that the speed change in the surface layer is negative (reduction of the jet) and twice as large as the changes in Experiment 3-1 due to the additional effect of mixing with relatively lower momentum from below. Immediately below the surface layer, the current speed has increased relative to the initial value. At 60 m depth, there is an area with reduced speeds. This is a layer in

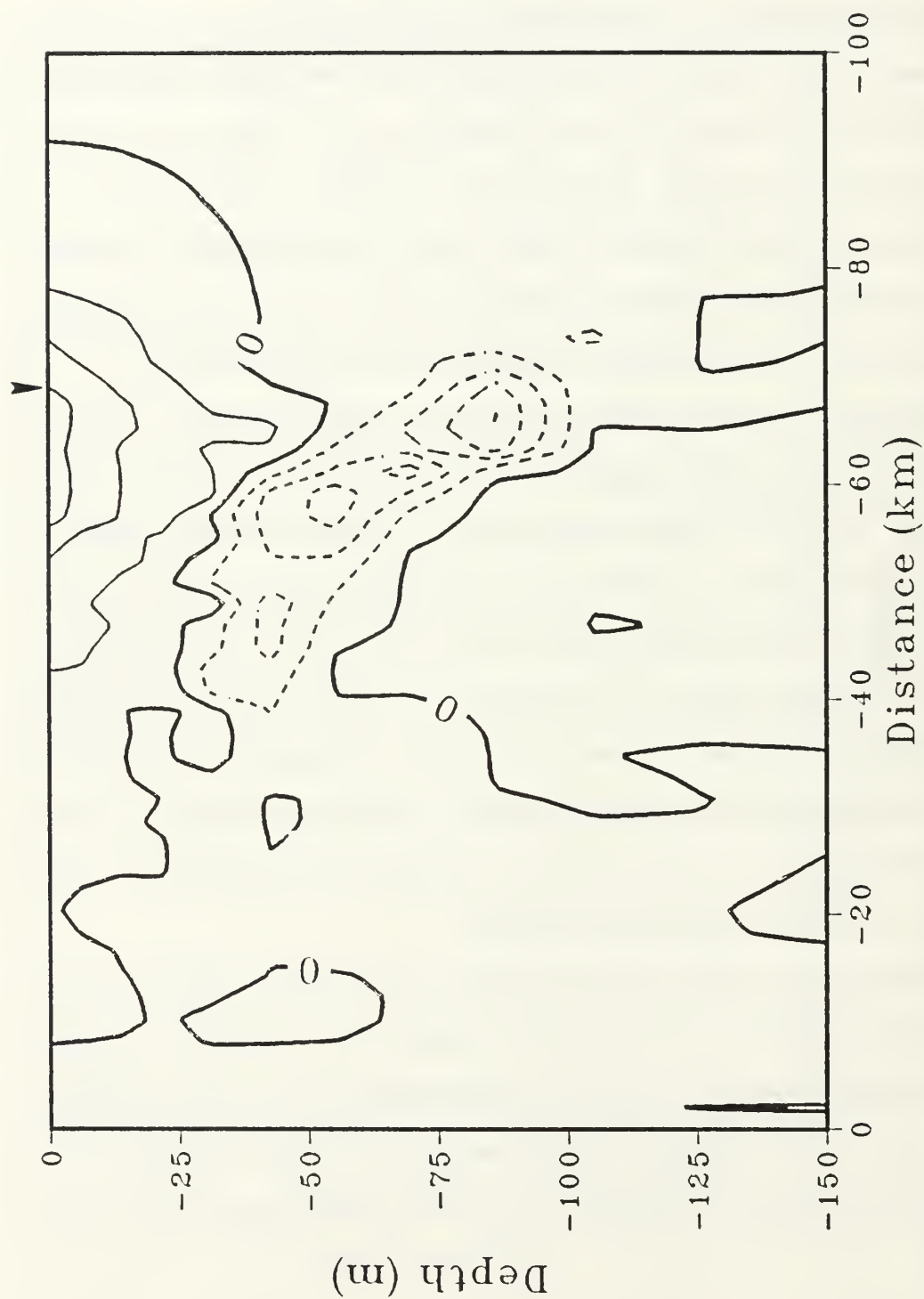


Figure 3-5. As in Fig. 3-1 except for Experiment 3-2 and the contour interval is 1 cm s^{-1} .

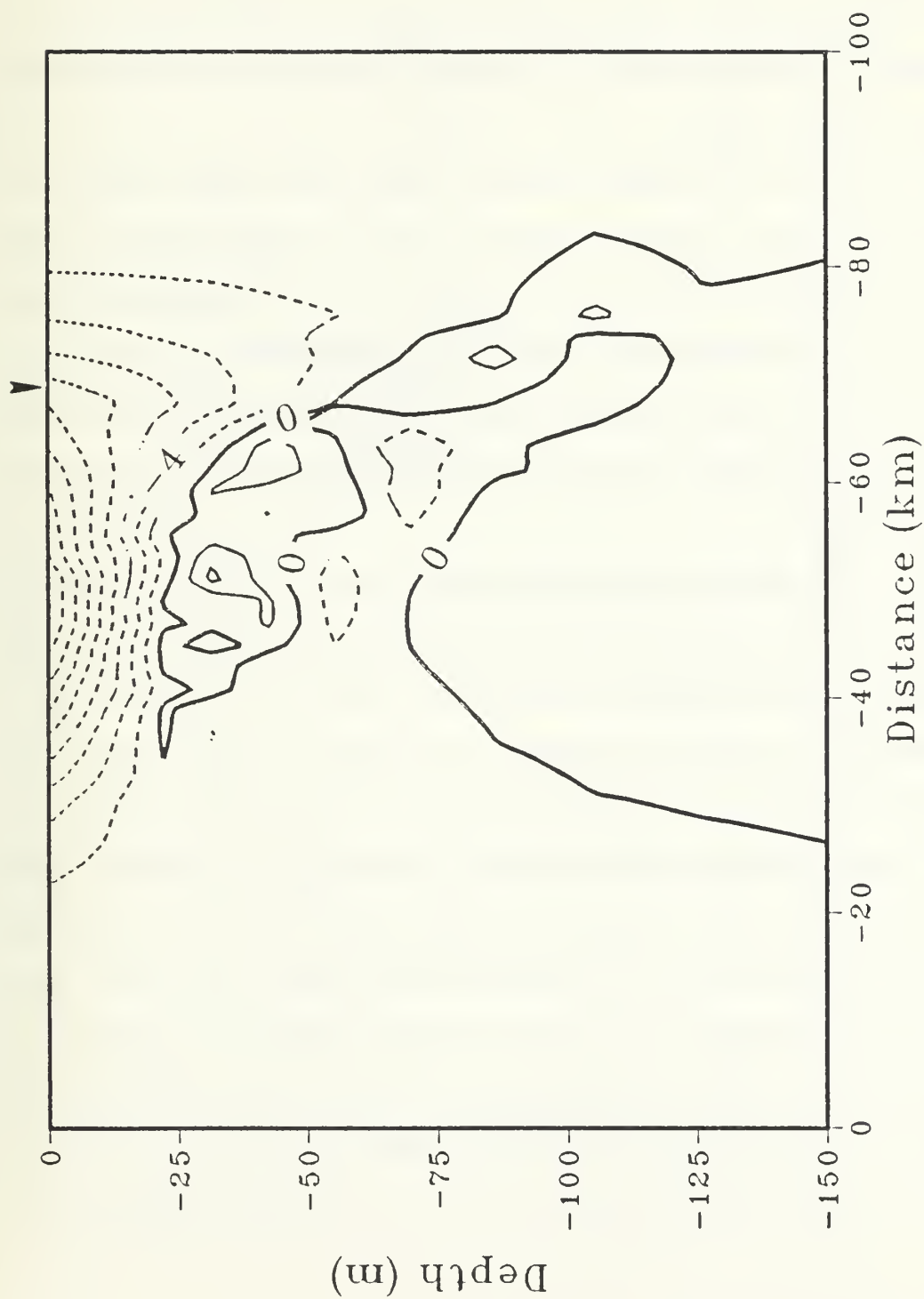


Figure 3-6. As in Fig. 3-2 except for Experiment 3-2 and the contour interval is 2 cm s^{-1} .

which the initial vertical shear in u is a maximum. Above this area, the shear is smaller and constant with depth. Locations where the vertical shear is large are locations where momentum mixing will also be very large. Plots of the instantaneous currents reveal a high variability in the currents at depth. The variability appears to be inertial. There is little evidence for propagation of the inertial energy vertically or horizontally. The oscillation remains confined to the upper 100 m toward the warm edge of the front.

The reversal in sign of the surface v components induces vertical velocities which tend to reduce the slope of the front. The vertical components of velocity at hour 72 are shown in Fig. 3-7. Notice the upwelling on the warm side of the front where downwelling occurred in the previous case. On the cool side of the front, downwelling is taking place. The sense of the vertical advection is direct (warm water rising and cold water sinking). The divergence on the warm side of the front and the convergence on the cold side of the front tend to diminish the temperature gradient across the front.

In the atmosphere, there have been several investigations that show that upper level fronts in the vicinity of jets are preferred regions for vertical mixing (e.g. Kennedy and Shapiro, 1980). Although large vertical eddy diffusivities are apparent in the upper atmosphere, care must be taken in applying those results to ocean surface fronts since upper-atmospheric fronts are far removed from the effects of a planetary boundary layer. In a numerical simulation of upper-atmospheric frontogenesis, Shapiro (1982) notes that if a maximum in the heat flux occurs in the vicinity of a front, the forced circulation is thermally indirect. However, if the turbulent momentum fluxes dominate the heat fluxes, the forced circulation will be thermally direct, which is consistent with the simulations in this study. Other studies have indicated a dominance of turbulent momentum exchanges over turbulent heat exchange. Gidel and Shapiro (1979) investigated the role of turbulent heat and momentum fluxes in the production of potential vorticity near an upper tropospheric front for a range of Prandtl numbers (K_M/K_T). For a

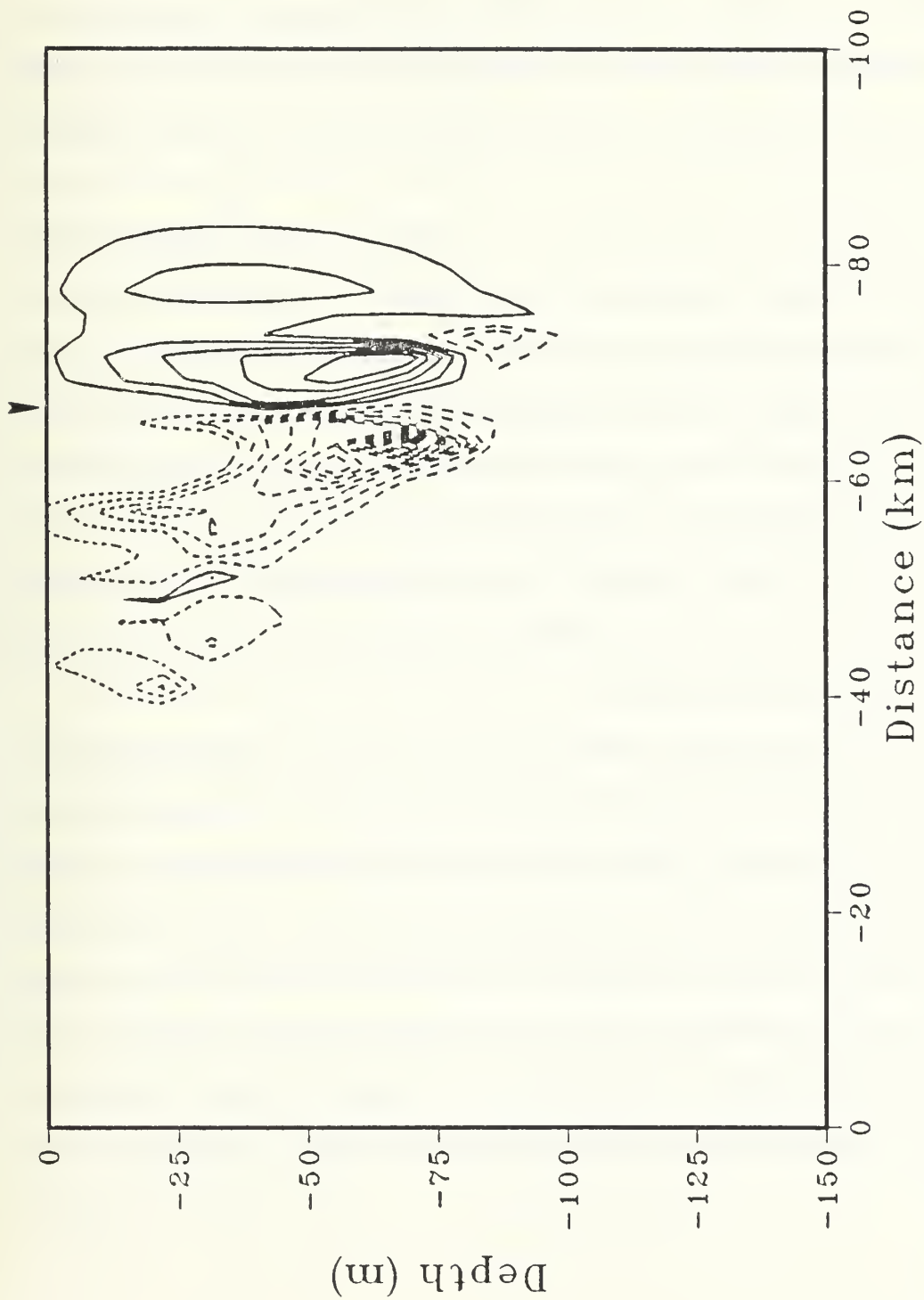


Figure 3-7. Average of the vertical velocity for hours 51-72 for Experiment 3-2. The contour interval is 0.002 cm s^{-1} and negative (downward) contours are dashed. The values have been multiplied by 100.

Prandtl number of 1, the change in vorticity due to the turbulent momentum flux dominated the change in vorticity due to the turbulent heat flux.

Each of the above simulations was repeated with different cooling rates. The sense of the ocean response is not dependent upon the magnitude of the cooling, however the magnitude of the response is nearly linearly dependent on the magnitude of the cooling. When the cooling rate is reduced by 50%, the changes in the temperature and current fields are similarly reduced by about 50%.

The simulations which included momentum mixing were repeated using a critical Richardson number of 0.25 to include possible dynamic instability effects. The response of the cross-stream and the along-stream velocity components are in the same direction as in the case with critical Richardson number equal to zero, but the magnitude of the currents is increased by about 30%. The increase in the response is due to relatively high momentum at the surface being mixed with relatively low momentum from below as the condition for instability (mixing) is satisfied more frequently. However, the large stratification in the thermocline restricts the effects due to momentum mixing to the upper layers. Although, the response in the currents is enhanced, the responses still occur in the same locations.

The role of momentum mixing in the ocean is not well documented. Numerical simulations by Adamec *et al.* (1981) show that including mixing of momentum alters significantly the oceanic response due to hurricane forcing. Schopf and Cane (1983) found that entrainment of momentum is a non-negligible process in maintaining equatorial undercurrents. The role of momentum mixing is particularly interesting in the simulations of the response of the Gulf Stream to surface cooling since the mixing of momentum produces a very different response in the along-front flow than in the simulations without it. Measurements of the change in the Gulf Stream velocity profile during a cold outbreak are required to document the importance of this process in the ocean.

C. EFFECT OF WIND FORCING (EXPERIMENTS 3-3 AND 3-4)

Two components of the total heat flux, sensible and latent heating, are directly proportional to wind speed in the bulk aerodynamic formulations. Large losses of heat by the ocean are normally accompanied by an increase in the wind speed. In the previous simulations that included the effects of cooling only, the treatment of the vertical structure of momentum was a critical factor in determining the magnitude and direction of the internal ocean response. In this section, a surface momentum flux is also included to determine if it is an important factor in determining the response of the ocean to a cold air outbreak.

Two wind forcings are considered: a cross-stream southward wind stress simulating an outbreak of cold air from polar regions, and such as the cold outbreak during AMTEX 74 (Agee and Howley, 1976), and a wind stress in the direction of the along-stream flow to simulate a cold air outbreak from the cold continental area to the west. For each of these simulations, the maximum wind stress is 0.2 N-m and is applied impulsively. This wind stress represents the low end of values observed by Agee and Howley (1976). The effects of the combined cooling and wind forcing are compared to the effects due to cooling only.

The change in u velocity for the simulation with cooling and a southward wind stress is shown in Fig. 3-8. The difference from the cooling-only simulation is a further decrease in the speed of the surface jet by 0.1 m s^{-1} . The reduction of the eastward component is consistent with an Ekman-type response to the southward wind stress. The reduction of the jet is evident throughout the surface layers as the convective overturning efficiently mixes momentum. There are areas below the warm edge of the surface front where the jet speeds have increased. Notice that the reduction in the jet in the cooling-only simulation is larger than the additional reduction due to the wind forcing alone (0.16 m s^{-1} as opposed to the additional 0.1 m s^{-1}). However, significant reductions in the initial jet penetrate to depths twice as large when the effect of wind forcing is included when compared to the cooling-only simulation.

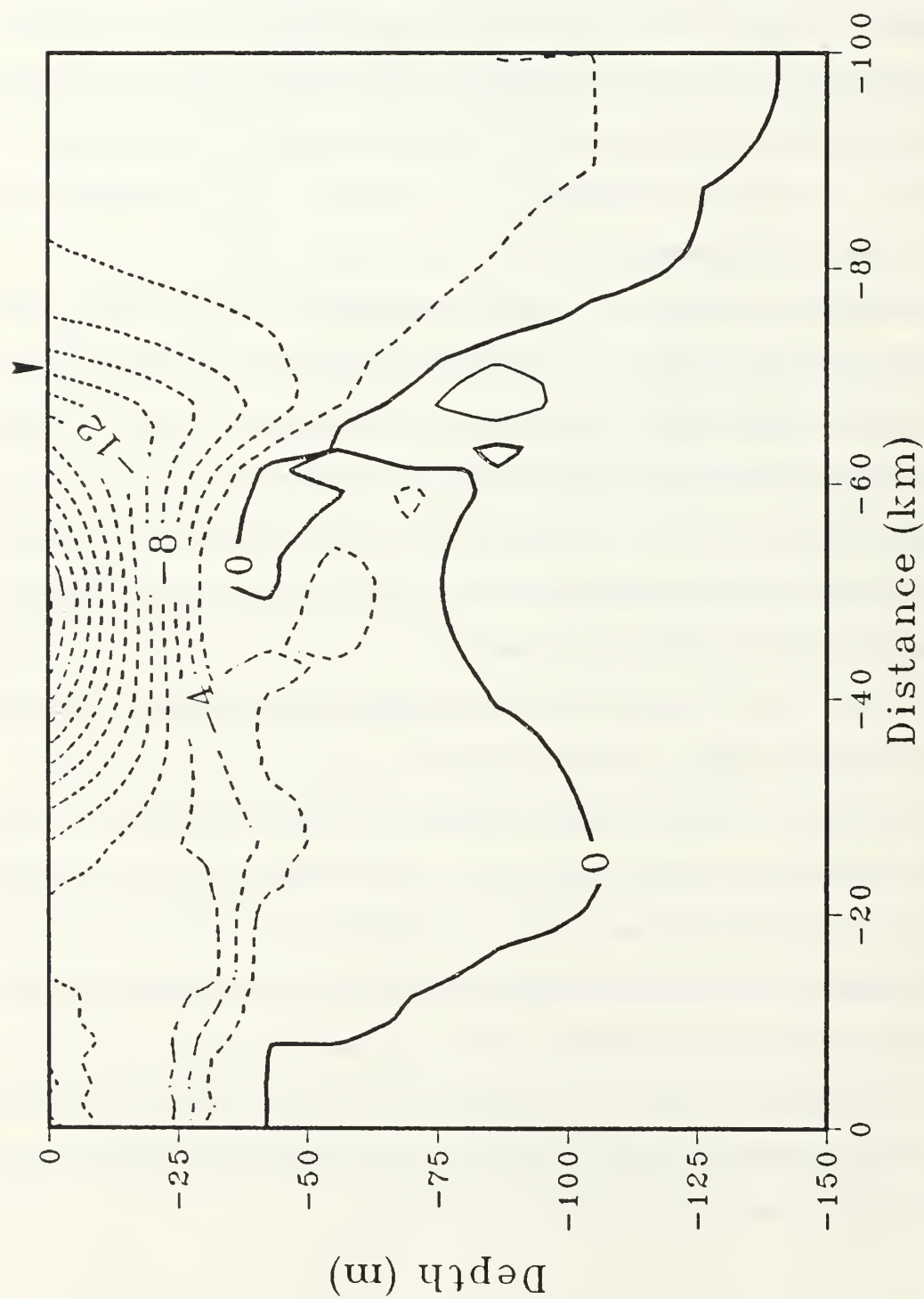


Figure 3-8. As in Fig. 3-2 except for Experiment 3-3 and the contour interval is 2 cm s^{-1} .

The effect of the southward wind stress on the v velocity is shown in Fig. 3-9. The large positive v components near the surface in the cooling-only simulation are greatly reduced. The tendency to produce a current toward the north due to momentum mixing (Fig. 3-5) is opposed by the effect of the wind stress. Farther to the north and south of the front, the v components are negative, which is in the direction of the applied wind stress. The response immediately below the surface front is also somewhat diminished due to the opposing tendencies of momentum mixing to produce a sub-surface current toward the south and the wind stress which forces a sub-surface current toward the north.

On the warm edge of the front the flow is divergent, and toward the cooler side, the flow is convergent. The response in this simulation, as in the cooling-only simulation, is a thermally direct circulation at the warm edge of the front. The strength and shape of the vertical circulation pattern (Fig. 3-10) is similar to the cooling-only simulation.

The response in the temperature field (not shown) is very similar to the cooling-only simulation. There is a slight southward shift in the temperature response due to the advection induced by the southward wind stress. The temperature response, as in the previous simulations, is dominated by the surface heat flux and not by the internal response of the ocean.

The response to the inclusion of an eastward wind stress is very dramatic. The sense of the Ekman advection for this simulation is southward. The changes in the near-surface v velocity at hour 72 (Fig. 3-11) are negative (southward) everywhere except for a small area at the surface. The maximum change occurs in the vicinity of the front where the v components are 0.04 m s^{-1} . In the cooling-only simulation, the maximum v components are in the same area and of the same magnitude, but in the opposite direction. Because the magnitude of the Ekman response is inversely proportional to mixed-layer depth, the surface v velocities are divergent at the front. In a similar simulation of the response of the Maltese ocean front to wind forcing, Adamec and Garwood (1985) found that the forced divergence was very effective in spreading the surface isotherms and reducing the intensity of the flow near the front.

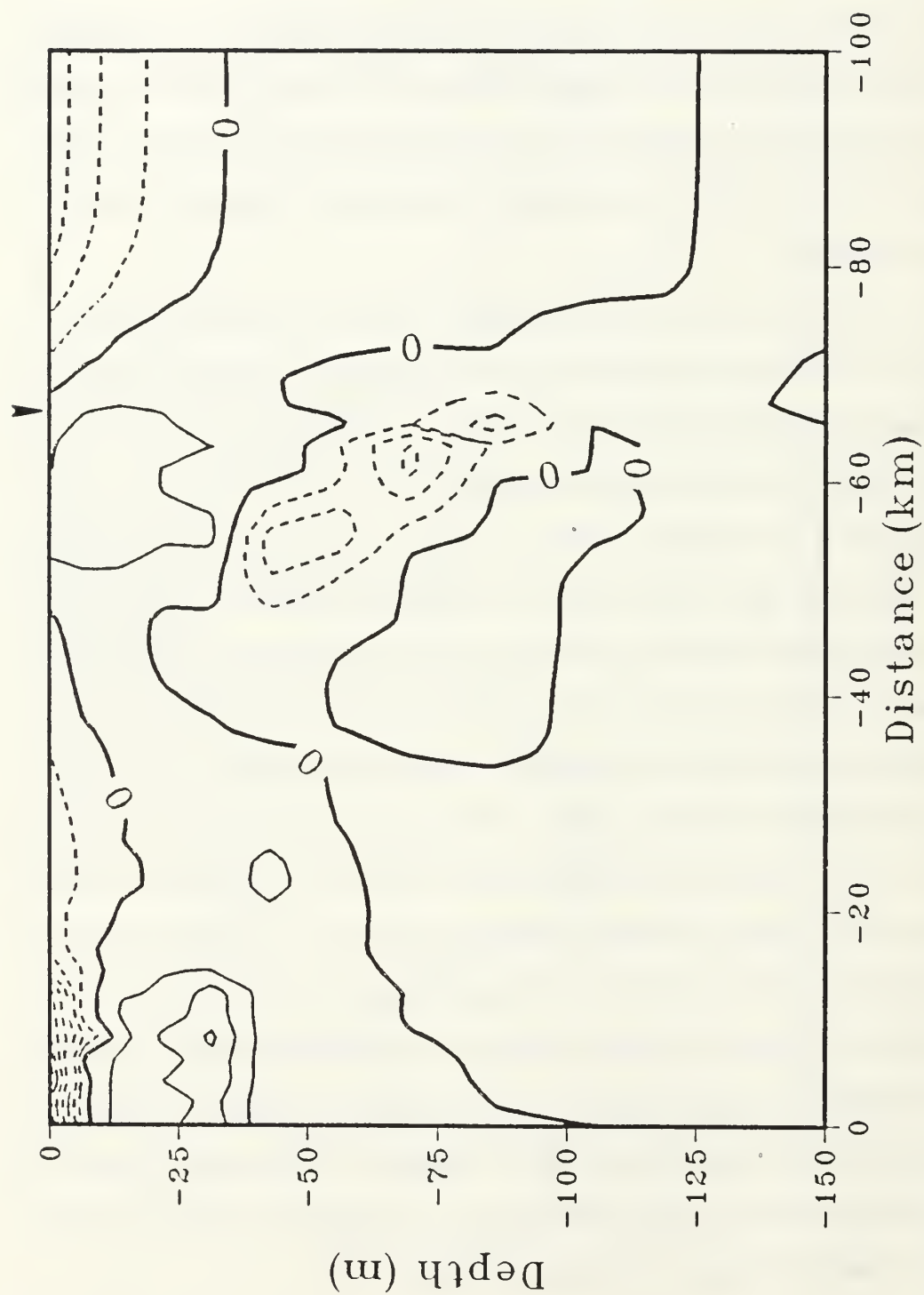


Figure 3-9. As in Fig. 3-1 except for Experiment 3-3 and the contour interval is 1 cm s^{-1} .

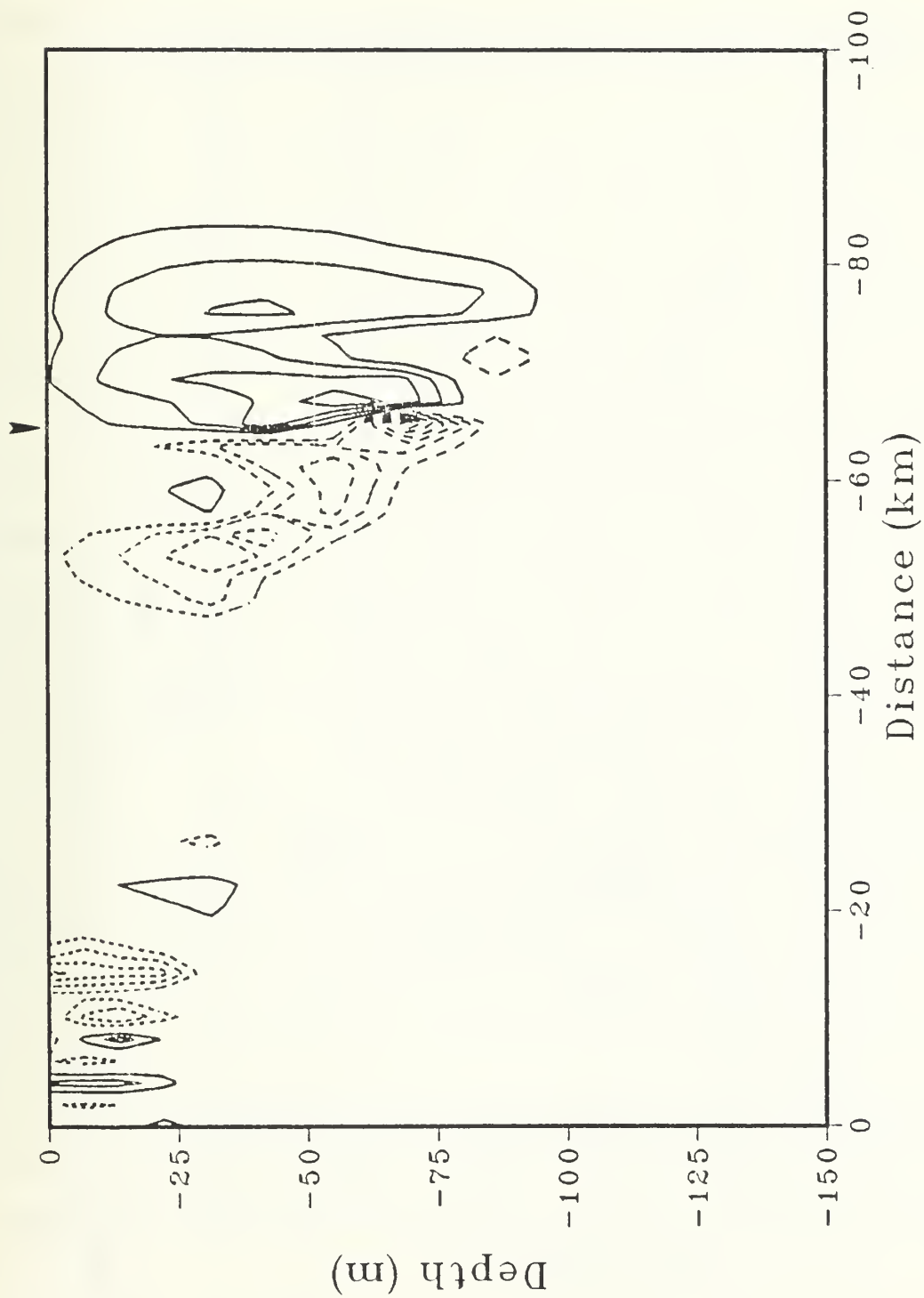


Figure 3-10. As in Fig. 3-7 except for Experiment 3-3.

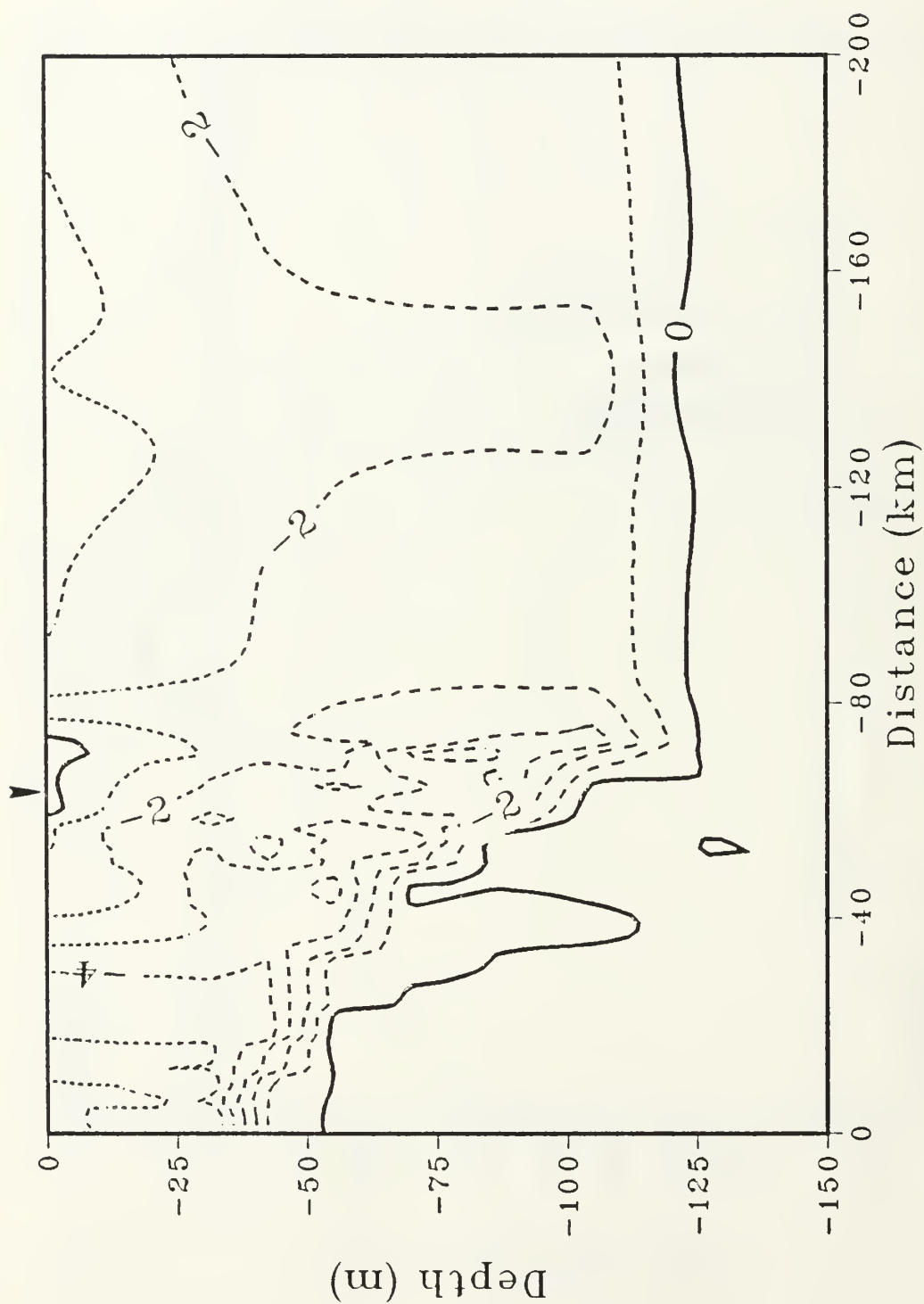


Figure 3-11. As in Fig. 3-1 except for Experiment 3-4, the contour interval is 1 cm s^{-1} , and for values of y between -200 and 0 km.

The u components for the simulation that included an eastward wind stress are shown in Fig. 3-12. Near the initial position of the front, the u components are decreased by over 0.38 m s^{-1} whereas the u components are increased by 0.12 m s^{-1} farther to the south. This southward shift of the jet is due to the geostrophic adjustment of the flow to a southward shift in the horizontal temperature gradient. Colder water from the north is advected southward and sinks as it encounters the warmer water in the south. The tendency for advection is to diminish the northern edge of the horizontal temperature gradient and form a relatively stronger temperature gradient to the south. As a result, the u components decrease on the northern side of the initial jet and increase to the south. In the region near -140 km , a southward advection causes positive (negative) changes in u where the initial $\partial u / \partial y$ is negative (positive).

The maximum surface temperature change (Fig. 3-13) at the front is more than 1.0°C lower than the temperature changes in the cooling-only simulation due to the southward advection of cold water. At $y = -30 \text{ km}$ and $y = -140 \text{ km}$, there are areas of temperature increases below the initial isothermal layer. This warming is due to the effect of downwelling occurring in those areas. The enhanced cooling at $y = -120 \text{ km}$ is similarly due to a local area of upwelling. As in all cases that included momentum mixing, the vertical circulation near the front (not shown) is thermally direct.

In summary, a moderate increase in the eastward wind stress has a greater effect on the position of the current system than does a strong cross-stream cooling gradient. Only the simulation which considers the response to an eastward wind stress has a noticeable shift in the position of the current system after three days of forcing. Nof (1983) considered a different mechanism to produce cross-stream currents. Nof assumed that an adjustment by the ocean to an along-stream cooling gradient produces a cross-stream current of sufficient magnitude to displace the Gulf Stream by as much as 90 km in a season. Nof's mechanism must be modelled in three dimensions. Since the direction and magnitude of the cross-stream current in the two-dimensional

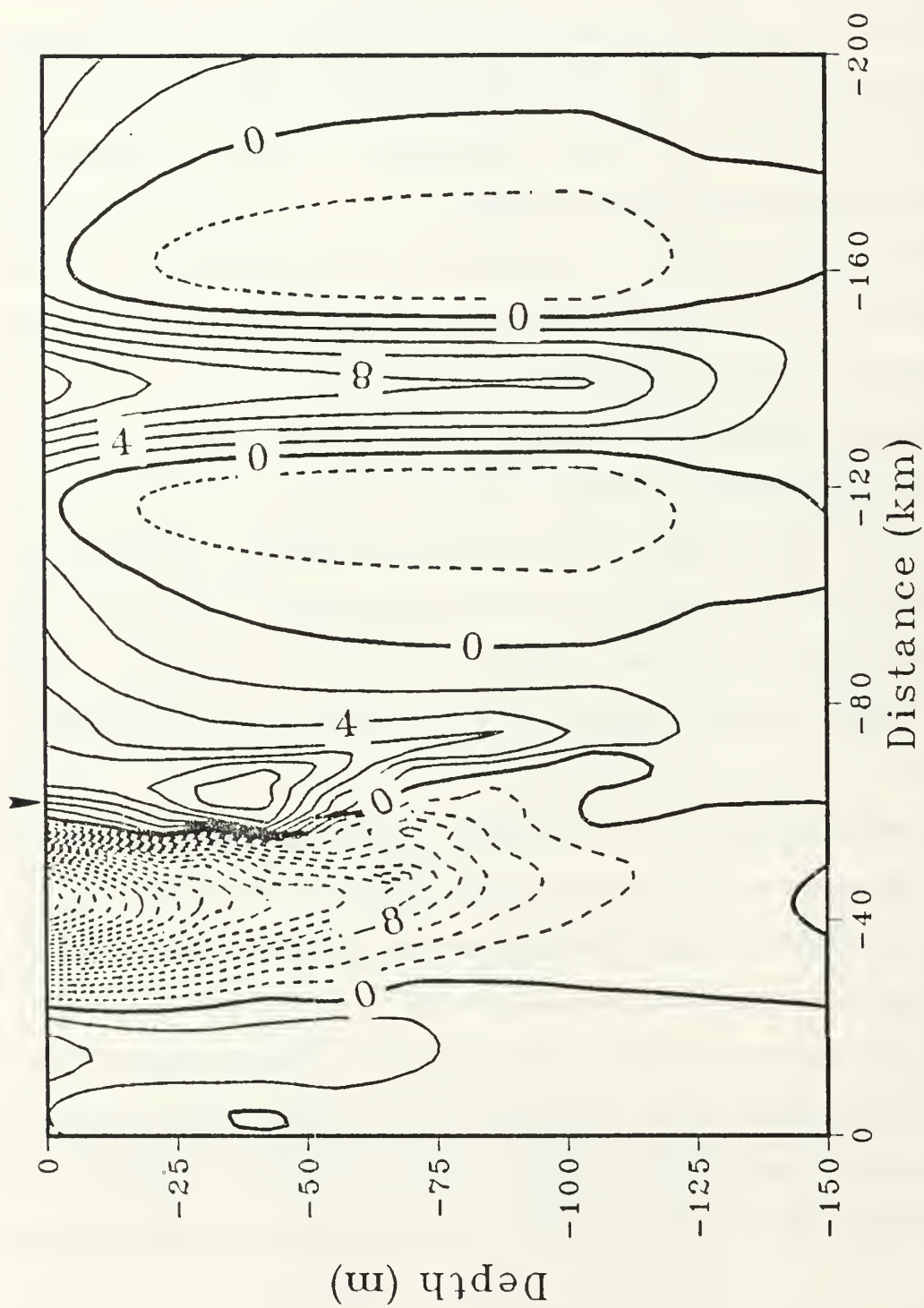


Figure 3-12. As in Fig. 3-2 except for Experiment 3-4 and for values of y between -200 and 0 km.

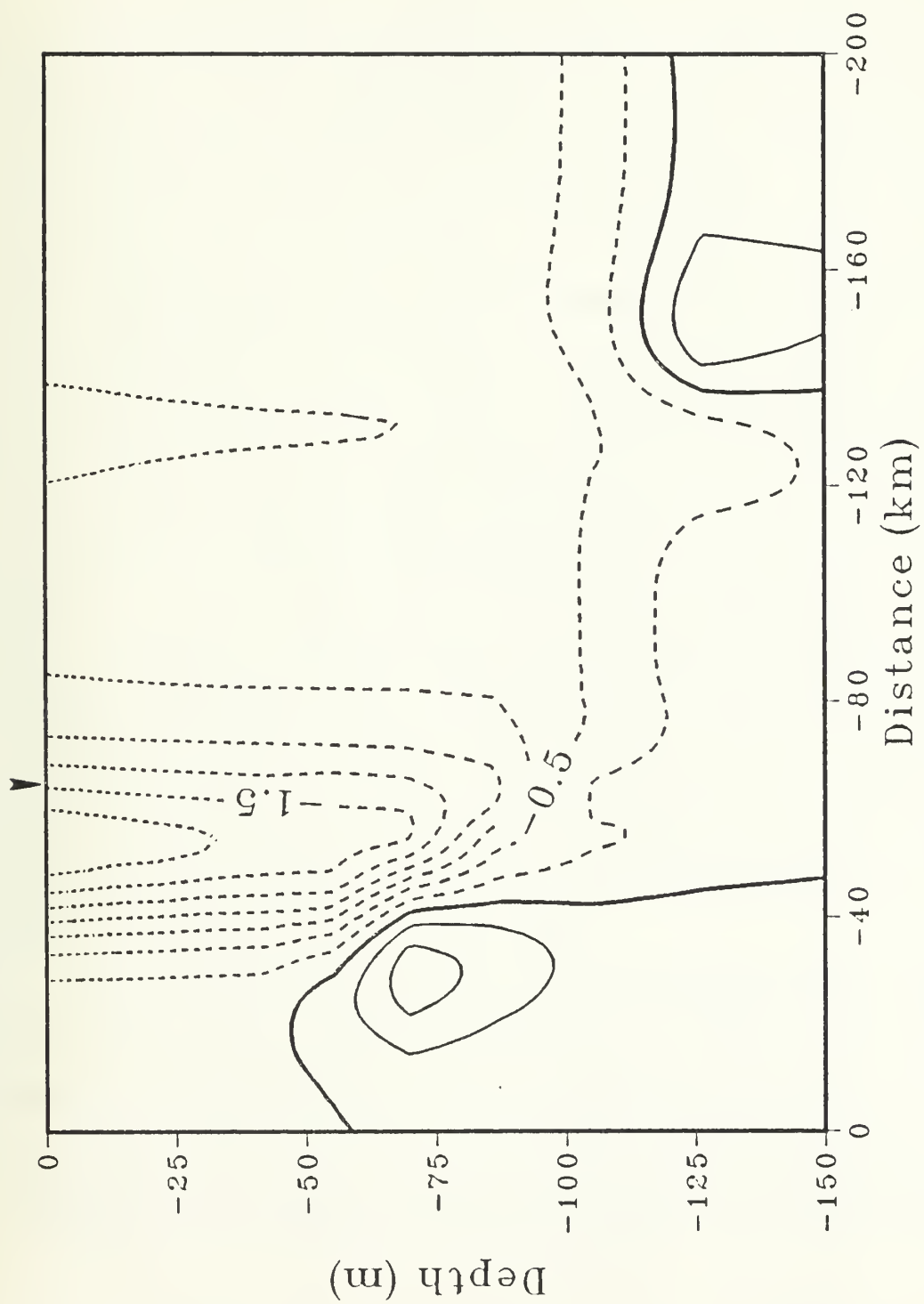


Figure 3-13. As in Fig. 3-4 except for Experiment 3-4 and for values of y between -200 and 0 km.

simulations are dependent on whether or not momentum mixing is included as part of the convective adjustment to surface cooling, it is expected that momentum mixing will also play an important role in three-dimensional simulations.

IV. THREE-DIMENSIONAL SIMULATIONS

Three sets of experiments are designed to investigate the three-dimensional response of a strong ocean current to local atmospheric forcing. The purpose of the first two sets of experiments is to compare the relative importance along-stream cooling gradients to the cross-stream cooling gradients treated in Section III in the two-dimensional simulations. The design of these experiments is similar to the design of the experiments in Section III. In the first experiment, only the vertical mixing of heat in the convective adjustment problem is considered. The second experiment is similar to the first but also includes the effect of vertical mixing of momentum as part of convective adjustment process. The third set of experiments considers the response of the ocean currents to an increase in the zonal wind stress. Part of the response in the horizontal velocity components when momentum mixing is included is due to inertial motion. Although inertial motion is not of primary interest to this investigation, an interesting effect occurs which is due to advection. The strong zonal advection alters the period of the oscillations in these simulations so that the period is near 15 hours rather than the expected 21-hour inertial period. An analysis of how advection affects the period of oscillation in these simulations is presented in Appendix A. For all the results presented, the flow fields have been low-passed filtered to remove the inertial response, and the fields are presented as a deviation from a control run with no surface forcing. The initial front is centered along $y = 192$ km.

The numerical simulations presented here treat three processes which were not considered in Nof's (1983) original work. Aside from the effects of an along-stream cooling gradient, the numerical simulations also consider: 1) the forced meridional response due to a cross-stream cooling gradient as outlined in Section III; 2) the effects of momentum mixing during convective adjustment; and 3) the time-dependent response of the zonal flow. These three effects are critical

in the simulations since they determine much of the response in the immediate vicinity of the surface front.

A. EFFECT OF VERTICAL MIXING OF HEAT ONLY (EXPERIMENT 4-1)

The surface v components at hour 72 for the simulation with no momentum mixing during convective adjustment are shown in Fig. 4-1. Within the region where there is a uniform along-stream cooling gradient (see Fig. 2-2), the v components are negative (southward) with maximum current speeds near 0.6 cm s^{-1} . The cross-stream components south of the front are in thermal wind balance as in Nof (1983). The magnitude of the v components in this simulation are five times smaller than Nof's predictions. Nof used an observed density increase (Gorshkov, 1978) of $1 \times 10^{-3} \text{ gm cm}^{-3}$ along the Gulf Stream extension. A surface cooling rate of 2000 W m^{-2} would have to persist for a period of 10 days to obtain such a density increase in the mixed layer. From the observations by Agee and Howley (1976) (Fig. 2-4) and Kondo (1977) (Fig. 2-6), such large cooling rates appear to be unrealistic, which implies the density increase used by Nof is not due to surface cooling alone.

There is also a relative maximum in the southward velocity immediately to the south of the initial zonal current maximum. The process for the inducement of cross-stream velocities near a jet in the presence of cross-stream cooling is described in Section III. The magnitude of the maximum cross-stream flow in Fig. 4-1 is only slightly larger than that from the two-dimensional (y - z) simulations. The slight increase is due to the adjustment of the flow to a weak zonal temperature gradient induced by the zonal cooling gradient. Most of the cross-stream velocity in the immediate vicinity of the current maximum appears to be due to the two-dimensional effect of cross-stream cooling and not the imposed along-stream cooling gradient. At the current maximum, the cross-stream flow is about half the magnitude of the cross-stream flow further to the south. Thus, displacements of the surface current system would be less than might be inferred from the southward velocities that develop where the zonal gradient in surface cooling is a maximum.

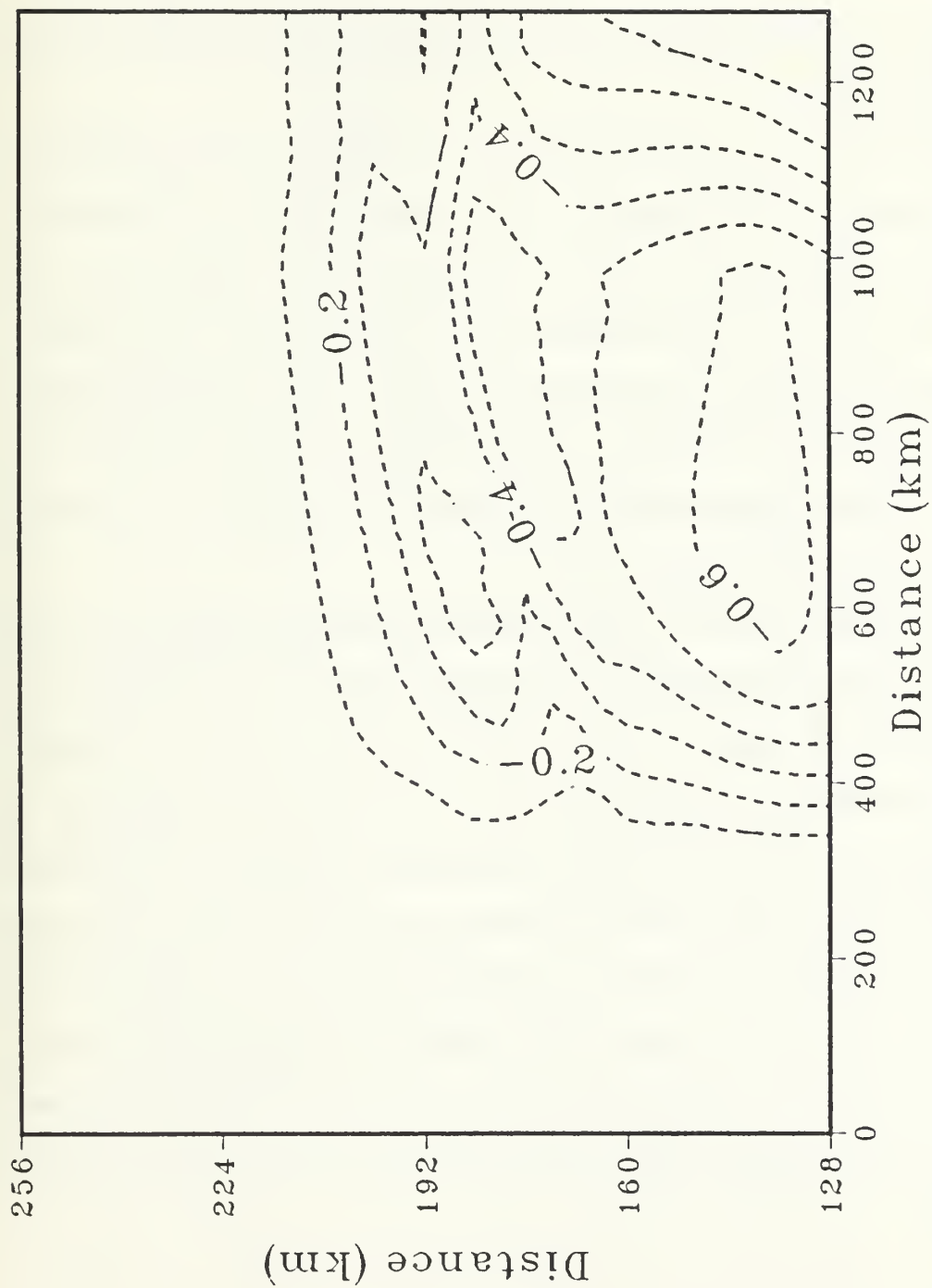


Figure 4-1. Surface v component at hour 72 for Experiment 4-1. Negative values indicate southward flow.

Relatively large zonal gradients in v occur where the zonal gradient of the cooling changes ($x = 320$ km and $x = 1000$ km), especially in the extreme southern portion of the domain where the zonal velocities are small. Between $y = 100$ and 190 km, the zonal gradient in v is more diffuse. Zonal advection of temperature tends to weaken the zonal temperature gradients near $x = 320$ km and $x = 1000$ km. Thus, the southward components, which are in thermal wind balance, are smaller in these areas.

The decreases in the surface temperature field and the change in the surface flow field at 72 hours are shown in Fig. 4-2. The pattern of the surface temperature changes is very similar to the pattern of the surface cooling (Fig. 2-2), which indicates that the changes in the surface temperature are due to the surface cooling and not the internal response of the ocean. The temperature changes near the western boundary of the surface cooling are slightly modified by the tendency of zonal advection to restore the temperature field to the initial conditions. As in the case with the velocity components, the maximum temperature change of 0.8°C is very close to the value in two-dimensional simulations.

The changes in the surface flow field are consistent with geostrophic adjustments in response to the changes in the surface temperature field. Because the cross-stream cooling gradient reduces the surface horizontal temperature gradient, the surface zonal components are diminished as denoted by the westward pointing arrows in Fig. 4-2. The maximum reduction in the surface zonal components of 8.0 cm s^{-1} is similar to the maximum decrease in the two-dimensional simulations and occurs along the current maximum at the downstream boundary of the domain. Smaller decreases in the zonal velocity occur to the north and to the south of the front where the cross-stream cooling gradient is smaller. West of 600 km, very small decreases in the zonal velocity occur due to the combination of a reduced cross-stream cooling gradient and the tendency of zonal advection to restore both the temperature and zonal velocity to their initial conditions.

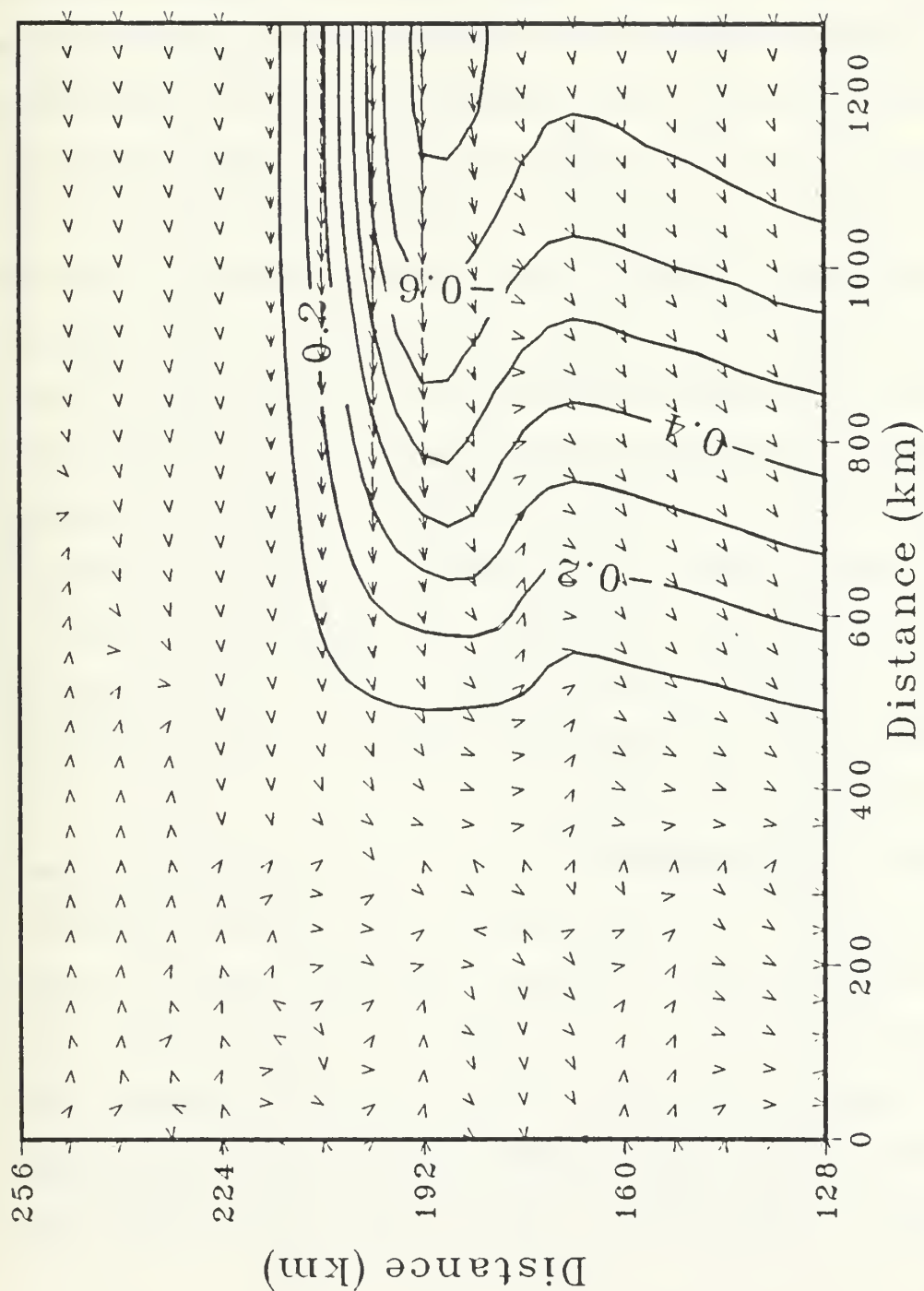


Figure 4-2. Changes in surface temperature (solid lines) and the velocities (arrows) at hour 72 for Experiment 4-1. The length of the arrows is proportional to the departure from a control run without forcing. The maximum departure is about 8 cm s⁻¹. The contour interval is 0.1 °C.

An 18-day integration using a cooling rate six times smaller than the previous experiment was performed to study the effect of having the same total cooling, but over a longer period of time. The magnitude of the cooling is very similar to the maximum average cooling during February computed by Gorshkov (1978) (Fig. 2-5). The cross-stream velocities at day 18 for the simulation with a lower cooling rate are shown in Fig. 4-3. In the immediate vicinity of the front, the cross-stream velocities are much smaller than in the previous simulation (Fig. 4-1). This is consistent with the analysis in Section III which shows that the cross-stream velocity response due to a cross-stream cooling gradient is only weakly time dependent and will be reduced when the cross-stream cooling gradient is reduced. The smaller cross-stream components also support the conclusion that it is the value of the cross-stream cooling gradient and not the along-stream cooling gradient that determines the cross-stream flow in the immediate vicinity of the front. South of the front, the meridional flow is slightly smaller than in the previous simulation. In this region, the tendency for the along-stream cooling gradient to establish a zonal temperature gradient is opposed by the tendency for zonal advection to restore the temperature field to the initial condition. The effect is most noticeable where the initial current is strong, between $y = 110$ and 190 km. In the extreme southern portion of the domain ($y < 110$ km) where the zonal advective effects are smaller, the meridional flow is comparable in magnitude to the flow in the earlier simulation.

In summary, the combined effects of a cross-stream and an along-stream cooling gradient induce a southward flow in these numerical simulations, but the magnitude of that flow is too small to produce displacements of the Gulf Stream of the magnitude suggested by Nof (1983). South of the current maximum the southward velocities are in thermal wind balance with the induced zonal temperature gradient, which is consistent with Nof's (1983) predictions. Near the front, the tendency for the formation of a southward flow is due more to the constant adjustment of the flow fields to the reduced meridional temperature gradient than the along-stream cooling

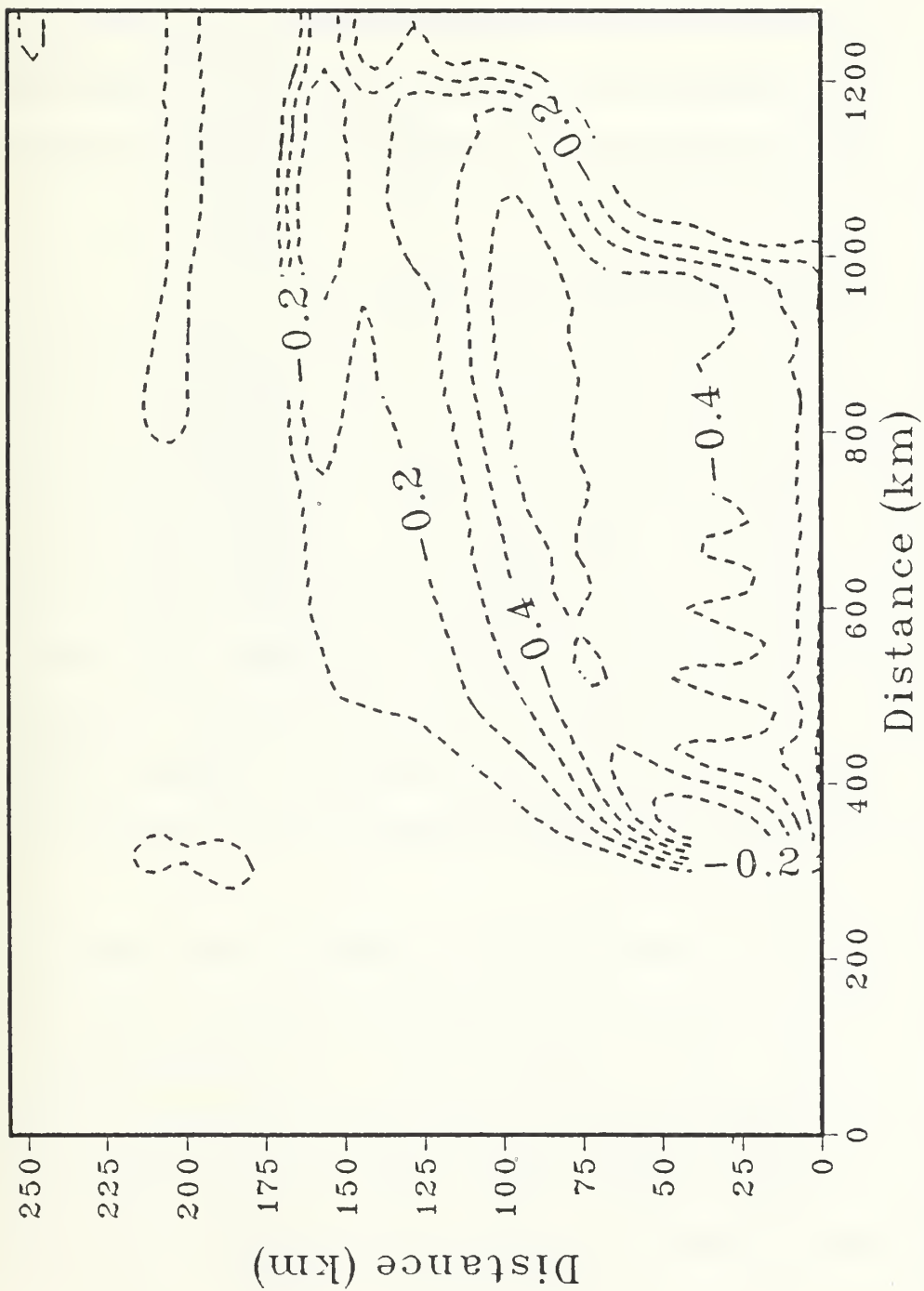


Figure 4-3. Surface v component at day 18 for a simulation using a cooling rate six times smaller than the first simulation of Experiment 4-1. The contour interval is 0.1 cm s^{-1} .

gradient. Much of the change in the magnitude in the initial jet can be explained by the reduced horizontal temperature (pressure) gradient. A strong short period of cooling is more effective in inducing cross-stream velocities in the immediate vicinity the front than is a steady prolonged, but smaller, cooling rate. The stronger short cooling event is also more effective in producing larger meridional velocities south of the current maximum. Because there is no surface forcing on the upstream flow in these simulations, there is a tendency for zonal advection to restore the fields to their initial condition. The tendency for zonal advection to restore the fields to their initial condition is larger over relatively longer integrations.

B. EFFECT OF MOMENTUM MIXING (EXPERIMENT 4-2)

It was shown in Section III that the inclusion of momentum mixing in the convective adjustment is critical in determining the magnitude and direction of the response of an intense oceanic flow to cross-stream cooling. With momentum mixing, surface cooling causes the relatively high zonal momentum near the surface to be mixed with relatively low zonal momentum immediately below, so that the surface currents decrease relative to their initial values. The horizontal gradient in the surface cooling, and the associated decrease in pressure gradient is not large enough to balance geostrophically the decrease in the momentum. Consequently, the surface flow becomes sub-geostrophic, and positive (northward) v components occur near the front. This behavior is opposite of that predicted (Experiment 4-1) when momentum mixing is not allowed.

The surface meridional velocities at hour 72 for the simulation that includes convective mixing of momentum are shown in Fig. 4-4. The maximum cross-stream speeds near the current maximum are now near 2.5 cm s^{-1} as opposed to -0.3 cm s^{-1} when momentum mixing is not included. South of the current maximum, the southward flow is only slightly smaller than in Experiment 4-1. The flows in this region are similar in the two experiments because there is little vertical current shear at the initial time, so momentum mixing has almost no effect. Thus, the

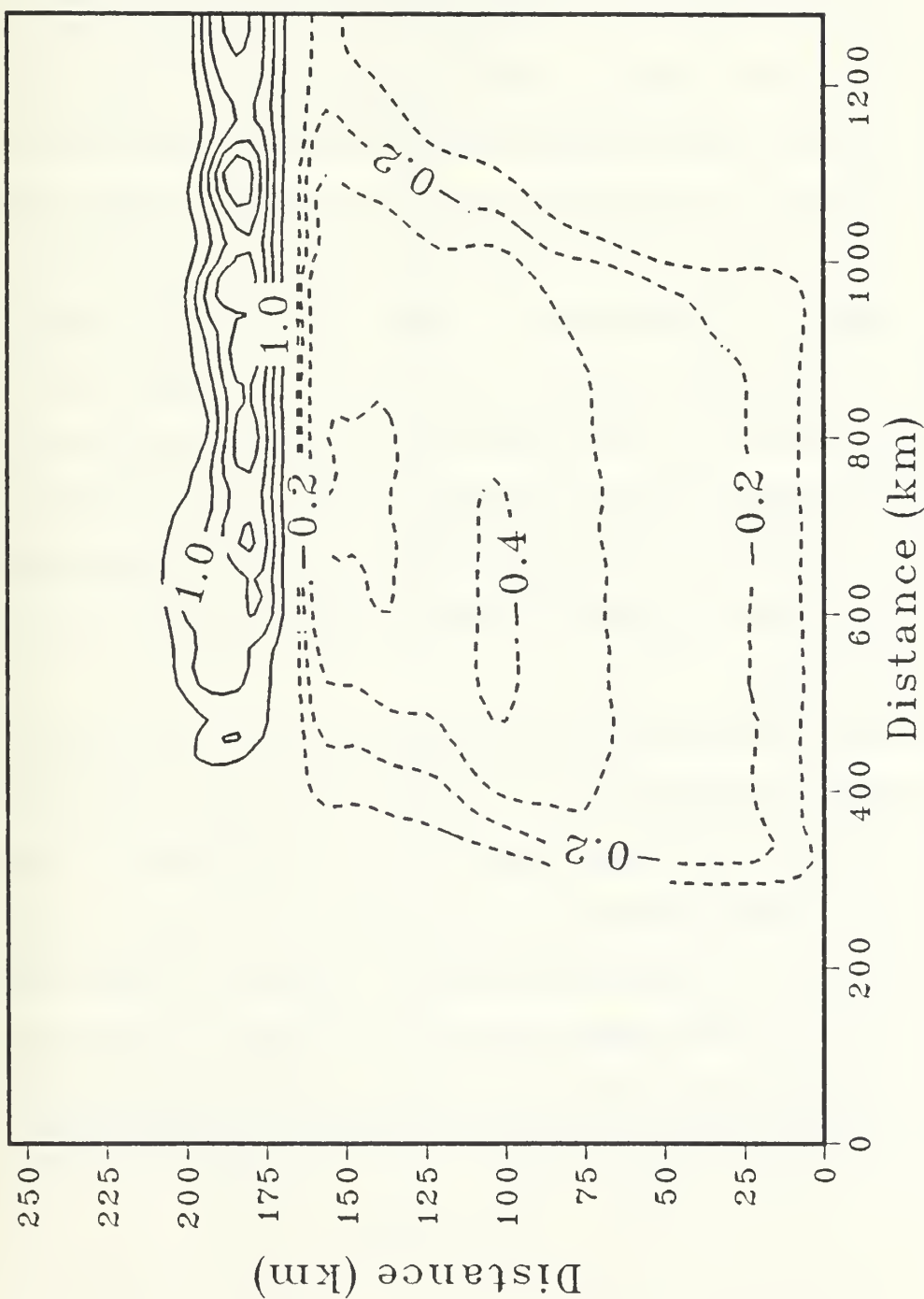


Figure 4-4. As in Fig. 4-1 except for Experiment 4-2 and the contour interval is 0.5 cm s^{-1} where the flow is positive (northward), and 0.1 cm s^{-1} where the flow is negative (southward).

drastic effect of including or excluding momentum mixing is confined to the region where the initial current has a sizeable vertical shear, i.e. near the front.

The maximum cross-stream component at the front is similar to the two-dimensional simulations, but the contribution from the along-stream differences is also noticeable. At the front, the cross-stream velocities near the western boundary of the cooling are only half the magnitude of the cross-stream components farther downstream. Between $x = 600$ km and $x = 1000$ km, the surface cross-stream components near the front are nearly constant in x even though the forcing is a function of x . The cross-stream response at the front depends more on the initial shear in the zonal velocity than the imposed surface cooling in these simulations. The surface cross-stream components at the front between $x = 300$ km and $x = 600$ km are smaller due to the tendency of zonal advection to restore the fields to their initial condition. Also, at the southern edge of the front near $y = 170$ km, there is an area of divergence, which also occurred in the two-dimensional simulations. However, the divergence in the three-dimensional simulations is larger due to the added effect of the southward meridional flow forced by the along-stream cooling gradient south of the front. The divergence, and hence upwelling, is nearly 20% larger in the three-dimensional simulation.

The disturbance with a wavelength of about 100 km along the front in Fig. 4-4 is not due to contamination by inertial components that are not removed by the filtering. A time series of the instantaneous v component and the filtered v component at $x = 1100$ km and $y = 188$ km is shown in Fig. 4-5. An inertial oscillation in the instantaneous flow (dashed line) is very evident. Although there is a 6 cm s^{-1} oscillation in the instantaneous v components, the low-pass filtered data show no sign of the inertial oscillation. Rather, the 100 km wave is due to the growth of perturbations on a baroclinically unstable flow. The wavelength for maximum growth rate for this flow was determined from separate simulations (not shown) to be on the order of 75-100 km.

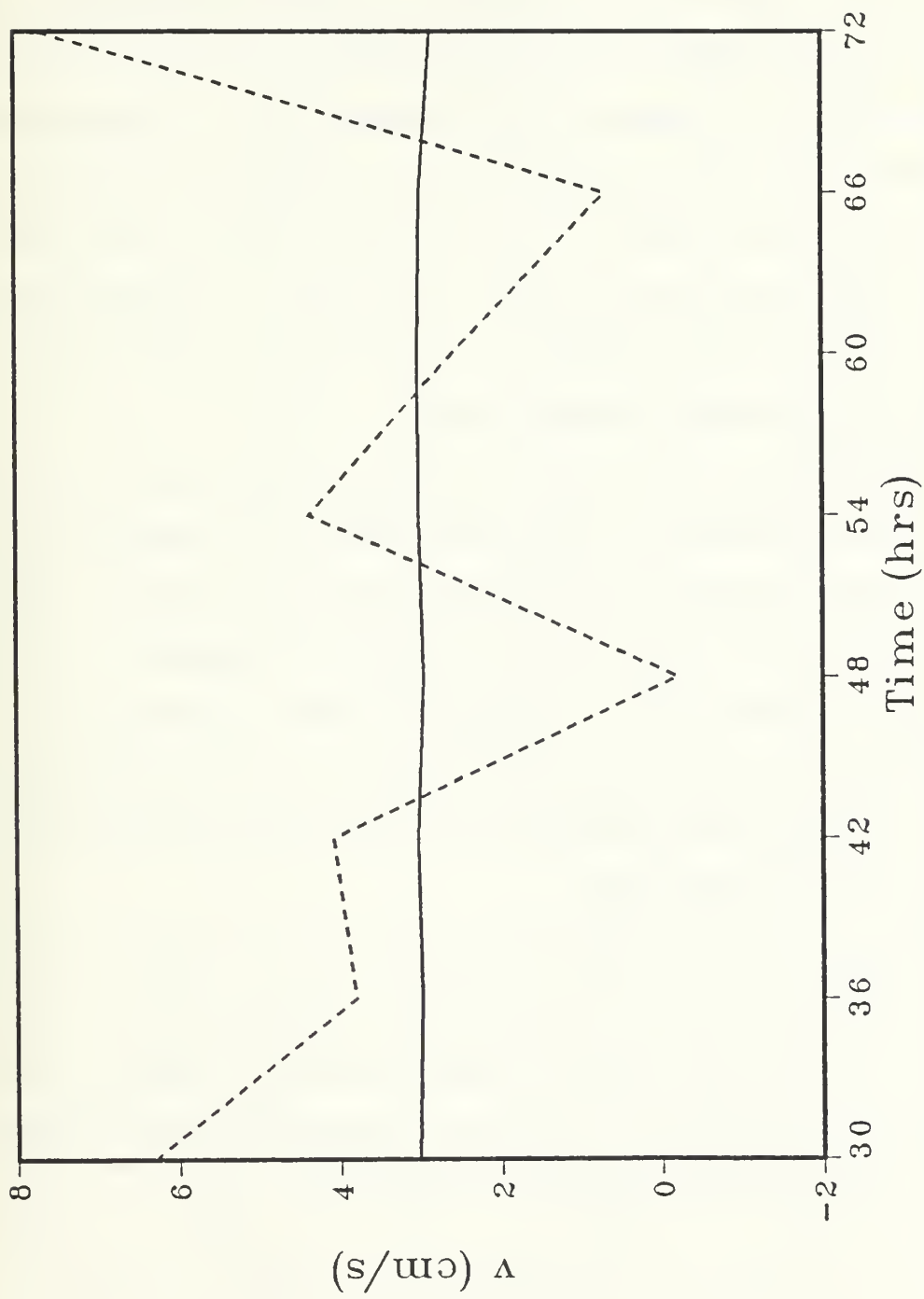


Figure 4-5. Time series of the instantaneous v component at the surface (dashed line) and filtered v component (solid line) at $x = 1100$ km and $y = 188$ km for Experiment 4-2.

The maximum reductions in the zonal components (Fig. 4-6) near the surface jet are almost twice as large as in Experiment 4-1. The change in the surface zonal components is due to a combination of the adjustment of the flow to a weakened meridional temperature gradient and the reduction of the flow through convective mixing with the sub-surface flow. The reductions in the zonal components extend farther to the south in this simulation than in Experiment 4-1. The larger southward extent of the reductions in the zonal components is due to the divergence of the cross-stream flow south of the front, which tends to weaken the horizontal temperature gradient there. The effect is most noticeable at the eastern boundary of the cooling where there are reductions in the zonal components south of the current maximum, and significantly smaller reductions north of the maximum. Away from areas of meridional cooling gradients and areas of vertical shear, there is little change in the surface zonal flow.

The change in surface temperature after 72 hours (Fig. 4-7) is similar to the surface temperature changes in Experiment 4-1 with only minor differences. As in Experiment 4-1, the temperature changes are primarily due to the surface heat flux rather than the ocean's internal response to the forcing. The maximum temperature decreases in Experiment 4-2 are shifted slightly to the north and the west of the decreases that occurred in Experiment 4-1. The northward shift is due to advection by the positive v components at the front, and the westward shift is due to the weakened current maximum and thus, weakened tendency for zonal advection to restore the fields to their initial condition.

The changes in the vector flow field after 72 hours (Fig. 4-7) are also similar to Experiment 4-1, except in the immediate vicinity of the front. There is a noticeable tendency for the vector flow to cross the lines of constant temperature change, indicating that the change in the flow is not as geostrophic as in Experiment 4-1. Away from the immediate vicinity of the surface front, the changes in the flow are parallel to the changes in the temperature.

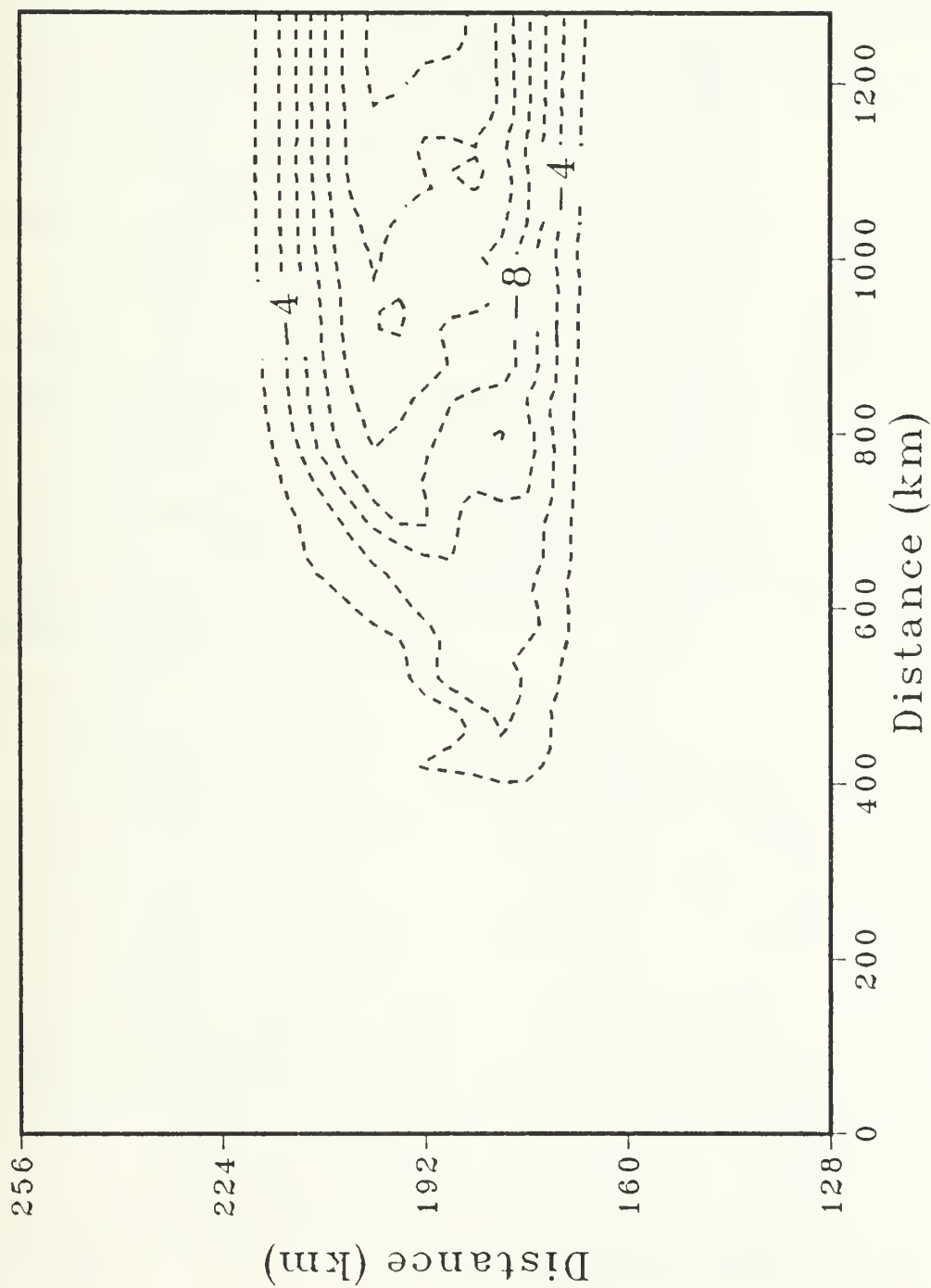


Figure 4-6. Change in surface u component of velocity at hour 72 for Experiment 4-2. Negative values indicate a reduction in the eastward current maximum. The contour interval is 2 cm s⁻¹.

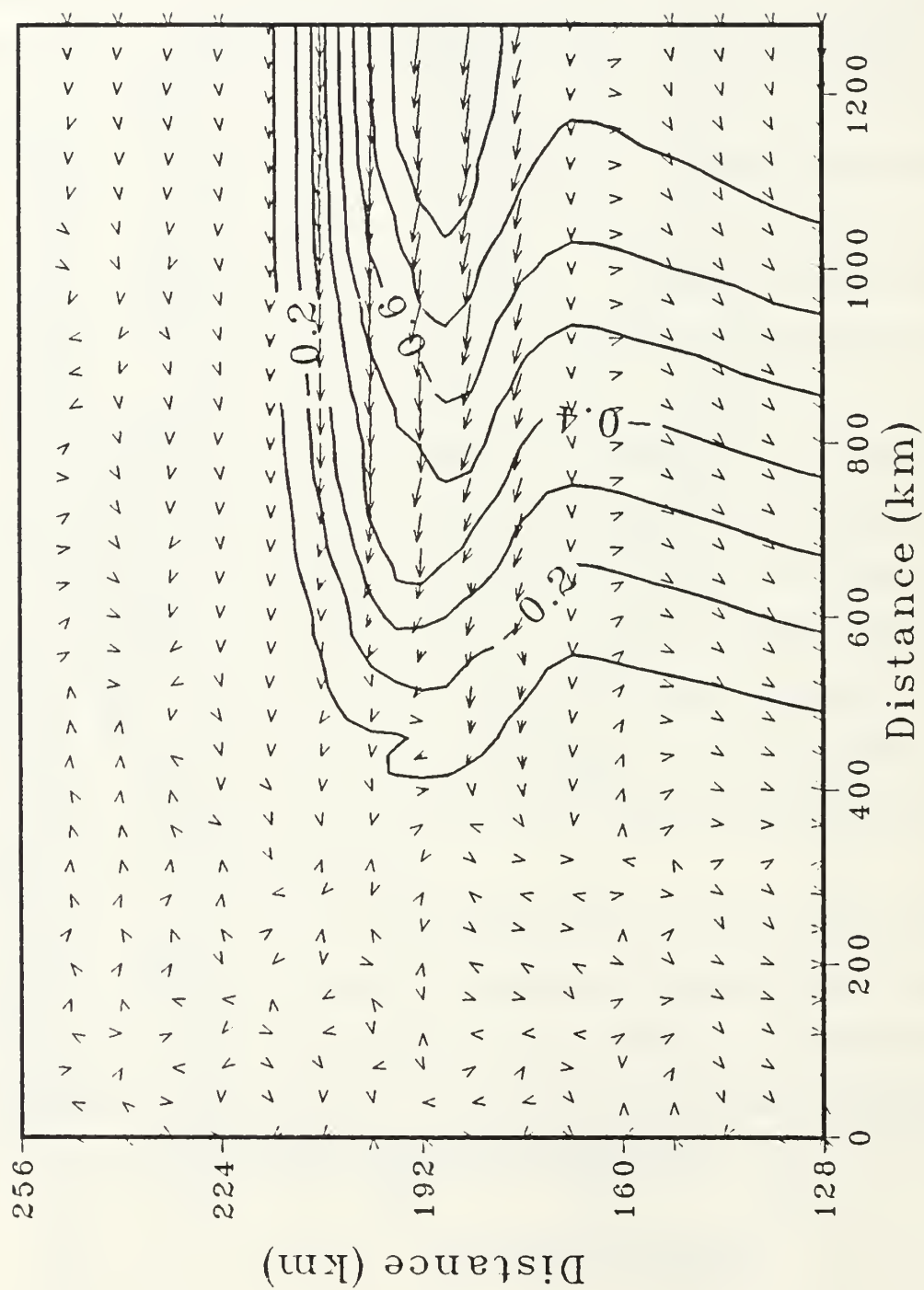


Figure 4-7. As in Fig. 4-2 except for Experiment 4-2, and the maximum departure is about 16 cm s^{-1} .

In summary, the cross-stream components in the immediate vicinity of an ocean front are larger, and in the opposite direction, to the simulation with no momentum mixing during convective adjustment. South of the current maximum, in the region of weak vertical shear, the induced southward flow is only slightly changed by the inclusion of vertical mixing of momentum. The reductions in the zonal component near the current maximum are twice as large as those that occurred in Experiment 4-1. As in Experiment 4-1, the changes in temperature are primarily due to the surface forcing rather than an internal adjustment of the ocean. The effects of vertical mixing of momentum dominate the effects of the imposed surface cooling gradients near the current maximum. The tendency to produce northward v components at the front when momentum mixing is included is large enough to compensate a cross-stream flow of the magnitude predicted by Nof (1983). The above conclusions obviously depend on the assumed initial vertical profile of zonal momentum, and on the assumed form of the vertical mixing of momentum (adjustment based on the value of the local Richardson number). At least for these simulations, strong cooling events alone cannot explain the observed southward shift of the mean position of the Gulf Stream during winter.

C. EFFECT OF WIND FORCING (EXPERIMENT 4-3)

It was suggested in Section III that an increase in the zonal wind stress during winter may be an alternate explanation for the observed southward shift of the Gulf Stream. An additional integration was performed to consider the response of a strong ocean current as it flows into a region of wind forcing. The wind stress increases in the along stream direction from 0 at $x = 320$ km to 0.2 N-m at $x = 1000$ km. There is no meridional dependence of the wind stress. To isolate first the effects due to wind forcing, there is no surface cooling specified in Experiment 4-3. The choice of wind stress which increases in the along-stream direction is supported by observations by Agee and Howley (1976) (Fig. 2-4). Simulations with a meridionally dependent wind stress were performed but did not significantly alter the results presented in this section.

The changes in the surface temperature field after 72 hours are shown in Fig. 4-8. The reductions along the northern boundary are due to the effect of upwelling forced by an Ekman divergence and are not of interest for this study. Reductions in the sea-surface temperature are evident in the eastern two-thirds of the domain, which suggests that the front has been shifted southward consistent with the direction of the Ekman flow. The maximum decreases along the current maximum are in excess of 1.4°C at the eastern boundary of the domain, which is equivalent to a 9 km southward shift in the front. The shifts in the previous simulations, which are due to cooling alone, are less than 1 km. The 9 km shift is comparable to the shift noted in the two-dimensional simulations. The temperature decreases farther to the west are not as large as those in the eastern domain due to the smaller southward advection where the wind stress is smaller. This integration was extended to 7 days to determine a limit for the southward shift of the front for this wind forcing. After seven days of forcing, the front was displaced 13 km southward. The rate of the southward advection of the front has been slowed which indicates a limit on the effectiveness of wind stress for shifting the front. As the front is advected southward, the slope of the front becomes larger, and the depth to which the frontal region is well-mixed becomes greater. Consequently, the effects due to advection become smaller since the Ekman (advecting) velocities are inversely proportional to the mixed-layer depth.

An integration similar to Experiment 4-3 but also including cooling similar to that described in Experiments 4-1 and 4-2 was performed to investigate the combined effects of the atmospheric forcings on strong ocean currents. The changes in sea-surface temperatures after 72 hours (not shown) are similar to the pattern in the wind-forcing only experiment, but the decreases in surface temperature are larger (especially south of the front) due to the extra effect of surface cooling. The effect of the cross-stream components (not shown) is also additive. The meridional flow south of the current maximum is enhanced due to the adjustment of the flow to the forced along-stream temperature gradient. At the front, the meridional flow is still southward, but at a reduced speed relative to the case with no surface cooling.

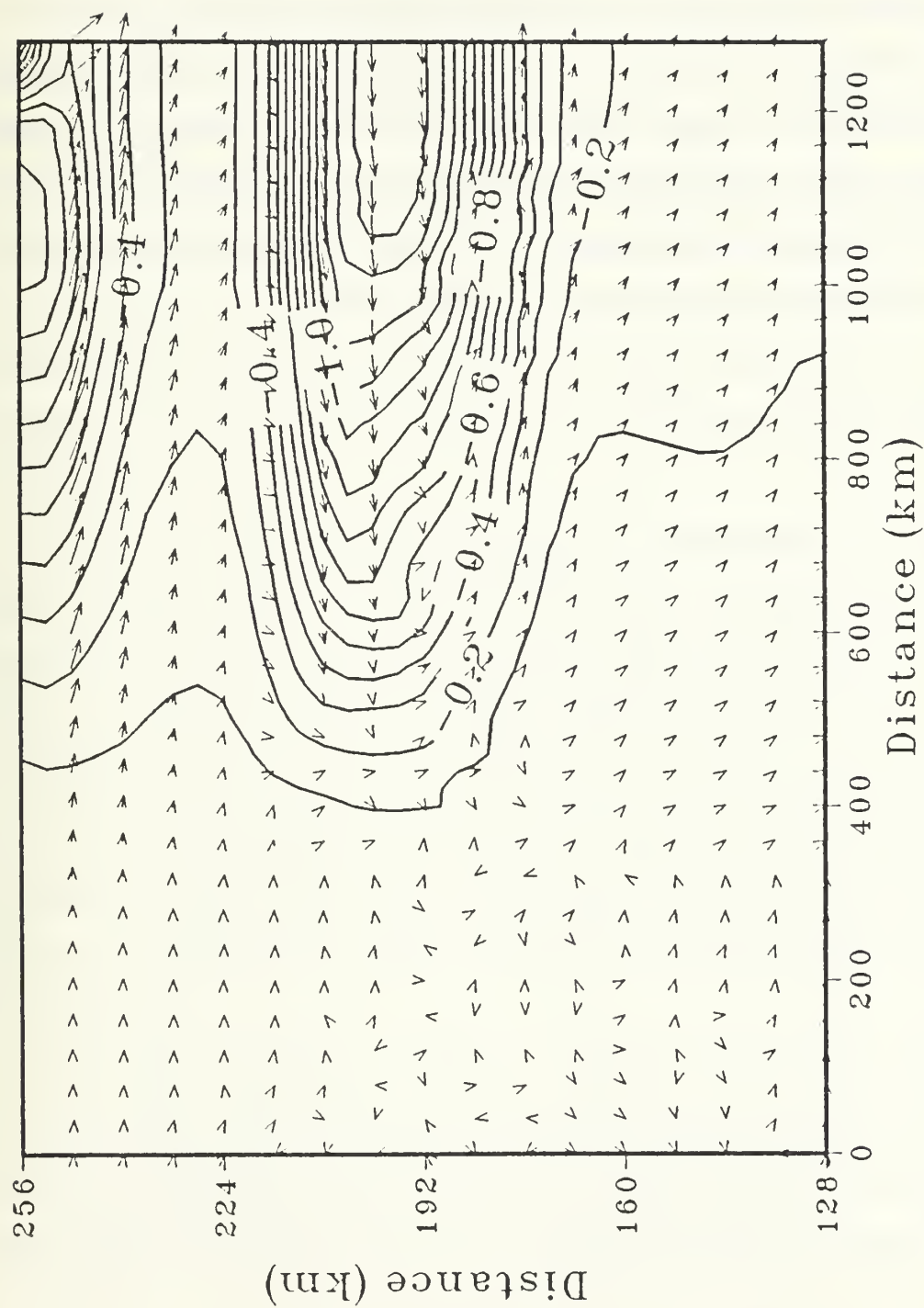


Figure 4-8. As in Fig. 4-2 except for Experiment 4-3, and the maximum departure is about 35 cm s^{-1} .

As in the two-dimensional simulations, the effect of wind forcing is more effective in shifting the position of a intense current system than are very strong gradients in the horizontal cooling. However, none of the simulations support the hypothesis that atmospheric forcing is capable of shifting an intense oceanic baroclinic zone (and the associated current system) far enough to cause significant feedback to the atmosphere. To this point, the effects of atmospheric forcing on a uniform zonal flow only has been considered. The Gulf Stream is a meandering current system that adjusts to changes in the bottom topography and perturbations on a strong baroclinic flow. It is possible that atmospheric forcing may affect the processes that produce meanders in the Gulf Stream, and ultimately lead to changes in the mean path of the flow.

V. THE EFFECTS DUE TO TOPOGRAPHY

The position of the Gulf Stream has been observed to change rapidly as it encounters topographic features associated with the New England Seamount Chain (NESC) (Vastano and Warren, 1975). Richardson (1981) observed that the NESC appears to be responsible for a 100 km southeastward deflection of the Gulf Stream and for a quasi-permanent warm ring-meander to the south of the seamount chain. Richardson also observed that areas downstream of the NESC are favored locations for large-scale meander development. The seamount chain affects the Gulf Stream because of the height of its topographic features, which in places rise to 3 km above the ocean floor, and also because the flow associated with the Gulf Stream penetrates deep into the water column.

In this section, the effect of atmospheric forcing on baroclinic flow moving over topography is studied to determine if the flow can be steered away or toward a topographic feature. A second objective of this section is to determine if the atmospheric forcing affects the actual adjustment of the flow to underlying topography. If the adjustment of the flow is sensitive to the surface forcing, then large changes in the position of the current system may occur. If the flow can be steered away from or toward topographic features, then the character of the flow downstream of the topography may change radically as observed by Richardson (1981). In either case, it may be possible to affect significantly the position of the surface front over time scales that are important to the atmosphere.

The simulations described in this section are very similar to a linear study by Smith (1984) who looked at the two-dimensional response of atmospheric flow over a mountain. In that study, as well as in this, the direction of the flow reverses with height. The reversal of the current with height in this study is due to the assumption of no barotropic component. The current reversal in

Smith's study was a necessary condition for the propagation of disturbances away from a topographic feature. Although the purpose of this section is not to reproduce Smith's results, his analytic work does provide a guideline for determining if the flow is adjusting to the topography in a realistic fashion.

An example of a cross-section of the initial zonal velocities used in this study is shown in Fig. 5-1. The flow is eastward in the upper 400-500 m and westward in the lower layers. Thus, the flow in the layer adjacent to the bottom is from east to west. The topography used in these simulations is a Gaussian-shaped seamount that rises 200 m above a 1 km deep ocean floor. The width of the seamount is approximately 120 km. Although this investigation considers the effect on stratified flow only, the conservation of potential vorticity is expected to be very important in these simulations as in Smith's (1984) results. The initial conditions are similar to the those in Section IV. The surface front is centered along $y = 128$ km for all the simulations, and the initial zonal velocities are prescribed to be in geostrophic balance

$$u = \frac{-1}{\rho_0 f} (P_y - \frac{\sigma}{D} P_\sigma D_y) \quad . \quad (5.1)$$

These simulations of the adjustment of the flow to topography neglect the barotropic component. In an atmospheric study of lee cyclogenesis, Hayes (1985) incorporated topographic effects into Eady's (1949) solution for baroclinic growth. Hayes found that the steady state solution for flow over a mountain decayed exponentially with height above the mountain. The vertical structure in these ocean simulations can be estimated (Fig. 5-2) from Hayes' solution using values of 100 km for the mountain width, 10 km for the baroclinic radius of deformation and -0.5 for the ratio of the mean current at the bottom to the change in the mean current up to the thermocline. Notice that the amplitude of the response changes sign with height and is almost totally baroclinic. The barotropic component does not seem to be important for the adjustment of the flow for the topographic scales in this study. Hayes shows that the vertical extent of the topographic effect is reduced as the horizontal scale of the topography decreases relative to the

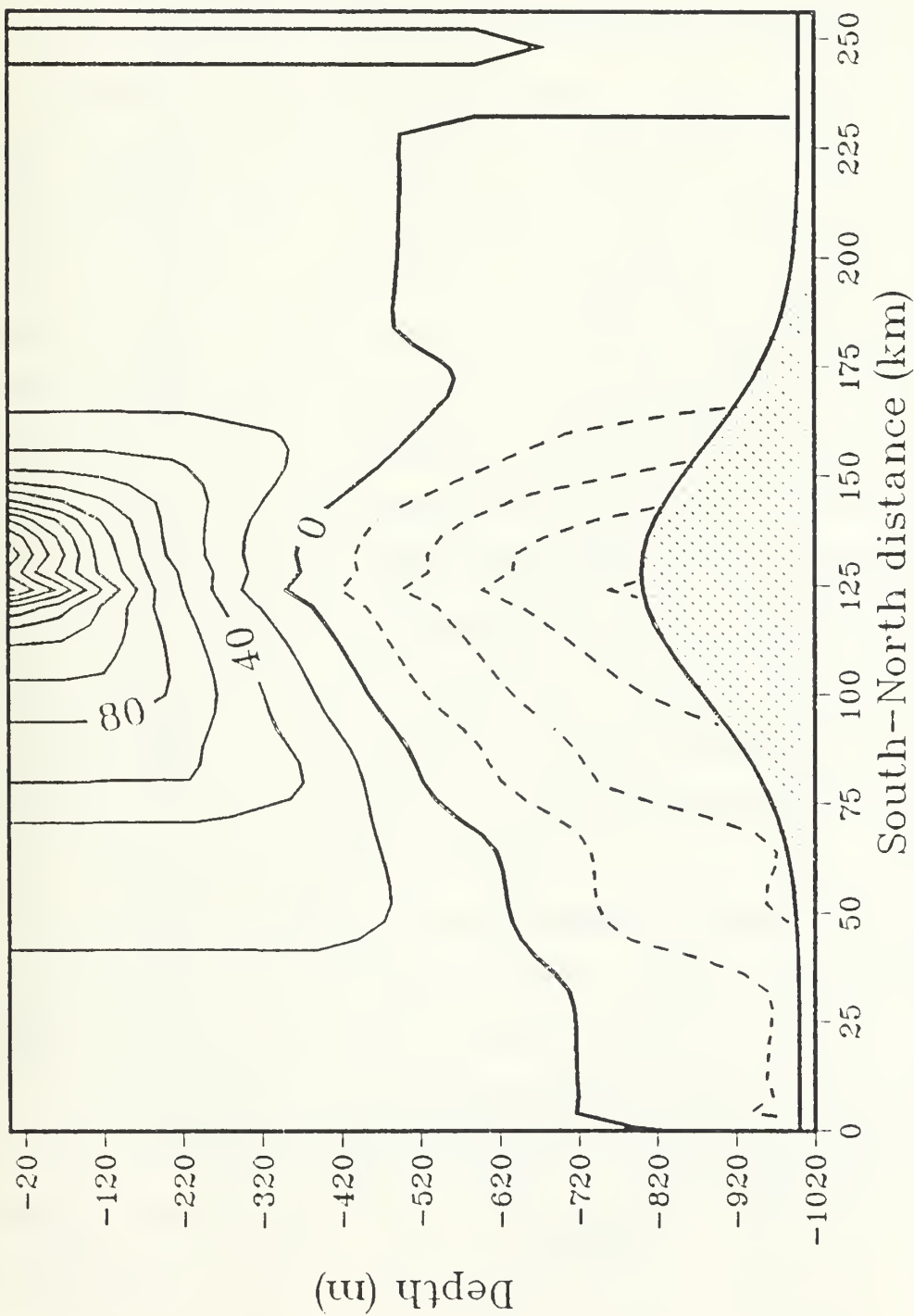


Figure 5-1. South-to-north cross-section of the initial zonal velocities used in the simulations which include effects due to topography. The contour interval is 20 cm s^{-1} , and positive flow is toward the east.

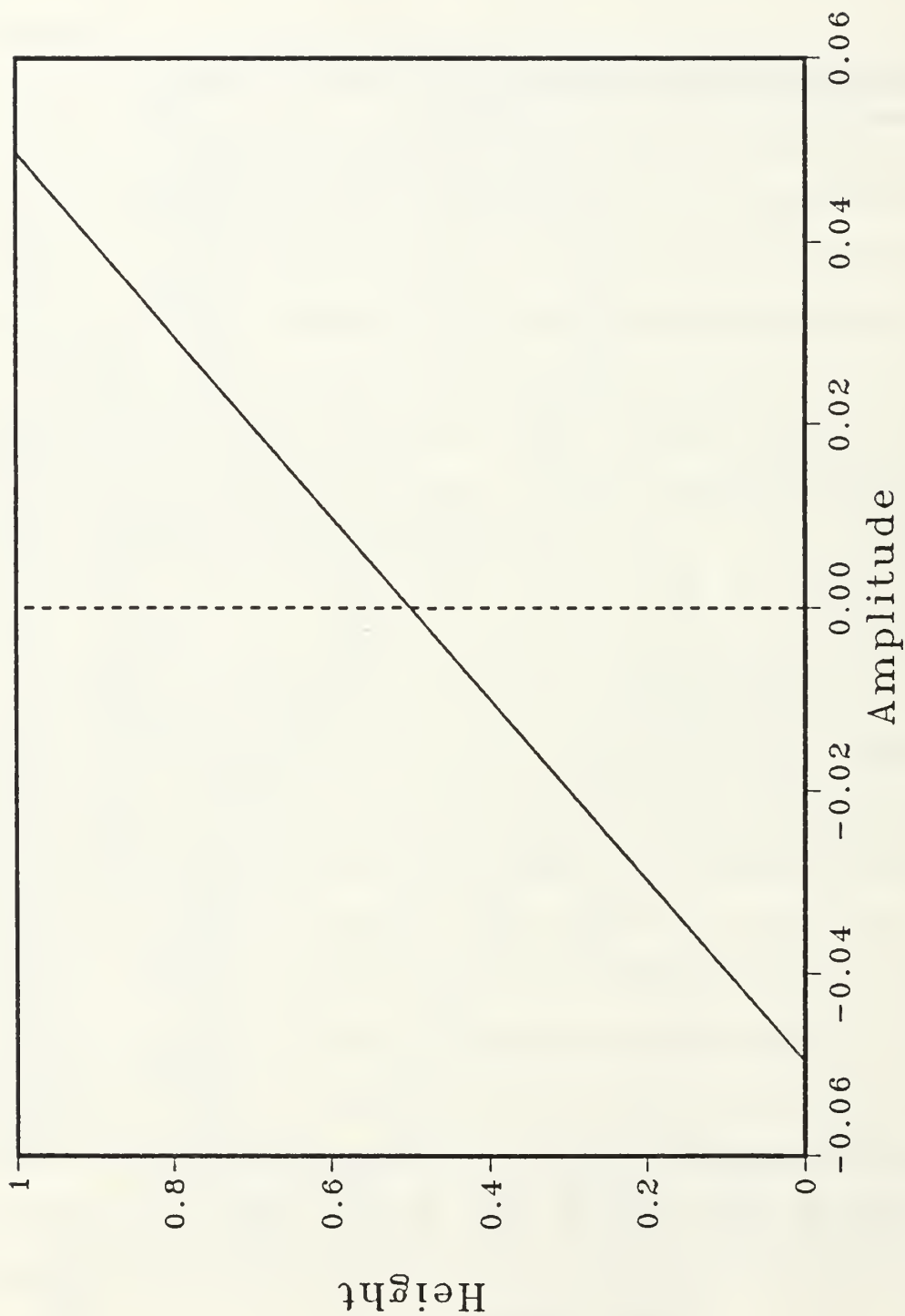


Figure 5-2. Dependence of the amplitude of the response of the flow on non-dimensional height for the initial conditions and topography used throughout Section V.

deformation radius. Since the wavelength of the seamount in the present study is relatively long compared to the baroclinic radius of deformation, the topographic effect should be felt all the way up to the surface. However, as shown in Fig. 5-2, the response will be primarily baroclinic as assumed in the numerical experiments.

The investigation is divided into two sets of experiments. The first experiment considers the effect on the flow when the maximum surface current will be forced away (south) from the seamount, and the second experiment considers the response of the flow when the maximum surface current is being forced toward the highest point of the seamount. Each experiment contains three simulations. The first simulation of each experiment is a control case which is integrated to 6 days to determine the response of the flow to topography alone. The second simulation is identical to the first except that the topography is shifted 16 km north relative to the first simulation. Thus, the first two simulations of each experiment highlight the adjustments of identical flows which are initially over a slightly different topography. The third simulation uses the fields from day 3 of the first simulation and then includes an eastward wind stress which is applied impulsively. The tendency of the Ekman advection in this simulation will be to shift the front south as in Sections III and IV. Surface wind stress is chosen to force the problem since it was shown to be effective in shifting the position of the surface current system in Sections III and IV. The wind stress increases from zero at $x = 120$ km to a maximum value of 0.2 N-m at $x = 260$ km. The wind stress has no meridional dependence.

By comparing the third simulation with the first simulation, it is possible to determine how the surface forcing affects the adjustment of the flow to the topography. By comparing the third simulation with the second simulation, it is possible to determine if the atmospheric forcing is effective in steering the flow toward or away from the topography. If the surface forcing is able to steer the flow, the adjusted flow in third simulation will resemble the second simulation more than the first. If the surface forcing is not effective in steering the flow, the adjusted flow will resemble the first simulation.

A. SURFACE CURRENT FORCED AWAY FROM SEAMOUNT (EXPERIMENT 5-1)

The first simulation considers the response of flow over a seamount which is centered at $x = 640$ km and $y = 128$ km. In this case, the maximum surface flow is directly over the highest point of the seamount. The surface temperature at day 6 for the simulation with no surface forcing is shown in Fig. 5-3. Upstream of the seamount near $x = 600$ km, the fluid particles encounter a shallower water column and curve anticyclonically consistent with the conservation of potential vorticity. Downstream of the seamount, the isotherms curve cyclonically as the flow moves over deeper water. Without surface forcing, the front is approximately at the same latitude downstream of the seamount as it is upstream of the seamount.

The conservation of potential vorticity is a powerful dynamic constraint in this simulation. However, because the fluid is stratified, a discussion in terms of density can explain the curvature in the surface isotherms. Fig. 5-4 is a west-to-east cross-section of the temperature field at day 6. A dramatic change from the initial temperature field is evident (there is no zonal dependence in the initial conditions; the isotherms are initially flat). There is a marked lifting of the isotherms on the eastern side of the seamount, while on the western side, the isotherms are depressed. Since the shear flow near the bottom is from east to west (Fig. 5-1), there is convergence (divergence) on the eastern (western) side of the seamount which induces an upward (downward) vertical motion. The convergence (divergence) at depth is balanced by a divergence (convergence) above so that the net divergence over the water column is zero. Notice that the upwelling on the eastern side of the seamount penetrates the thermocline. The pattern of vertical motion produces a column of relatively cold water above the eastern side of the seamount and relatively warm water above the western side. The zonal pressure gradient induced by this warm-cold pattern is negative above the western side of the seamount, positive over the seamount and negative above the eastern flank of the seamount. The surface meridional geostrophic flow for these pressure gradients is northward above the eastern and western sides of the seamount and southward over the seamount. Thus, v_x

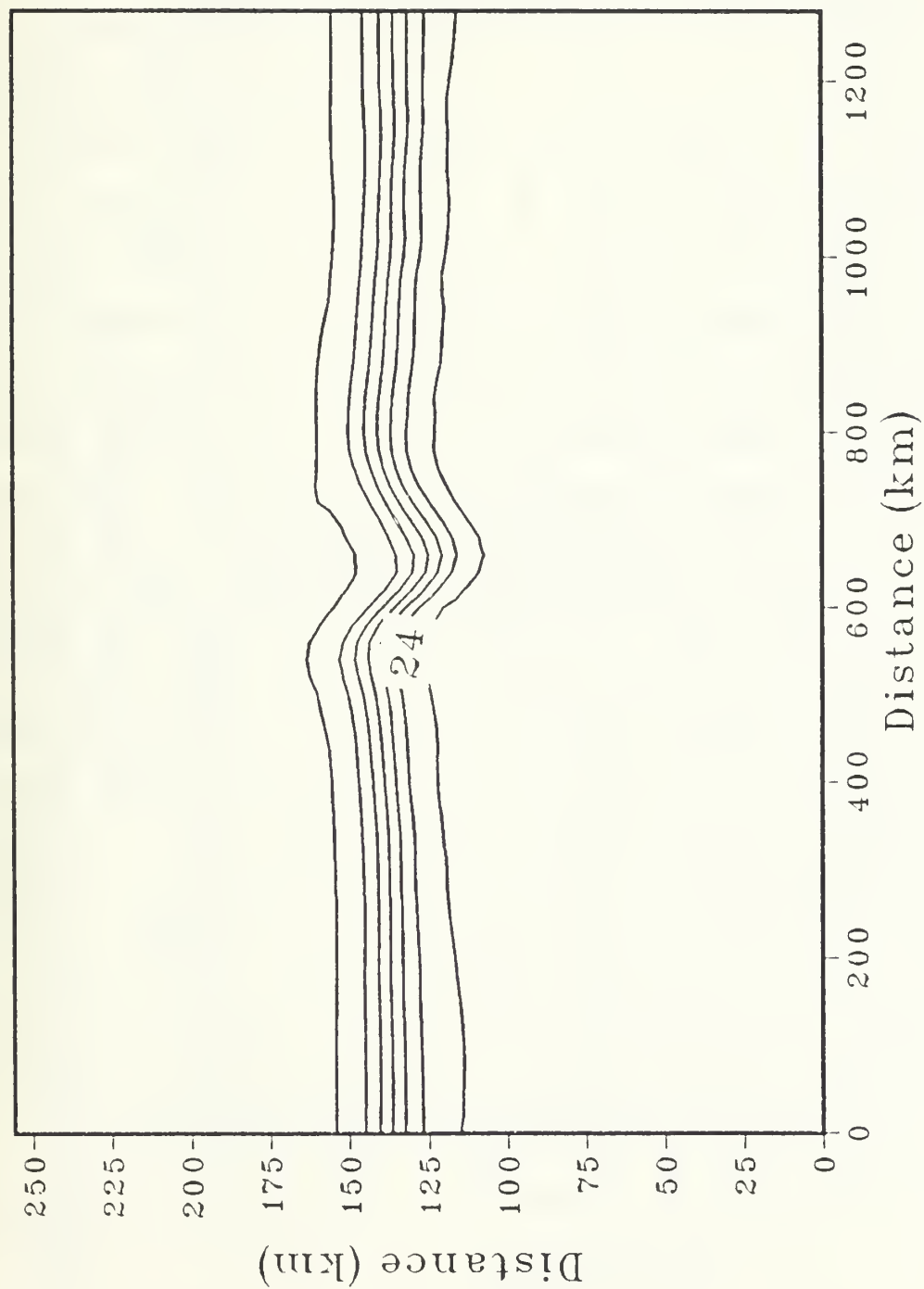


Figure 5-3. Surface temperature at day 6 for the first simulation of Experiment 5-1. The contour interval is 1.0 °C.

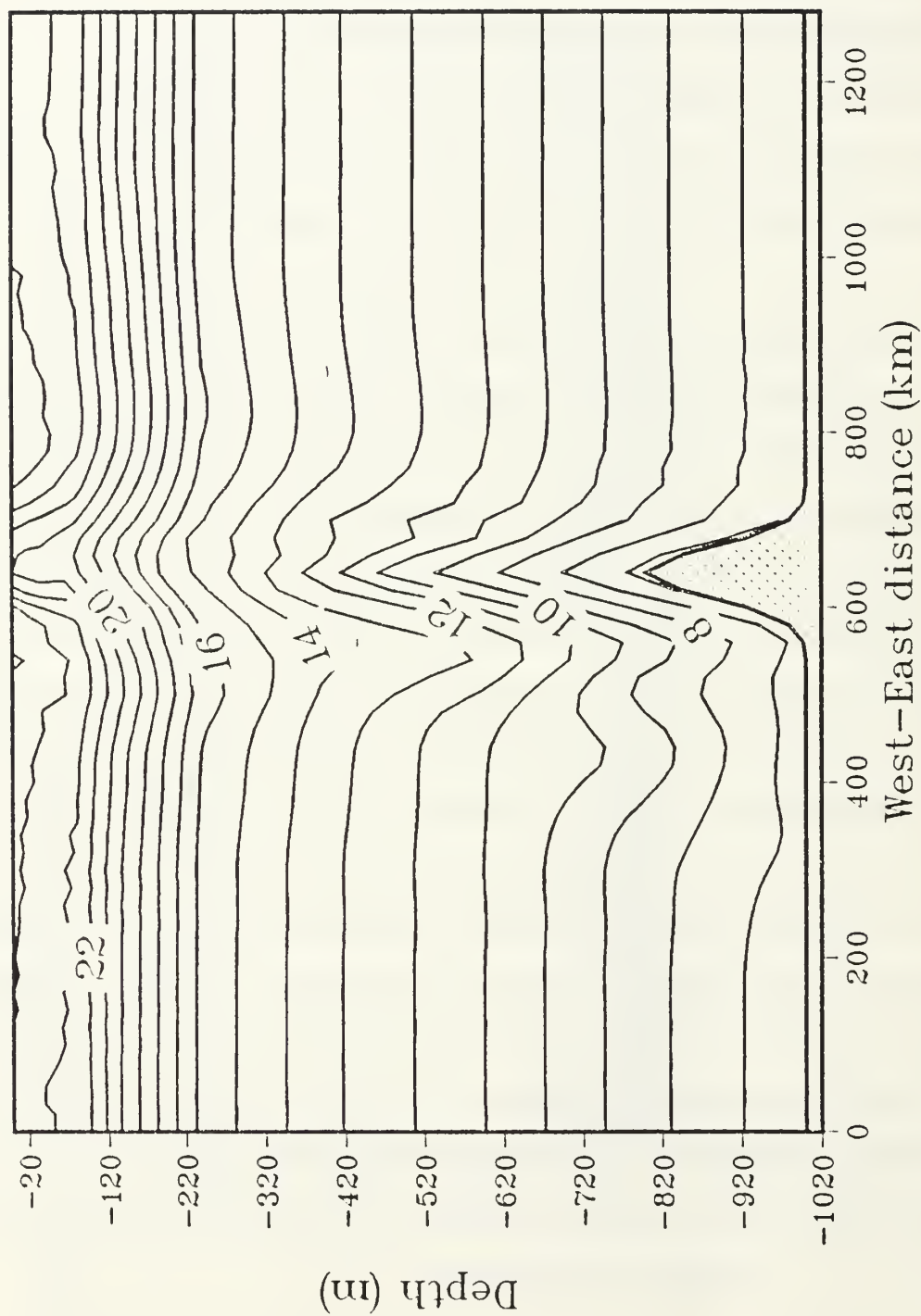


Figure 5-4. West-to-east cross-section of temperature across $y = 128$ km at day 6 for the first simulation of Experiment 5-1. The contour interval is 1.0°C .

< 0 (anticyclonic) on the western slope of the seamount and $v_x > 0$ (cyclonic) on the eastern slope of the seamount. In this simulation, potential vorticity is conserved by an adjustment to the local areas of upwelling and downwelling generated as the flow moves over the topography. The train of lee waves to the west of the seamount is an effect that was noticed by Smith (1984). The appearance of these waves in this study is an indication that the flow is adjusting in a fashion similar to previous investigations.

The second simulation of this experiment considers the response of flow over a seamount which is centered at $x = 640$ km and $y = 144$ km. Thus, the initial surface flow in this simulation is south of the center of the seamount. The surface isotherms at day 6 are shown in Fig. 5-5. The response of the flow is very different from the first simulation. Although the initial flow is located over smaller topographic features, the amplitude of the meander is nearly two times larger than in the earlier simulation. The larger amplitude meander develops because the initial adjustment of the surface flow west of the seamount is anticyclonic to the north and the flow is forced toward larger changes in the topography. By contrast, the flow in the first simulation adjusts so that it is shifted away from the largest slopes in the topography.

The first simulation is repeated with a 0.2 N-m wind stress in the eastward direction which is applied impulsively at day 3. The difference in the surface temperatures at day 6 between the simulations with and without forcing is shown in Fig. 5-6. The decreases in the surface temperature are due to a southward advection of the front. The maximum decrease of 2.0 °C occurs along the current maximum and is comparable to the decrease described in Section IV for a flat bottom case. The contours of temperature difference parallel the surface flow which indicates a uniform advection. Along the northern boundary of the domain, the decreases are due to upwelling forced by an Ekman divergence at the boundary and are not of interest in this study.

The temperature response below the surface layer (not shown) is remarkably similar to that in the simulation without surface forcing. The fluid below the surface layer is protected against the

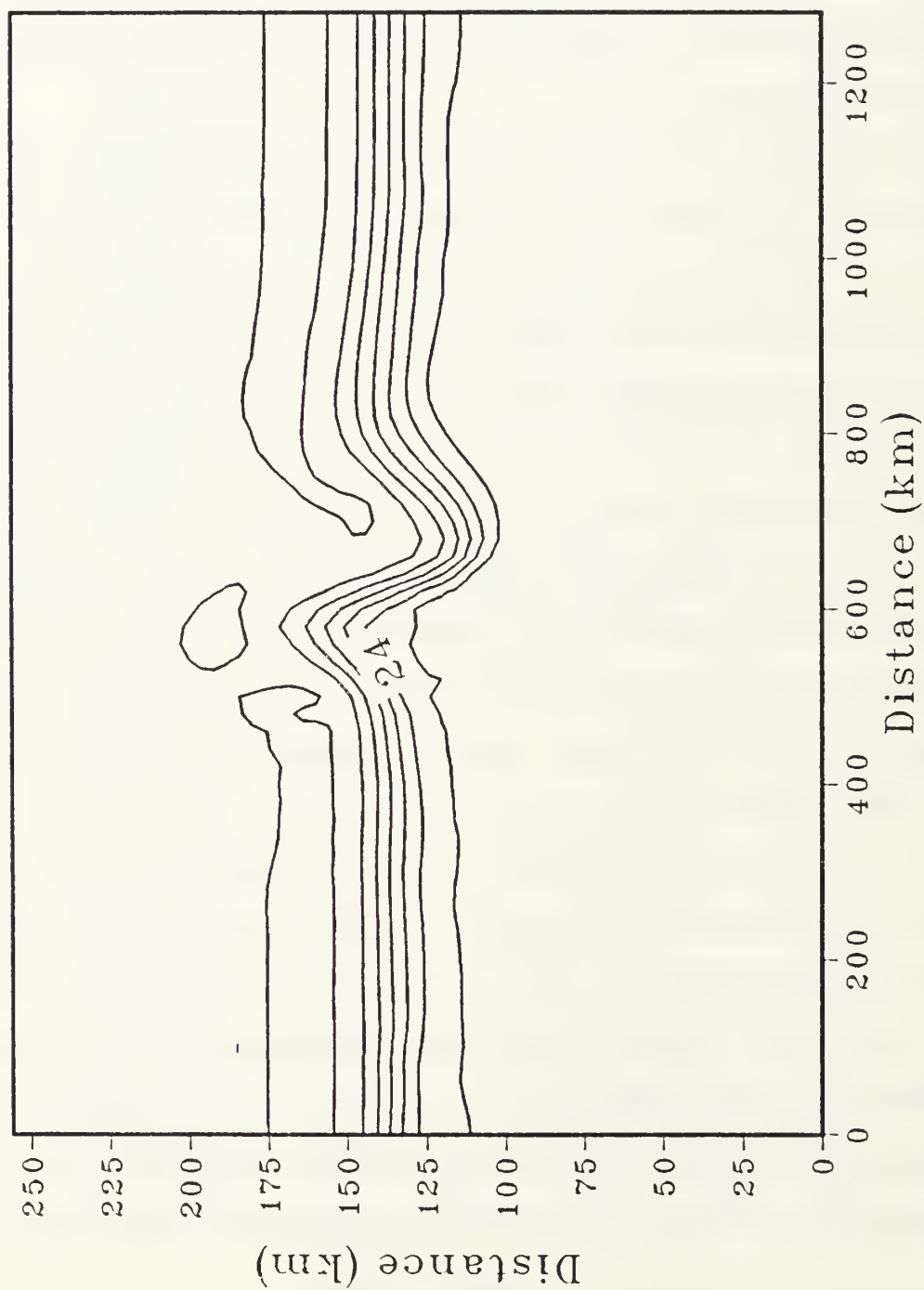


Figure 5-5. As in Fig. 5-3 except that the seamount is centered at $x = 640$ km and $y = 144$ km.

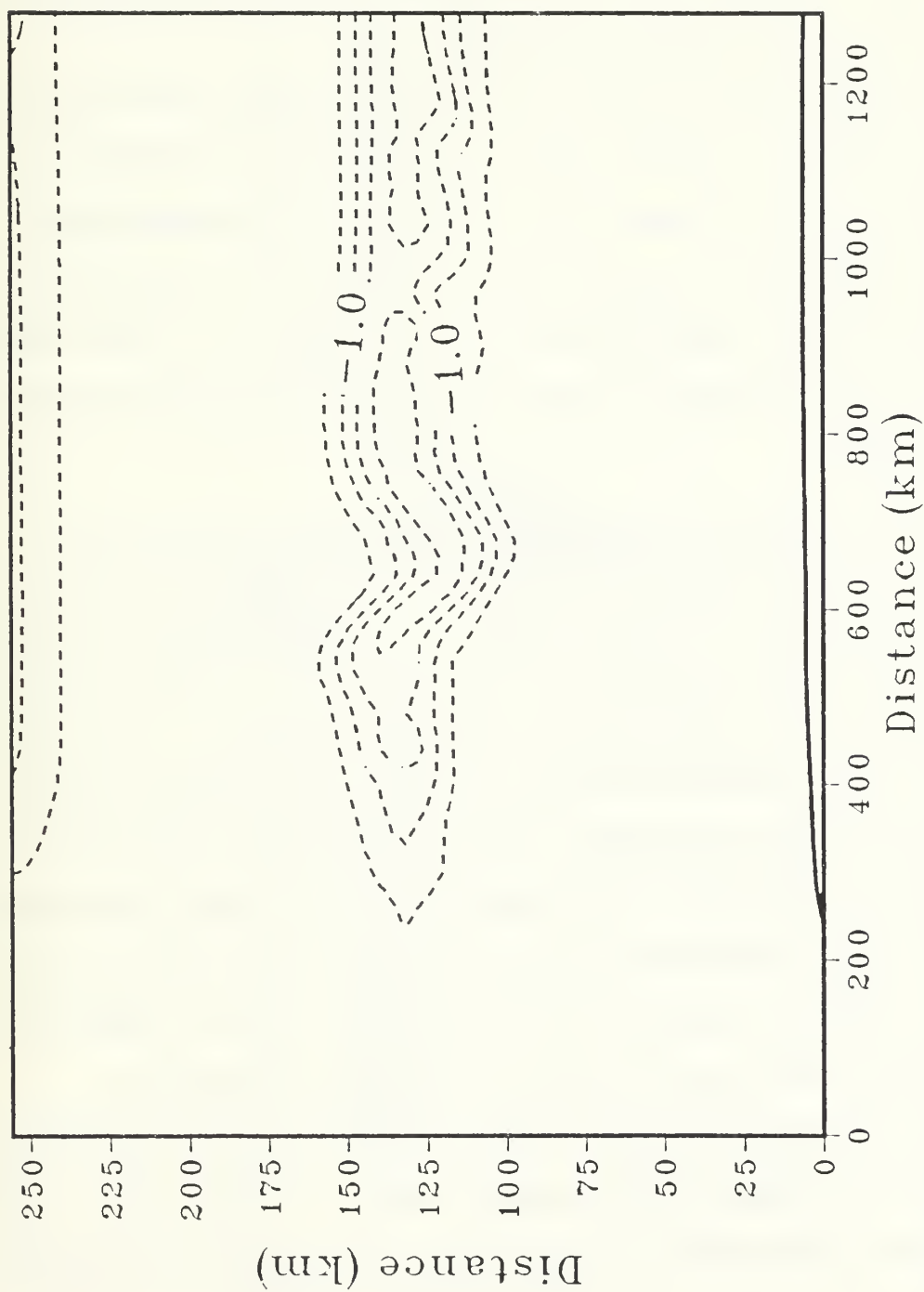


Figure 5-6. Difference in surface temperature fields at day 6 for Experiment 5-1 between the simulation which is forced by an eastward wind stress and the simulation which is not forced. The contour interval is 0.5 °C.

action of the wind stress by the initial stratification. Thus, the flow adjusts in a similar manner as when forcing is not included, and does not depend on the upper layers in this simulation. When the simulations are extended to 8 days, the effect of Ekman advection becomes reduced as the front steepens, as in Experiment 4-3. The surface temperature decreases are only slightly larger (2.5°C) than at day 6 and still parallel the surface flow.

Although Ekman advection has shifted the surface flow south of the seamount in the wind-forced case, the flow does not develop as large a meander as in the second simulation when the flow is initially south of the seamount. Thus, the forcing does not affect the actual adjustment of the flow in these simulations. Also, the forcing has not steered the flow so that the adjustment evolves from the smaller amplitude meander of the first simulation to the larger amplitude meander of the second simulation. The meander in the third simulation is similar to the meander in the first simulation.

B. SURFACE CURRENT FORCED TOWARD SEAMOUNT (EXPERIMENT 5-2)

The three simulations of Experiment 5-1 were repeated with the highest point of the seamount shifted southward 40 km for each case. In these simulations, the initial surface current maximum is always north of the center of the seamount, which is along $y = 88$ km in the first simulation. The surface isotherms for the control simulation without forcing at day 6 are shown in Fig. 5-7. The amplitude of the meander is much larger in this simulation (100 km) than in any of the simulations of Experiment 5-1. The amplitude of the meander is large in this simulation because the adjustment of the flow to the topography forces the flow over the highest point of the seamount. Although the amplitude of the meander is about 100 km, the surface front is approximately at the same latitude west of the seamount as it is east of the seamount.

A 16 km shift in the initial conditions produces a radically different response in the amplitude of the meander. The simulation with the seamount centered at $x = 640$ km and $y = 104$ km produces a surface isotherm pattern that is very similar to the pattern in the first simulation of

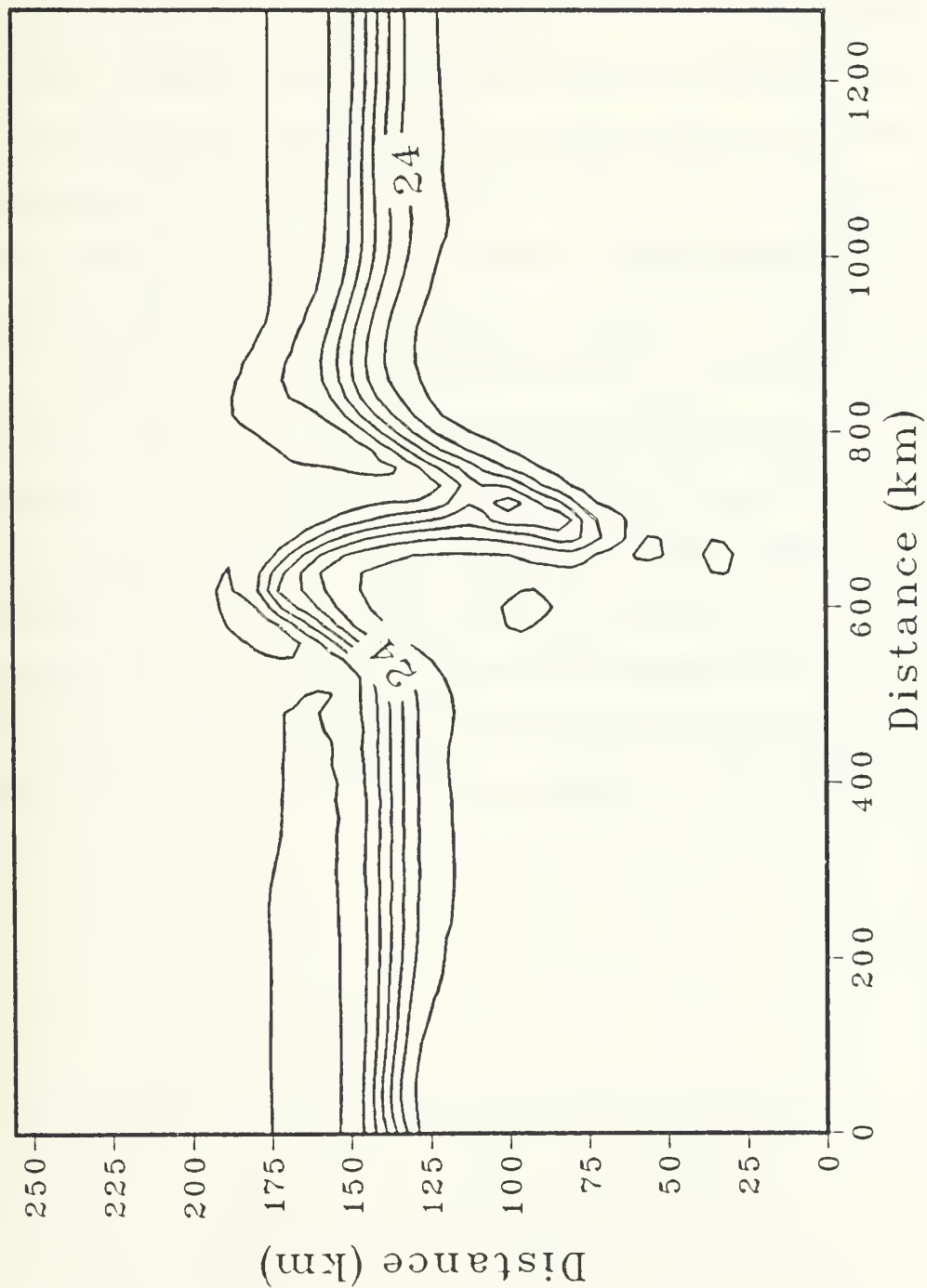


Figure 5-7. As in Fig. 5-3 except for Experiment 5-2.

Experiment 5-1. (Fig. 5-3). As the adjustment of the flow to the topography is very sensitive at this location, it may also be sensitive to the effects of surface forcing.

The first simulation of this experiment is repeated with the effect of wind forcing included to determine whether or not the forcing is able to shift the adjustment of the flow from the large amplitude meander to the smaller amplitude meander. The differences in the surface isotherms at day 6 between the integration which included wind forcing and the first simulation are shown in Fig. 5-8. Notice that the temperature differences in this experiment tend to parallel the surface flow as in Experiment 5-1. Also, the amplitude of the meander has not changed. Although Ekman advection has shifted the surface front 10 km in this simulation, the effect of the wind stress is confined to the upper layers by the initial stratification, and the adjustment of the flow does not change from the large amplitude meander mode to the smaller amplitude meander mode.

In summary, the response of the flow in the simulations without surface forcing is consistent with the conservation of potential vorticity. When the effects of an eastward wind stress are included, Ekman advection induces a uniform southward displacement of the surface front. Although the position of the surface current system is changed due to advection, the adjustment of the sub-surface flow to the topography and the amplitude of the meanders which are produced does not change in these simulations. The effects due to atmospheric forcing cause no significant changes in the position of the front or changes in the character of the downstream flow in these simulations.

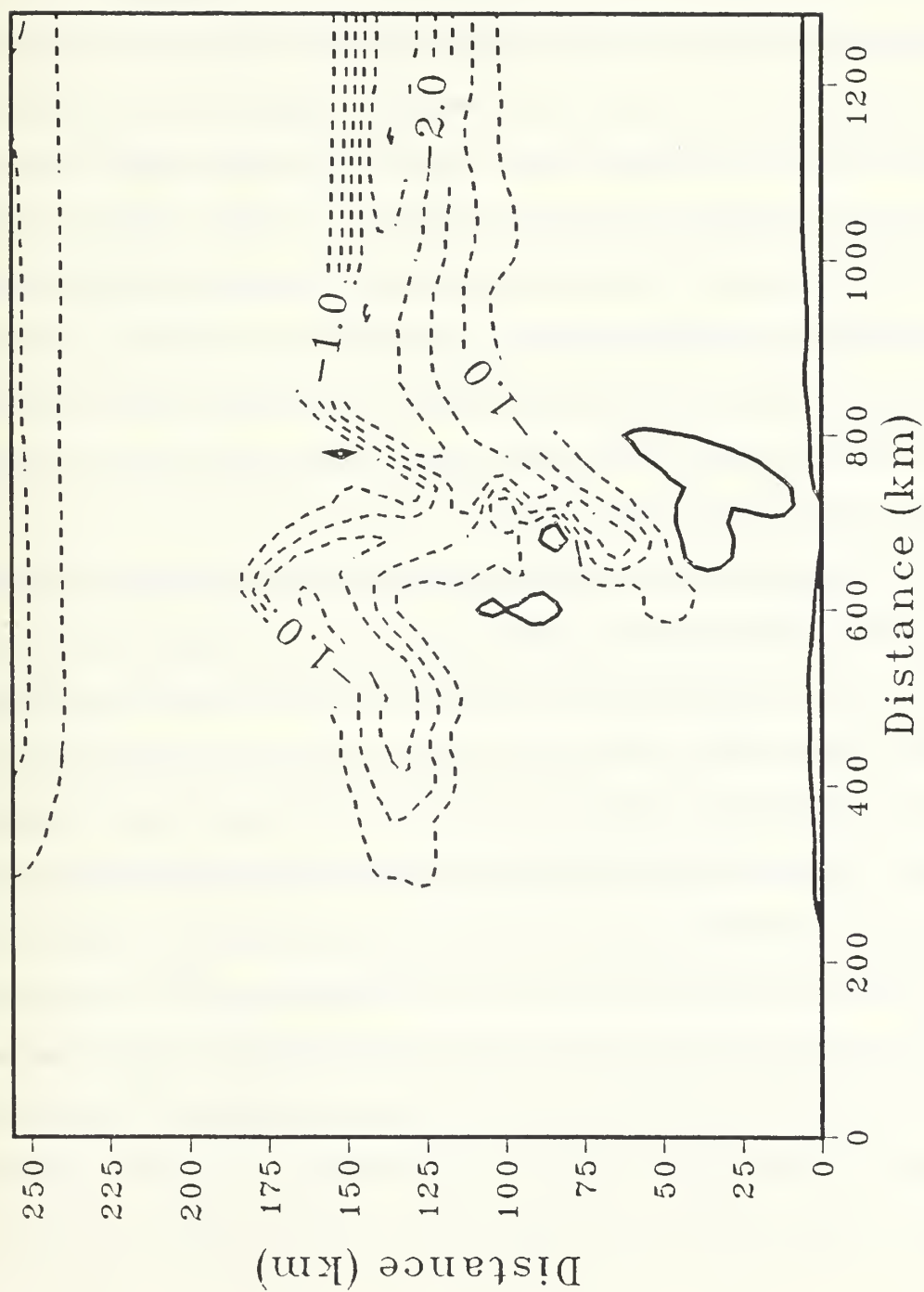


Figure 5-8. As in Fig. 5-6 except for Experiment 5-2.

VI. SUMMARY AND CONCLUSIONS

The objective of this study is to investigate the effect of atmospheric forcing on the location of the mean path of the Gulf Stream. Associated with the Gulf Stream is a strong baroclinic zone that extends eastward from the continental United States for hundreds of kilometers. A shift in the position of the Gulf Stream may have important consequences for the atmosphere such as in the case for predicting explosive cyclogenesis events (Sanders and Gyakum, 1980). One of the emphases of this study has been on the role of surface cooling in determining the path of the Gulf Stream. Nof (1983) has proposed that an observed southward shift of the Gulf Stream of 90 km during winter may be due to the effects of surface cooling. This investigation deals mainly with the ocean's response to strong atmospheric forcing on time scales of about 3 days, which should contribute to the seasonal effects of surface forcing.

The two-dimensional response of the current system to surface cooling is highly dependent on the vertical mixing of both heat and momentum in these numerical simulations. In a convective overturning case with no momentum mixing, the magnitude of the horizontal pressure gradient is reduced, which induces a weak cross-stream flow toward the warmer water. A thermally indirect circulation is centered on the warm edge of the surface front. Although the sense of the cross-stream current is to advect the front southward at the surface, the vertical circulation acts to increase the horizontal temperature gradient and maintain the front at its initial position. When momentum mixing is also included, the decrease in the along-stream current at the surface is larger than the change in the horizontal pressure gradient, and a cross-stream velocity toward the cooler water occurs near the surface. The v components are an order of magnitude larger than in the simulation that did not include the momentum mixing, but they are in the opposite direction. The sense of the vertical circulation is also changed when the momentum mixing is allowed. The

vertical circulation becomes thermally direct and tends to diminish the horizontal temperature gradient. As high momentum is transferred downward into a layer of diminished horizontal pressure gradient, strong cores of southward velocity occur immediately below the surface layers.

During winter, there is an increase in the mean eastward wind stress associated with the stronger and more frequent synoptic disturbances in the atmosphere. The inclusion of a southward wind stress to simulate a cold outbreak from the north in the two-dimensional model produces an Ekman-type advection above the main thermocline. The Ekman component is directed upstream which reduces the magnitude of the initial jet. The magnitude of the cross-stream velocity is also reduced relative to the simulation with no wind stress. Except for a slight southward shift, the net effect on the temperature field is minimal. Imposing an eastward wind stress in the two-dimensional model to simulate a cold outbreak from the west, induces a larger response than does the southward wind stress. The sense of the Ekman advection is to displace the front southward which affects both the along-front velocities and the temperature field. Due to the strength of the Ekman advection, the cross-stream velocities are in the opposite direction from the simulation without the wind stress. The divergence at the front and the horizontal gradient in cooling both act to reduce the intensity of the surface horizontal temperature gradient.

In these simulations, a modest wind stress of 0.2 N-m has a greater effect on the position of the Gulf Stream than does a very strong horizontal gradient in the cooling. Ekman advection due to an eastward wind stress displaces the current system southward and increases the vertical tilt of the front. The strong response in the simulation with an eastward wind stress suggests an alternate explanation for the observed shift in the Gulf Stream position and increased vertical tilt of the associated temperature front (Worthington, 1976). Horton (1984) also found that the main response of the Gulf Stream to forcing by hurricane Dennis was that the surface layer was shifted by Ekman advection.

The three-dimensional response of an intense oceanic current system as it enters a region of cooling was also numerically simulated. In the immediate vicinity of the associated surface front, the flow response is primarily due to a cross-stream gradient in cooling rather than the along-stream cooling gradient. As in the two-dimensional simulations, relatively small southward velocities (-0.3 cm s^{-1}) occur when momentum is not mixed vertically during convective adjustment. When momentum mixing is included, larger northward velocities (2.5 cm s^{-1}) occur. Performing an 18-day integration with a reduced but steady cooling function produced a very weak (-0.1 cm s^{-1}) cross-stream response in the immediate vicinity of the front. These simulations do not support the hypothesis that downstream surface cooling alone is responsible for an observed southward shift in the mean position of the Gulf Stream during winter.

Away from the immediate vicinity of the front, the response in the flow field is entirely due to the prescribed along-stream cooling gradient. In both experiments, a southward flow field develops in response to cooling that increases toward the east. The cooling produces a zonal pressure gradient to which the flow adjusts geostrophically. That is, the meridional component is in the thermal wind balance as in Nof (1983).

Because the upstream flow is not forced, there is a strong tendency in the three-dimensional simulations for zonal advection to return the temperature and flow fields to their initial condition. The effect is most evident near the region where the strong currents first encounter cooling. The restoring advection is not important in areas of weak zonal flow, and effects due to the cooling can be seen farther upstream than in areas where the initial zonal flow is strong.

The inclusion of a moderate increase in the eastward wind stress shifts the surface front southward 9 km after 3 days of integration. However, an additional 4 days of integration results in a further shift in the surface front of only 4 km. The steepening of the frontal interface limits the effectiveness of the wind stress in advecting the front farther southward.

Investigations into the large-scale forcing of these current systems to explain observed seasonal shifts seems warranted. The position of the Gulf Stream is not displaced enough by the local atmospheric forcing to significantly affect feedback by the ocean to the atmosphere on the time scale of 3-6 days. Although an increase in the zonal wind stress is able to displace the upper layer of a strong current system in these simulations, the effect does not extend below the thermocline. The sub-surface front is a effective anchor of the current system in these simulations.

Because the Gulf Stream penetrates very deep into the water column, the effect of gradients in the underlying topography may be important in determining the path of the Gulf Stream. A primitive equation model in σ -coordinates is used to simulate the adjustment of ocean flow to bottom topography. The conservation of potential vorticity is a strong dynamical constraint for flow that is adjusting to topography in the numerical simulations. The flow acquires anticyclonic curvature as it moves toward the seamount, and cyclonic curvature as it move away from the seamount. The inclusion of a surface wind stress produces a nearly uniform Ekman advection of the surface front, but does not affect the flow's adjustment to the underlying topography. The initial stratification protects the lower layers against the effects of the wind and from affecting the main adjustment of the flow.

The experiment was repeated with the seamount moved south 40 km relative to the maximum surface current. In control experiments, the maximum surface current has a much larger amplitude meander than occurred when the initial current maximum is directly over the seamount. The adjustment of the flow to the topography shifts the front so that the maximum currents flow over the highest points in the topography and larger amplitude meanders occur. The inclusion of surface forcing is not able to shift the adjustment from the large amplitude meander to the smaller meander. The difference in the surface temperatures is parallel to the surface flow, though not as uniformly distributed along the flow as in Experiment 5-1. The inclusion of atmospheric forcing does not affect the adjustment of the flow to the topography so that there will be feedback to the atmosphere on time scales of 3-5 days.

This study numerically simulates the effects of atmospheric forcing on intense ocean currents. These simulations provide little support for the hypothesis that surface forcing is capable of shifting ocean current systems so that there is an effect felt by the atmosphere over time scales of about three days. However, each of the experiments isolates effects which are important to the local balance of forces near strong ocean currents. These simulations aid in understanding the response of the ocean on short-time scales, and hopefully will be helpful in the understanding and prediction of the large-scale flow.

APPENDIX A

STABILITY ANALYSIS

The instantaneous flow fields along the current maximum display an oscillatory behavior in the experiments when momentum mixing is included. These oscillations have a period near 15 hours rather than the 21-hour inertial period. The purpose of this appendix is to demonstrate the effect of advection on the inertial frequency in a numerical model by use of a stability analysis.

Consider the equations for a flow where changes in the velocity are due to inertial motion and zonal advection only. The linearized equation for the horizontal flow is

$$w_t = -U w_x - ifw \quad (\text{A.1})$$

where $w = u + iv$. Numerical simulations involve approximations to the derivatives and may alter the frequency of the response. Consider the numerical approximation to (A.1)

$$w_j^{n+1} - w_j^{n-1} = -\frac{U\Delta t}{\Delta x} (w_{j+1}^n - w_{j-1}^n) - 2if\Delta t w_j^n \quad (\text{A.2})$$

where the subscripts refer to the position in space and the superscripts refer to levels in time. If a solution for w is assumed to have the wave form

$$w_j^n = W^n \exp(i k j \Delta x)$$

then one obtains

$$W^{n+1} = W^{n-1} - 2i W^n \left(\frac{U\Delta t}{\Delta x} \sin(k\Delta x) + f\Delta t \right) \quad (\text{A.3})$$

Assume an amplification matrix, μ , such that $W^{n+1} = \mu W^n$ and $\mu^{-1} W^n = W^{n-1}$. Substitution into (A.3) yields a quadratic for μ

$$\mu^2 + 2i \left(\frac{U\Delta t}{\Delta x} \sin(k\Delta x) + f\Delta t \right) \mu - 1 = 0, \quad (\text{A.4})$$

or solving for μ

$$\mu = -i (S \sin(k\Delta x) + f \Delta t) \pm (S^2 \sin^2(k\Delta x) - 2 f \Delta t S \sin(k\Delta x) - f^2 \Delta t^2 + 1)^{1/2} \quad (\text{A.5})$$

where $S = U \Delta t / \Delta x$.

The radical is always real for the values of S used in the present study. It is possible to obtain phase information from the expression for μ . The amount of phase change ϕ in a single time step in the numerical solution is given by

$$\phi = \tan^{-1} \frac{\text{imag}(\mu)}{\text{real}(\mu)} \quad (\text{A.6})$$

For ϕ to be zero, $f \Delta t$ must be equal to $-S \sin(k \Delta x)$. Unlike the analytic solution, ϕ can never be zero for the values of S in this study, because the argument of \sin^{-1} would have to be greater than one. The period of the response for a given wavelength is given by

$$\tau = \frac{2\pi}{\phi} \Delta t \quad (\text{A.7})$$

The oscillations along the current maximum in the numerical simulations have a wavelength near 75 km. Using a basic current speed of 2.0 m s^{-1} and wavelength of 75 km in (A.5), (A.6) and (A.7) yields a period near 15 hours for the oscillations. This result has several implications for the simulations presented in this investigation: 1) the equation (A.1) is describing much of the time dependence of the flow in the complete numerical model; and 2) zonal advection appears to be responsible for the shift in the response away from the inertial frequency.

Another interesting result of (A.6) and (A.7) is that the change in the advective-inertial frequency is dependent upon the direction of the advecting flow. For $U > 0$, the period of the response will decrease, and for $U < 0$, the period of the response will increase. The range of the periods for different wavelengths at 36°N is between 15 and 21 hours when $U > 0$, and 21 and 27 hours when $U < 0$.

LIST OF REFERENCES

- Adamec, D., R.L. Elsberry, R.W. Garwood Jr., and R.L. Haney, 1981: An embedded mixed layer - ocean circulation model, *Dyn. Atmos. Ocn.*, *6*, 69-96.
- Adamec, D., and R.W. Garwood Jr., 1985: The simulated response of an upper ocean density front to local atmospheric forcing, *J. Geophys. Res.*, *90*, 917-928.
- Agee, E.M., and R.P. Howley, 1977: Latent and sensible heat flux calculations at the air sea interface during AMTEX 74, *J. App. Meteor.*, *16*, 443-447.
- Baker, D.J., 1979: Ocean-atmosphere interactions in high southern latitudes, *Dyn. Atmos. Ocn.*, *3*, 213-229.
- Barker, E.H., and T.L. Baxter, 1975: A note on the computation of atmospheric surface layer fluxes for use in numerical modelling, *J. Appl. Meteor.*, *14*, 620-622.
- Budyko, M.I., 1963: *Atlas of the heat balance of the earth sphere*, Joint Geophysical Committee, Presidium of the Academy of Sciences, Moscow, 5pp. and 69 plates.
- Camerlengo, A.L., and J.J. O'Brien, 1980: Open boundary conditions in rotating fluids, *J. Comp. Phys.*, *35*, 12-35.
- Camerlengo, A., 1982: Large-scale response of the Pacific Ocean subarctic front to momentum transfer: a numerical study, *J. Phys. Oceanogr.*, *12*, 1106-1121.
- Cushman-Roisin, B., 1981: Effects of horizontal advection on upper ocean mixing: a case of frontogenesis, *J. Phys. Oceanogr.*, *11*, 1345-1356.
- Cushman-Roisin, B., 1984: On the maintenance of the subtropical front and its associated countercurrent, *J. Phys. Oceanogr.*, *14*, 1179-1190.
- DeSzoeke, R.A., 1980: On the effects of horizontal variability of wind stress on the dynamics of the ocean mixed layer, *J. Phys. Oceanogr.*, *10*, 1439-1454.
- Eady, E.T., 1949: Long waves and cyclone waves, *Tellus*, *1*, 33-52.
- Eliassen, A., 1962: On the vertical circulation in frontal zones, *V. Bjerknes Memorial Vol.*, *24*, 147-160.
- Fuglister, F.C., 1972: Cyclonic rings formed by the Gulf Stream. 1965-1966. In: *Studies in physical oceanography*, vol. 1, A.L. Gordon Ed., Gordon and Breach, N.Y., 194 pp.
- Gidel, L.T., and M.A. Shapiro, 1979: The role of clear air turbulence in the production of potential vorticity in the vicinity of upper tropospheric jet stream-frontal systems, *J. Atmos. Sci.*, *36*, 2125-2138.

- Gorshkov, S.G., 1978: *World ocean atlas, vol.2, Atlantic and Indian oceans*, Pergamon Press, N.Y., 306 pp.
- Halliwel, G.R. Jr., and C.N.K. Mooers, 1983: Meanders of the Gulf Stream downstream from Cape Hatteras 1975-1978, *J. Phys. Oceanogr*, *13*, 1275-1292.
- Hayes, J.L., 1985: An analytic and numerical study of lee cyclogenesis, Ph.D. dissertation, Naval Postgraduate School, 110 pp.
- Horton, C.W., 1984: Surface front displacement in the Gulf Stream by hurricane/tropical storm Dennis, *J. Geophys. Res.*, *89*, 2005-2012.
- Huh, O.K., L.J. Rouse Jr., and N.D. Walker, 1984: Cold-air outbreaks over the northwest Florida continental shelf: heat flux processes and hydrographic changes, *J. Geophys. Res.*, *89*, 717-726.
- Huppert, H.E., and K. Bryan, 1976: Topographically generated eddies, *Deep Sea Res.*, *23*, 655-679.
- Kennedy, P.J., and M.A. Shapiro, 1980: Further encounters with clear air turbulence in research aircraft, *J. Atmos. Sci*, *37*, 987-993.
- Kondo, J., 1976: Heat balance of the East China Sea during the air mass transformation experiment, *J. Meteor. Soc. Jap.*, *54*, 382-398.
- McWilliams, J.C., 1974: Forced transient flow and small-scale topography, *Geophys. Fluid Dyn.*, *6*, 49-79.
- Nof, D., 1983: On the response of ocean currents to atmospheric cooling, *Tellus*, *35A*, 60-72.
- Orlanski, I., 1976: A simple boundary condition for unbounded hyperbolic flows, *J. Comp. Phys.*, *21*, 251-269.
- Richardson, P.L., 1981: Gulf Stream trajectories measured with free-drifting buoys, *J. Phys. Oceanogr.*, *11*, 999-1010.
- Roden, G.I., 1976: On the structure and prediction of oceanic fronts, *Nav. Res. Reviews*, *29*, 18-35.
- Sanders, F., and J.R. Gyakum, 1980: Synoptic-dynamic climatology of the "bomb", *Mon. Wea. Rev.*, *108*, 1589-1606.
- Sandgathe, S.A., 1981: A numerical study of the role of air-sea fluxes in extratropical cyclogenesis, Ph.D. dissertation, Naval Postgraduate School, 134 pp.
- Sawyer, J.S., 1956: The vertical circulation at meteorological fronts and its relation to frontogenesis, *Proc. Roy. Soc. Lond.*, *A234*, 346-362.
- Schopf, P.S., and M.A. Cane, 1983: On equatorial dynamics, mixed layer physics and sea surface temperature, *J. Phys. Oceanogr.*, *13*, 917-935.

Semtner, A.J., and Y. Mintz, 1977: Numerical simulation of the Gulf Stream and mid-ocean eddies, *J. Phys. Oceanogr.*, 7, 208-230.

Shapiro, M.A., 1981: Frontogenesis and geostrophically forced secondary circulations in the vicinity of jet stream-frontal zone systems, *J. Atmos. Sci.*, 38, 954-973.

Shapiro, M.A., 1982: Mesoscale weather systems of the central United States, CIRES/NOAA report, Boulder, Co., 78 pp.

Smith, R.B., 1984: A theory of lee cyclogenesis, *J. Atmos. Sci.*, 41, 1159-1168.

Thompson, J.D., and H.E. Hurlburt, 1982: A numerical study of the influence of the New England seamount chain on the Gulf Stream, In: *Proceedings of the Workshop on Gulf Stream Structure and Variability*, University of North Carolina, 346-362.

Thorpe, S.A., 1973: Turbulence in stably stratified fluids: A review of laboratory experiments, *Bound. Layer Meteor.*, 5, 95-119.

United States Naval Oceanographic Office, 1970: Monthly summary, *The Gulf Stream*, 5, Number 11, 10 pp.

Vastano, A.C., and B.A. Warren, 1976: Perturbations to the Gulf Stream by Atlantis II Seamount, *Deep Sea Res.*, 23, 681-694.

Veronis, G., 1981: Dynamics of the large-scale ocean circulation, in *Evolution of Physical Oceanography*, edited by, B.A. Warren and C. Wunsch, MIT Press, Cambridge, MA, 623pp.

Wei, M., 1979: The energy budgets of a developing cyclone over the East China Sea during the 1975 Air Mass Transformation Experiment, OU AMTEX Contribution No. 79-1, University of Oklahoma, 136 pp.

Worthington, L.V., 1976: *On the North Atlantic Circulation*, The Johns Hopkins University Press, Baltimore, MD, 110pp.

INITIAL DISTRIBUTION LIST

	No. Copies
1. Defense Technical Information Center Cameron Station Alexandria, VA 22314	2
2. Library, Code 0142 Naval Postgraduate School Monterey, CA 93943	2
3. Chairman (Code 63Rd) Department of Meteorology Naval Postgraduate School Monterey, CA 93943	1
4. Chairman (Code 68Mr) Department of Oceanography Naval Postgraduate School Monterey, CA 93943	1
5. Professor R.L. Elsberry (Code 63Es) Department of Meteorology Naval Postgraduate School Monterey, CA 93943	5
6. Adj. Res. Professor D. Adamec (Code 63Ac) Department of Meteorology Naval Postgraduate School Monterey, CA 93943	5
7. Director Naval Oceanography Division Naval Observatory 34th and Massachusetts Avenue, NW Washington, D.C. 20390	1
8. Commander Naval Oceanography Command NSTL Station Bay. St. Louis, MS 39522	1

9. Commanding Officer 1
Naval Oceanographic Office
NSTL Station
Bay St. Louis, MS 39522
10. Chief of Naval Research 1
800 N. Quincy Street
Arlington, VA 22217
11. Naval Ocean Research and 1
Development Activity
NSTL Station
Bay St. Louis, MS 39522
12. Professor R.L. Haney (Code 63Hy) 1
Department of Meteorology
Naval Postgraduate School
Monterey, CA 93943
13. Professor R.T. Williams (Code 63Wu) 1
Department of Meteorology
Naval Postgraduate School
Monterey, CA 93943
14. Adj. Professor M.A. Rennick (Code 63Rn) 1
Department of Meteorology
Naval Postgraduate School
Monterey, CA 93943
15. Professor G.E. Latta (Code 53Lz) 1
Department of Mathematics
Naval Postgraduate School
Monterey, CA 93943
16. Associate Professor R.W. Garwood (Code 68Gd) 1
Department of Oceanography
Naval Postgraduate School
Monterey, CA 93943

211069

Thesis

A223

Adamec

c.1

Numerical simulations
of the response of in-
tense ocean currents to
atmospheric forcing.

19 NOV 82

70 37 -

211069

Thesis

A223

Adamec

c.1

Numerical simulations
of the response of in-
tense ocean currents to
atmospheric forcing.

thesA223

Numerical simulations of the response of



3 2768 001 90903 9

DUDLEY KNOX LIBRARY